


12-1-2020

Numerical and Experimental Investigation of Aeration Self Mixing By Using Pulsating and Continuous Air Flow

Ahmed Ali Alkhafaji
University of Wisconsin-Milwaukee

Follow this and additional works at: <https://dc.uwm.edu/etd>

 Part of the [Environmental Engineering Commons](#), [Mechanical Engineering Commons](#), and the [Water Resource Management Commons](#)

Recommended Citation

Alkhafaji, Ahmed Ali, "Numerical and Experimental Investigation of Aeration Self Mixing By Using Pulsating and Continuous Air Flow" (2020). *Theses and Dissertations*. 2447.
<https://dc.uwm.edu/etd/2447>

This Dissertation is brought to you for free and open access by UWM Digital Commons. It has been accepted for inclusion in Theses and Dissertations by an authorized administrator of UWM Digital Commons. For more information, please contact scholarlycommunicationteam-group@uwm.edu.

NUMERICAL AND EXPERIMENTAL INVESTIGATION OF
AERATION SELF MIXING BY USING PULSATING AND
CONTINUOUS AIR FLOW

by

Ahmed Alkhafaji

A Dissertation Submitted in
Partial Fulfillment of the
Requirements for the Degree of

Doctor of Philosophy
in Engineering

at

The University of Wisconsin-Milwaukee

December 2020

ABSTRACT

NUMERICAL AND EXPERIMENTAL INVESTIGATION OF AERATION SELF MIXING BY USING PULSATING AND CONTINUOUS AIR FLOW

by

Ahmed Alkhafaji

The University of Wisconsin-Milwaukee, 2020
Under the Supervision of Professor Ryoichi S. Amano

Wastewater treatment is considered one of the most common forms of pollution control in the united states. Considered as an integral part of the wastewater treatment, the aeration process is the most energy-consuming process among all the processes that take place in any wastewater treatment plant. According to the United States Environmental Protection Agency (EPA), a wastewater treatment plant is expected to remove at least 85% of the suspended solids and dissolved organic compounds from the wastewater before discharging it to a river or a lake. The normal operation of the aeration process is by compressing air continuously to basin diffusers for subsurface diffusion or agitate the water at the surface to create water droplets that can be mixed with atmospheric air. The goal of the aeration process is to bring the air in contact with the wastewater to provide the necessary oxygen for the biological flocculation and mixing in the wastewater. Aeration systems utilize subsurface diffusion employ diffusion equipment submerged at the bottom of water tanks called aeration diffusers. These diffusers introduce the air to the water in the aeration tank in the form of air bubbles. The rising of air bubbles in water

is important for many engineering applications. This importance comes from the need to keep the oxygen in water at certain levels. When considering these applications, the first question that arises is how to increase the rate of oxygen transfer and make the process more efficient. In this study, it was shown that the extent of bubbles diffusion in water has a significant influence on the aeration efficiency. When rising in the water, these bubbles will convert the flow to rotational flow with high vorticity and circulation which will increase the mixing and the rate of oxygen transfer. Experimental and computational studies were conducted to obtain the standard oxygen transfer efficiency (SOTE), Standard aeration efficiency (SAE), vorticity, and circulation. The SOTE and SAE obtained from the experimental approach is considered as a measure of the aeration efficiency. While the vorticity and circulation from the computational fluid dynamics (CFD) as a measure of the extent of mixing in the aeration tank. The SOTE and SAE are considered important design parameters that can render the efficiency of the aeration process when studied experimentally. Experimental lab measurements to obtain the dissolved oxygen concentration under standard conditions were conducted at the UWM aeration lab using full scale aeration systems with all the required equipment are built and set up to complete the experimental measurements. High-speed camera with 2000 frames per second was also used for visualization of the bubble's behavior. From both experimental and CFD results, it was proven that the method used to diffuse the air from sub-surface diffusion system can also alter the system efficiency. Normally, continuous air diffusion method is considered in typical aeration systems. A new method utilizes diffusing the air in pulsating order was proven to increase the aeration efficiency to up to 50%. When investigating for the effect of different pulsating times, it was obtained from the experimental results that when pulsating time is decreased to 0.5 S, the SOTE is increased. Also, experimental results of three water columns height showed that as

water column height is increased, the SOTE is also increased. On the other hand, the computational (CFD) method was also implemented in this work. The CFD is a very useful tool in many applications and it can be used for modeling the aeration systems. Due to lab limitations to conduct experimental studies for large scale aeration systems (larger than 1.8 m), CFD method was used to investigate the effect of water column of 2, 2.5, and 3 m water columns. After solving the flow and mass transfer models, results of the dissolved oxygen evolution in time were processed to obtain the SOTE results, which showed the higher water column gives the higher SOTE. This is similar to the experimental study conducted for investigating the effect of water column height. Another study using the CFD method to investigate the effect of diffusion order considering inline and staggered orders showed that vorticity and circulation can render the effect of mixing on the rate of oxygen transfer and the potential to develop this method to consider more general cases without the need to evolve in time to obtain the dissolved oxygen time dependent profile and save a lot of computation time. In all experimental and CFD studies, the results were showing strong influence of the oxygen transfer rate on mixing and this conclude the consideration of increase the mixing in the aeration tank can lead to significant increase in the aeration efficiency and reducing the high energy cost characterized by the aeration systems.

To
my parents,
my wife,
and my Kids

TABLE OF CONTENTS

1. Introduction	1
1.1 Aeration process	1
1.2 Types of Aeration systems	3
1.3 Coarse vs fine pore diffusers	4
1.4 Energy consumption of the aeration process	5
2. Literature review	7
2.1 Mass transfer	7
2.2 Bubbles formation, bubble rising velocity and bubble frequency	11
2.3 Hydrostatic forces acting on bubbles	13
2.4 Liquid degassing	16
2.5 Mixing in the aeration tank	18
3. Method of approach	22
3.1 Experimental approach	22
3.2 Theory for the experimental approach	24
3.3 Numerical approach	30
3.3.1 Volume fraction	31
3.3.2 Hydrostatic forces	31
3.3.3 Henry's law	33
3.3.4 Mass transfer coefficient	34
3.4 Use of image processing technique	38
4. Experimental studies on aeration	43
4.1 Aeration study using pulsating air flow	43
4.1.1 Conclusions	46
4.2 Effect of water column height	47
4.2.1 Effect of water column on the standard oxygen transfer efficiency	48
4.2.2 Conclusions	56
4.3 Froude number	56
4.4 Aeration from ceramic diffusers and comparison with membrane diffusers	59

4.4.1 Standard oxygen transfer efficiency	60
4.4.2 Standard aeration efficiency	68
4.4.3 Conclusions	75
4.5 Cyclone study	76
5. CFD studies on aeration	81
5.1 Effect of water column-CFD modeling	81
5.1.1 CFD results validation	86
5.1.2 CFD results of full-scale aeration systems	90
5.1.3 Conclusions	92
5.2 Effect of diffusers diffusion order	92
5.2.1 Computational method	92
5.2.2 Experimental method.....	95
5.2.3 Experimental results	97
5.2.4 CFD results	101
5.2.5 Application to real case	108
5.2.6 Conclusions.....	110
Chapter 6 Recommendations for future research	111
References	113
Appendix A: Image Processing Code	116
Curriculum Vitae	121

LIST OF FIGURES

Figure 1.1: (a) Typical wastewater treatment processes, (b) Primary treatment, (c) secondary treatment (EPA, How wastewater treatment works...The basics, 1998).....	2
Figure 1.2: (a) Subsurface diffusion. (b) Surface agitation.....	4
Figure 1.3: Examples of fine and course diffusers: (a) Fine bubbles diffuser, (b) Coarse bubbles diffuser.....	5
Figure 1.4: Energy consumption for wastewater treatment (Walther, 2009).....	6
Figure 2.1: C_T for small bubbles.....	15
Figure 2.2: C_T for large bubbles	16
2.3: Dissolved oxygen concentration in water with and without ultrasonic	17
Figure 2.4: Dissolved oxygen concentration in liquid (mg/liter); a. before the bubble passes, b. as the bubble passes, c. after the bubble passed.....	19
Figure 3.1: Experimental set up.....	23
Figure 3.2: Air diffusers; (a) Membrane, (b) Porous	24
Figure 3.3: Dissolve oxygen concentration variation with time.....	25
Figure 3.4: Vacuum degasification set up.....	27
Figure 3.5: Data collection of the DO.....	27
Figure 3.6: Bubbles average rising velocity at 0.5 second; a) Experiment, b) CFD	37
Figure 3.7: Bubbles average rising velocity at 1 second; a) Experiment, b) CFD	38
Figure 3.8: images processed for CFD and experiment cases at 0.5 second physical time	39
Figure 3.9: images processed for CFD and experiment cases at 1 second physical time	40
Figure 3.10: images processed for CFD and experiment cases at 1.5 second physical time	41
Figure 3.11: images processed for CFD and experiment cases at 2 second physical time	42
Figure 4.1: System set up.....	43
Figure 4.2: Control circuit	44
Figure 4.3: SOTE % variation with AAA	45
Figure 4.4: Normalized SOTE variation with AAA	46
Figure 4.5: SOTE variation with AAA parameter for 0.6 m water column.....	49
Figure 4.6: SOTE variation with AAA for 1.2 m water column	50
Figure 4.7: SOTE variation with AAA for 1.8 m water column	51
Figure 4.8: SOTE variation with flow rate at 0.5 sec pulsating time.....	52
Figure 4.9: SOTE variation with flow rate at 1.5 sec pulsating time.....	52

Figure 4.10: SOTE variation with flow rate at 2.5 sec pulsating time.....	53
Figure 4.11: Measurement uncertainty of SOTE for the 1.2 m water column.....	54
Figure 4.12: Schematic illustration of waves (pulsating flow).....	57
Figure 4.13: Surface wave with 1.14 Froude number.....	58
Figure 4.14: Froude number vs water column.....	58
4.15: SOTE variation with flow rate for 0.6 m water column.....	61
4.16: SOTE variation with flow rate for 1.2 m water column.....	61
4.17: SOTE variation with flow rate for 1.8 m water column.....	62
Figure 4.18: SOTE variation with flow rate for 0.6 m water column and 0.5 S pulsating	63
Figure 4.19: SOTE variation with flow rate for 0.6 m water column and 1.5 S pulsating time....	64
Figure 4.20: SOTE variation with flow rate for 0.6 m water column and 2.5 S pulsating time....	64
Figure 4.21: SOTE variation with flow rate for 1.2 m water column and 0.5 S pulsating time....	65
Figure 4.22: SOTE variation with flow rate for 1.2 m water column and 1.5 S pulsating time....	66
Figure 4.23: SOTE variation with flow rate for 1.2 m water column and 2.5 S pulsating time....	66
Figure 4.24: SOTE variation with flow rate for 1.8 m water column and 0.5 S pulsating time....	67
Figure 4.25: SOTE variation with flow rate for 1.8 m water column and 1.5 S pulsating time....	67
Figure 4.26: SOTE variation with flow rate for 1.8 m water column and 2.5 S pulsating time....	68
Figure 4.27: SAE variation with flow rate for 0.6 m water column and 0.5 S pulsating time	70
Figure 4.28: SAE variation with flow rate for 0.6 m water column and 1.5 S pulsating time	70
Figure 4.29: SAE variation with flow rate for 0.6 m water column and 2.5 S pulsating time	71
Figure 4.30: SAE variation with flow rate for 1.2 m water column and 0.5 S pulsating time	71
Figure 4.31: SAE variation with flow rate for 1.2 m water column and 1.5 S pulsating time	72
Figure 4.32: SAE variation with flow rate for 1.2 m water column and 2.5 S pulsating time	73
Figure 4.33: SAE variation with flow rate for 1.8 m water column and 0.5 S pulsating time	73
Figure 4.34: SAE variation with flow rate for 1.8 m water column and 1.5 S pulsating time	74
Figure 4.35: SAE variation with flow rate for 1.8 m water column and 2.5 S pulsating time	74
Figure 4.36: experimental set up.....	77
Figure 4.37: Forces acting on the bubbles soon after emerging from the pipe	78
4.38: Suggested set up for deflecting air bubbles	80
Figure 5.1: CFD model for the aeration system	82
Figure 5.2: Experimental model to validate the CFD results	83
Figure 5.3: Experimental set up for CFD validation.....	86
Figure 5.4: Dissolved oxygen evolution with time.....	88

Figure 5.5: DO profile of experiment vs CFD.....	89
Figure 5.6: DO evolution with time for 2, 2.5, and 3 m water columns	91
Figure 5.7: SOTE% vs water column-CFD.....	91
Figure 5.8: Experimental set up; a-Inline order, b-Staggered order	97
Figure 5.9: SOTE% variation with flow rate at 0.5 Sec pulsating time.....	98
Figure 5.10: SOTE% variation with flow rate at 1.5 Sec pulsating time.....	99
Figure 5.11: SOTE% variation with flow rate at 2.5 Sec pulsating time.....	99
Figure 5.12: SOTE of the 0.5, 1.5, and 2.5 S pulsating time for inline case	100
Figure 5.13: SOTE of the 0.5, 1.5, and 2.5 S pulsating time for staggered case	101
Figure 5.14: Water jump at the air-water interface.....	102
Figure 5.15: Vorticity variation with time at a plane on the water surface	103
Figure 5.16: Circulation variation with time at a plane on the water surface	104
Figure 5.17: Vorticity variation with time at a plane 0.2 m below the water surface.....	105
Figure 5.18: Circulation variation with time at a plane 0.2 m below the water surface	105
Figure 5.19: Curve fitting of the circulation variation for the inline order from figure 9 starting at 2.5 s time	106
Figure 5.20: Curve fitting of the circulation variation for the staggered order from figure 9 starting at 2.5 s time	107
5.21: Suggested staggered order layout for implementing the diffusion order on real case	109

LIST OF TABLES

Table 4.1: Measurement uncertainty of SOTE for the 1.2 m water column	55
Table 4.2: Dynamic wet pressure.....	69
Table 4.3: Percentage of experimental error	75

LIST OF ABBREVIATIONS

A	Interfacial area, m^2
AAA	Amano-Alkhafaji-Alkhalidi parameter, $4Q/\pi D^2 H$
AE	Aeration efficiency, $kgO_2/kw.h$
C	Coefficient, dimensionless
C _g	Oxygen concentration, $mg/liter$
D	Diameter of water reservoir, m
DO	Dissolved oxygen, $mg/liter$
DWP	Dynamic wet pressure, $mm H_2O$
d	Diameter of the bubble, m
F	Force, N
g	Acceleration of gravity, m/s^2
H	Height of water column, m
K _L	Local mass transfer coefficient, m/s
K _L a	Overall mass transfer coefficient, $1/s$
K _L a ₂₀	Overall mass transfer coefficient at 20°C, $1/s$
N	Mass flux of species, kg/s
P	Power, W
P _g	Gas pressure, Pa
Q	Flow rate, L/min
Re	Reynolds number
S	User defined mass transfer source, kg/s

SAE	Aeration efficiency at standard conditions, kgO ₂ /kw.h
Sc	Schmidt number
Sh	Sherwood number
SOTE	Standard oxygen transfer efficiency, dimensionless
SOTR	Standard oxygen transfer rate, kg/s
T	Temperature, °C
t	Time, second
U	Velocity, m/s
V	Volume of the water, liter
We	Weber number, dimensionless
Y	Volume fraction of gas or liquid, dimensionless
\dot{m}_{O_2}	Mass flow rate of the oxygen in the air, kg/s
D	Diffusion coefficient, m ² /s
ρ	Density, kg/m ³
ν	Kinematic viscosity, m ² /s
μ	Dynamic viscosity of fluid, Pa.s
τ	Shear stress, Pa
σ	Surface tension, N/m

Subscripts:

D	Denote to drag force, dimensionless
g	Denote to oxygen gas, dimensionless
<i>i, j</i>	Denote to the dispersed and continuous phases, dimensionless

- L Denote to lift force, dimensionless
- s Denote to slip velocity, dimensionless
- vm Denote to virtual mass force, dimensionless
- in and ∞ Denote to initial and steady state condition

ACKNOWLEDGEMENTS

First and foremost, Thanks god for all the blessings

My deepest gratitude and thanks go to my advisor, Professor Amano, who guided me from the beginning until this moment with his invaluable and unforgettable directions. Without him, I would not be able to pass all the hard obstacles I experienced through my study journey. His motivating guidance kept me always engaged with my coarse work and research. I deeply appreciate his encouragement and patience.

I would like to express my sincere thanks to my thesis committee members, Prof. Deyang Qu, Prof. Rudi Strickler, Prof. Istvan Lauko and Prof. John Reisel, for their time and valuable discussion and recommendations.

I also would like to thank my current and previous colleagues for sharing all information I needed regarding software packages, research lab equipment and instructions.

My biggest thanks to my parents, my wife and my kids for the support and patience while pursuing my degree.

1. Introduction

1.1 Aeration process

Wastewater contains different kinds of solids ranging from settleable to dissolved particles depending on the size of the particles. One cubic meter of wastewater weighs approximately 1000 kg contains 0.5 kg of solids (Davis, 2010). One half of the solids will be dissolved solids such as calcium and sodium salts as well as organic compounds. The other half will be settleable solids. Therefore, wastewater must be treated to properly remove a great portion of these solids before discharging to the lakes or rivers to protect the environment from pollution. Wastewater treatment involves series of processes to achieve the removal process and meet the EPA effluent requirements. The treatment of wastewater is mainly incorporated of two stages, first the wastewater is flowing through a filtration process by using different screens, this is called the primary treatment (Fig. 1.1, b), where larger particles are removed from the wastewater. Then in the next stage, small suspended and dissolved particles are removed from the wastewater during the secondary treatment (Fig. 1.1, c). The wastewater treatment was limited to the primary treatment only but demands for higher purity wastewater urged wastewater plants to consider implementing a secondary treatment for the wastewater. In the secondary treatment, the wastewater is admitted to the aeration tank first, where it will be brought to contact with the air supplied at the bottom of the aeration tank. In this aeration tank, the oxygen in the air is dissolved in the water. This oxygen absorption is called the aeration process.

As mentioned earlier, the wastewater contains dissolved organic compounds, these organic compounds can be used as substrate as to stimulate their growth to form biological flocs called activated sludge. Keeping required dissolved oxygen levels in the wastewater is necessary to efficient activated sludge operation. The activated sludge plays an important role in the secondary

treatment, and the percentage of the recycled or the wasted activated sludge determines the sufficiency or deficiency of the biological flocculation, hence the removal of pollutants.

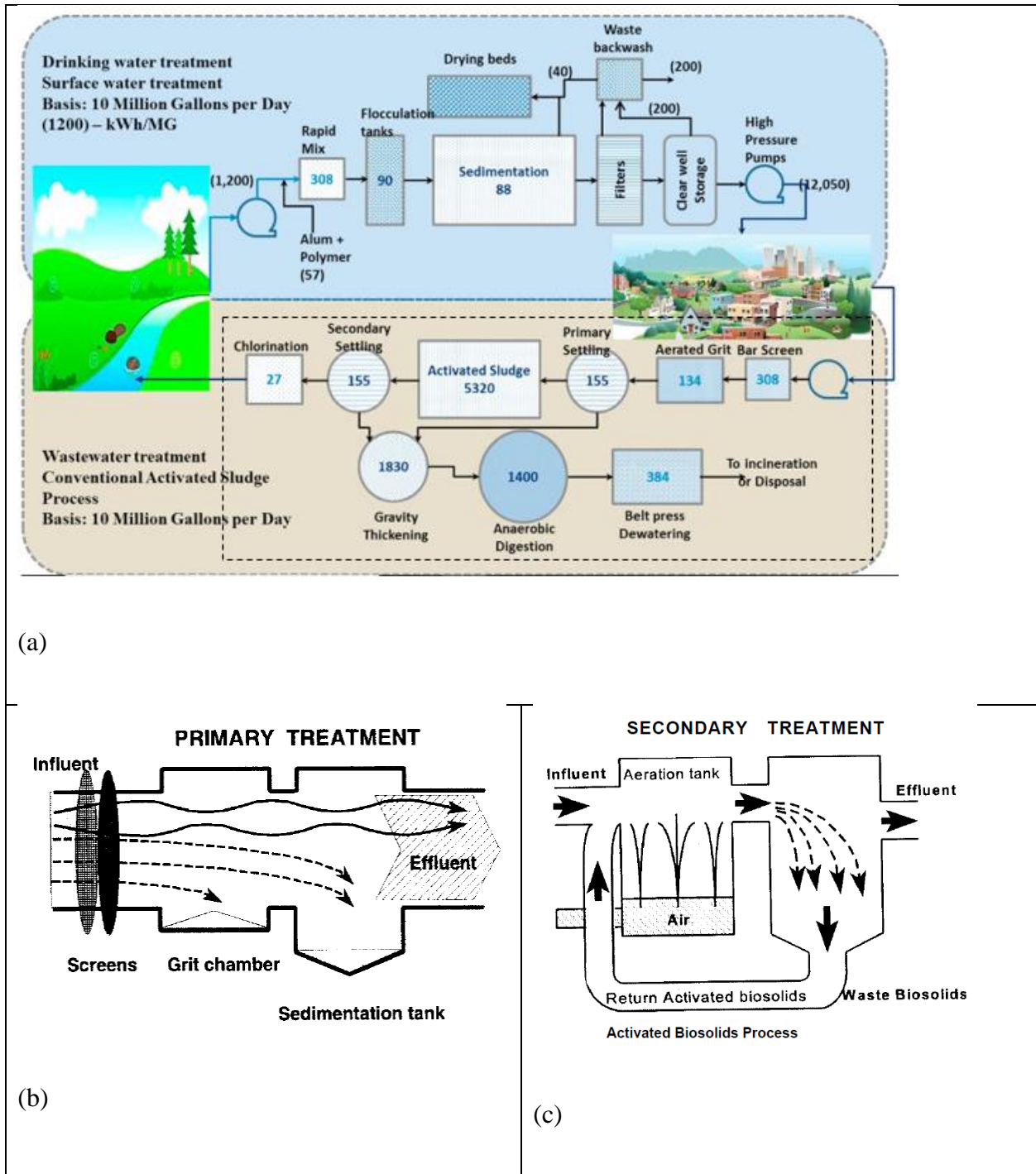


Figure 1.1: (a) Typical wastewater treatment processes, (b) Primary treatment, (c) secondary treatment (EPA, How wastewater treatment works...The basics, 1998)

1.2 Types of Aeration systems

For the aeration process to be efficiently operated, the wastewater must be brought into contact with air to keep the dissolved oxygen in the wastewater at a certain level, this level is determined by the biological oxygen demand (BOD).

Aeration systems fall into two categories, either air introduced to water or water to air. When air introduced to water, air bubbles are injected in water. When water introduced to air, water droplets are mixed with air. Both of these methods are designed to create a great surface area for oxygen molecules to transfer.

In general, there are two methods (Lawrence, Yung, & Nazih, 2006) used in wastewater treatment plants to mix the air with the wastewater, these are:

- 1- Subsurface air diffusion: In this method, the wastewater is brought into contact with air by diffusing the air into the water using air diffuser installed in a water basin as shown in Fig. 1.2 (a).
- 2- Surface agitation: In this method, surface agitators or mixers are used to bring the wastewater into contact with the atmospheric air as shown in Fig. 1.2 (b).

The subsurface air diffusion is used in the current study, where the air is supplied to air diffusers submerged at the bottom of the aeration tank. The efficiency of this system is depending on the type and set up of the aeration diffusers as it will be discussed further in details based on the results of the current work.



(a)



(b)

Figure 1.2: (a) Subsurface diffusion. (b) Surface agitation

1.3 Coarse vs fine pore diffusers

The main component of the aeration systems is the aeration diffuser, the aeration diffuser is used to diffuse the air into the wastewater which is necessary to keep the oxygen at certain levels and promote the microbial growth in the wastewater converting the small suspended and dissolved particles to larger particles that can be easily separated in post treatment processes. In addition, the diffusion of the air into the wastewater creates a better mixing environment which helps in disturbing the particles and bring them into contact with the diffused air. There are two kinds of diffusers used for the aeration process in industry, depending on the size of the bubbles generated, these diffusers are classified as fine and coarse diffusers (figure 1.3). It is common practice to consider the diffuser fine when the bubbles size is less than 3 mm and coarse for that greater than 3 mm (Mooers Products Inc., 2013). Fine pore diffusers generate fine bubbles which have been proven to transfer oxygen faster than coarse bubbles. Therefore, fine diffusers are more efficient than coarse diffusers. Due to the larger number and the small size of the holes contained in the fine diffuser, it experiences larger pressure drop than coarse diffuser which is not only a waste of energy

but also requires more operating maintenance to work efficiently. However, fine diffuser requires 30 to 40 % less air than coarse diffuser (EPA, Wastewater technology fact sheet fine bubble aeration, 1999) which significantly decrease the power requirement of the air blowers used in the aeration process.

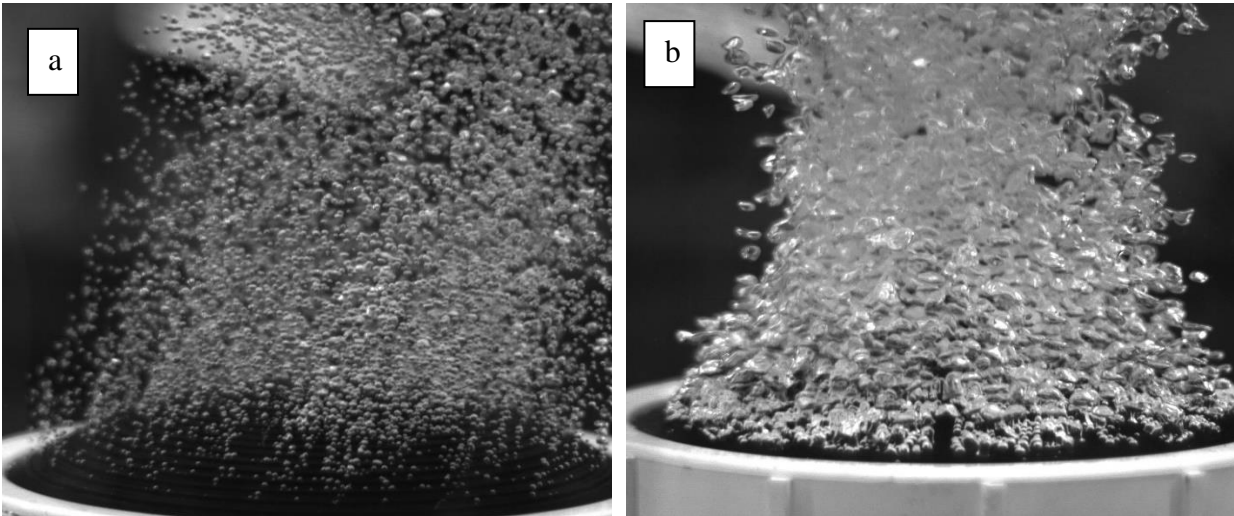


Figure 1.3: Examples of fine and course diffusers: (a) Fine bubbles diffuser, (b) Coarse bubbles diffuser

1.4 Energy consumption of the aeration process

Wastewater treatment was limited to only primary treatment prior to discharge to the receiving rivers or lakes, but the Clean Water Act in 1972 have imposed regulations on most wastewater treatment plants to provide secondary treatment in addition to the primary treatment. Secondary treatment, which includes the aeration process, is considered the principal energy-consuming process in the wastewater treatment that uses approximately 50 to 65% of the net energy consumption for a typical activated sludge wastewater treatment plant. Figure 1.4 (Walther,

2009) shows an illustration for the energy consumed by each process in the wastewater treatment plant. Based on that, the aeration process has the biggest potential for the energy savings and any design that contributes towards increasing the efficiency of the aeration process will have a positive impact on the energy consumption of the wastewater treatment process as whole.

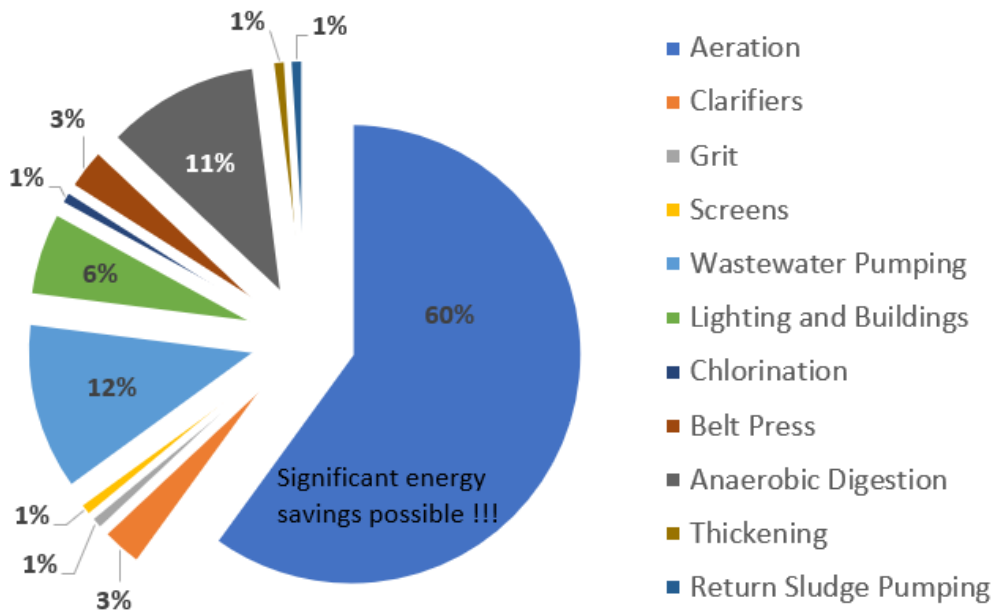


Figure 1.4: Energy consumption for wastewater treatment (Walther, 2009)

2. Literature review

The aeration process is the most energy consuming process among all the wastewater treatment processes, consuming more than 50% of the total energy of typical municipal wastewater treatment plants. The environmental protection agency (EPA 1999) reported that 85 % of the total biodegradable and suspended solids should be removed from the wastewater before discharging to the recipient rivers or lakes. In view of the increased importance to decrease the energy consumed by the aeration process, a considerable emphasis has brought to the attention of researchers to develop efficient aeration systems. Since the aeration efficiency is proportional to the rate of oxygen transfer, the mass transfer of the oxygen from the air to the water is of great importance.

2.1 Mass transfer

Gas – liquid transport process has important influence in many engineering applications and specifically in wastewater treatment process. In wastewater aeration, the mass transfer process that takes place to transfer the molecules from the solute to the solvent fluid Plays an important role in the efficiency of this process. Therefore, many researches have been conducted in this matter. These researches are studying the effect of different factors on the mass transfer coefficient. Most of the studies derive empirical models to determine the mass transfer coefficient for isolated bubbles, these models are based on the penetration theory (Higbie, 1935). In this theory, also known as the Boussinesq solution, the depth of penetration is estimated for water exposed to Carbon Dioxide (CO_2) for a short period of exposure to determine the gas concentration and the liquid film coefficient. The later was found inversely proportional with time which is consistent with common experience that shortening the period of exposure increase the coefficient. The penetration theory showed that the coefficient increased to infinity as the exposure time decreased

indefinitely. The Boussinesq solution has also been used as a closure law in Eulerian–Eulerian two-fluid simulations of industrial ozonation towers (Cockx, Do-Quang, Line, & Roustan, 1999) and aeration tanks for urban wastewater treatment (Fayolle, Cockx, Gillot, Roustan, & Hédut, 2007) at low to moderate volume fractions ($\alpha \leq 10\%$).

In most of the industrial applications, swarms of bubbles are rising at the same time. This brings the attention to the significance of turbulence experienced by such flow conditions. Turbulence and bubbly flow, when combined, are considered one of the most challenging flow problems. The already complicated nature of the carrier phase turbulence is further complicated by the random coalescence and breaking of the dispersed bubbles. This effect becomes more significant as the volume fraction of the dispersed phase becomes closer to that of the continuous phase. Therefore, the presence of the dispersed bubbles makes both experimental measurements and numerical simulations of multiphase flow conditions more difficult than those of single-phase flow conditions.

Computational investigations using Eulerian and Lagrangian techniques have provided useful tools for simulating multiphase flow. A detailed discussion on the formulation of various mathematical models of two-phase flow conditions based on the conservation laws of mass, momentum, and energy is presented by Ishii (Ishii, 1975). Special emphasis was considered on the local instant formulation and the time averaged macroscopic model. Two important models were presented; The two-fluid model, which is formulated by considering each phase separately, and the mixture model, which is formulated by considering the two-phase fluid as a mixture, which is expressed in terms of three mixture conservation equations of mass, momentum, and energy, in addition to one diffusion equation.

Due to this complexity, there is limited information on the effect of bubbles dispersion (dispersed phase) on the hydrodynamic behavior of the water (continuous phase). McGinnis (McGinnis & Little, 2002) considered a discrete bubbles model to predict the rate of oxygen transfer from air to water at different air flow rates considering initial bubbles size distribution. The model is applied for hypolimnetic oxygenation systems with 14 m deep water, which entails to consider the effect of hydrostatic pressure and the resident time on the bubble size.

The effect of increasing the gas volume fraction on the gas–liquid mass transfer coefficient has been experimentally investigated by (Colombet, et al., 2011) for air bubbles in water. They used a high-speed camera with fixed focal lens, and the particle tracking velocimetry (PTV) method was able to measure bubbles volumes, shapes and velocities for gas volume fractions from 0.45 to 16.5 %. In this range, the mass transfer coefficient is found very close to that of a single bubble provided that the Reynolds number is based on the mean equivalent diameter and the average rising velocity of a bubble in the swarm, which suggests a weak influence of the collective effect on the mass transfer at high Péclet number.

A bench scale experimental study was conducted by (Ashley, Hall , & Mavinic, 1991) to examine the effect of four design variables on the mass transfer coefficient (K_{La}) in a tap water tank with fine pore diffused aeration system. The design parameters are air flow rate, airflow rate per diffuser, orifice diameter and tank surface area. The study demonstrated that the K_{La} and the oxygen transfer rate (OTR) increased to about 90% when increasing air flow rate from 9.41 to 18.81 liter/min. The number of diffusers produced the next most significant result; by increasing the number of diffusers from 1 to 2 at a constant air flow rate, K_{La} and OTR increased to about 25%. Two fine pore diffusers were used with orifices size of 40 and 140 μm , both orifices gave no significant difference in K_{La} and OTR. A reduction in the tank surface area had a marginally

significant inverse effect on K_{La} and OTR. The mean bubbles size generated by the 40 and 140 μm diffusers were 4.0 and 4.2 mm, respectively. There was no consistent effect of air flow rate on bubble size within the range of flow rate used in their experiment.

(Khudenko & Shpirt, 1986) evaluated the effect of different hydrodynamic parameters on the oxygen transfer efficiency utilizing dimensional analysis for large scale aeration system. These parameters include the bubble diameter, submergence of the aerators, the liquid water height, the aeration tank length and width, aeration intensity, and liquid physical properties. Also, the effect of longitudinal dispersion in the aeration tank was investigated as functions of the Reynolds number and the dimensions of the aeration tank.

(Colombet, Legendre, Risso, Cockx, & Guiraud, 2014) considered the collective effect on both bubble dynamics and mass transfer in a dense homogeneous bubble swarm for gas volume fractions up to 30 %. The experimental investigation was carried out for air bubbles rising in a square water column. The bubble size and shape were determined by using a high – speed camera. The gas volume fraction and bubble velocity were measured by using an optical probe. Then, measurements from these two methods were combined to determine the interfacial area between the gas and the liquid. The oxygen transfer from the bubble to the water was measured by using a gassing – out method. The results showed that the average vertical velocity is decreasing when the gas volume fraction increases as follows:

$$V = V_0[0.28 + 0.72 \exp(-15\alpha)]^{0.5} \quad (2.1)$$

Where $V_0 = 0.32 \text{ m/s}$

Regarding the mass transfer process, their results show that the evolution time of the oxygen concentration to reach to the saturation is decreasing when the gas volume fraction is increasing. Also, the mass transfer coefficient is decreasing when the gas volume fraction is increasing according to:

$$K_L = K_{L_0}(1 - \alpha) \quad (2.2)$$

Where $K_{L_0} = 4.45 \times 10^{-4}$ m/s

The Sherwood number was derived from their experimental measurements and was expressed as:

$$Sh = Sh_0(1 - \alpha)(1 + 2.3\alpha^{0.5}) \quad (2.3)$$

Where $Sh_0 = 445$

While the bubble agitation was independent on the gas volume fraction. The Sherwood number was found to be close to that of the single bubble, that was based on the average vertical bubble velocity. The conclusion was valid for low diffusion coefficient or high Peclet number.

2.2 Bubbles formation, bubble rising velocity and bubble frequency

Bubbles formation and frequency determines the size of the bubbles which is considered one of the most effective factors in the transfer process of the molecules from the gas to the liquid phase. On the other hand, bubble rising velocity is depending on the bubble size and the forces acting on the bubble as well. That arise the importance for the researchers to look in deep at this subject and utilize their findings towards enhancing the mass transfer process. Bubble size,

terminal velocity and shape was investigated by (Miyagi, 1925) experimentally and theoretically, relating the velocity as functions of bubble size and shape. He found out that the critical velocity of the rising bubble is about 28 cm/sec and it occurs when the bubble radius is about 0.16 cm. Also, the terminal velocity was linearly increasing with the bubble size for bubble's radius less than the critical radius, while it was decreasing parabolically for bubble's radius larger than the critical radius. On the other hand, as the bubble rise, it takes a helical course; its shape was taking a flattened outline with the major axis lies perpendicular to its course. He also found out that the resistance to the bubble motion is proportional to its volume.

The effect of gas flow rate on the bubbles frequency was studied by (Das, Das, & Saha, 2011), using a new method to estimate the bubble release frequency from a submerged orifice in water, for three orifices diameters and different water heights. The bubbles count was estimated using a conductivity probe. The bubble release frequency was estimated using a simple analytical algorithm. Three bubbles frequencies regimes were detected depending on the gas flow rate. For low flow rates, discrete bubbles can be seen as they rise. When the flow rate increases, it will be difficult to recognize the bubbles individually. Further increasing of the flow rate lead to what is called bubble jetting, where bubbles formed at the orifice coalesce with the preceding bubbles.

(Wilkinson & Haringa, 1994), investigated the effect of gas density on the bubble size. A new empirical equation was developed based on a photographic bubble size evaluation for water, mono-ethylene glycol, cyclohexane and n-heptane. The new equation defines the bubble diameter as functions of gas density and liquid properties according to:

$$D = \frac{3\sigma^{0.34}\mu^{0.22}}{g^{0.44}\rho_i^{0.45}\rho_j^{0.11}U_j^{0.02}} \quad (2.4)$$

(Alkhalidi & Amano, 2015) investigated the effect of some operation factors on the bubble size for air bubbles rising in the water. Computational fluid dynamics results were obtained and validated with experimental measurements. It was found that the computational bubbles size and shape closely match the experimental results. From their results, they concluded that the major influential effect on the bubble size was obtained from changing the air flow rate. The punch length and direction seemed to have minimal effects on the bubble size.

2.3 Hydrostatic forces acting on bubbles

When bubbles are introduced to a liquid and the two – phase flow can be called as dispersed flow, it becomes inevitable to consider the effect of the forces acting on the bubbles. These forces are the buoyancy, lift, drag and surface tension; these are the main forces which have influential effects on the flow dynamics of bubbles. In order to determine the dominance of these forces, it is more convenient to define the dimensionless numbers associated with the bubbly flow. Which are the Reynolds number (Re), which gives the effect of inertial to viscous forces. Eotvos number (Eo), which gives the effect of buoyancy to surface tension. Morton number, which is a property group for the two – phase flow. All these numbers can be defined as:

$$Re = \frac{\rho_i U d_j}{\mu_i} \quad (2.5)$$

$$Eo = \frac{g(\rho_i - \rho_j)d_j^2}{\sigma} \quad (2.6)$$

$$M = \frac{g\mu_i^4(\rho_i - \rho_j)}{\rho_j^2\sigma^3} \quad (2.7)$$

(Tomiyama, Kataoka, Zun, & Sakaguchi, 1998) developed empirical correlations for drag coefficient under a wide range of fluid properties, bubble diameter and gravity based on the

balancing forces acting on a bubble in stagnant fluid and available empirical correlations of terminal rising velocity of a single bubble. Terminal velocity of a single bubble is considered under the condition of $10^{-2} < Eo < 10^3$, $10^{-14} < M < 10^7$ and $10^{-3} < Re < 10^5$. Three cases were considered; pure, slightly contaminated and contaminated systems. The three correlations for the coefficient of drag (C_D) for each case was found as:

1- Pure system

$$C_D = \max \left\{ \min \left[\frac{16}{Re} (1 + 0.15Re^{0.687}), \frac{48}{Re} \right], \frac{8}{3} \frac{Eo}{Eo + 4} \right\} \quad (2.8)$$

2- Slightly contaminated system

$$C_D = \max \left\{ \min \left[\frac{24}{Re} (1 + 0.15Re^{0.687}), \frac{72}{Re} \right], \frac{8}{3} \frac{Eo}{Eo + 4} \right\} \quad (2.9)$$

3- Contaminated system

$$C_D = \max \left\{ \frac{24}{Re} (1 + 0.15Re^{0.687}), \frac{8}{3} \frac{Eo}{Eo + 4} \right\} \quad (2.10)$$

(Tomiyama, Tamai, Zun, & Hosokawa, 2002) conducted experimental work to determine the transverse lift force acting on a single bubble under the conditions of $-5.5 \leq \log_{10} M \leq -2.8$, $1.39 \leq Eo \leq 5.74$, $0 \leq |dV_i/dy| \leq 8.3 \text{ s}^{-1}$, where dV_i/dy is the velocity gradient of the shear flow. The coefficient of lift C_T of the small bubbles ($d < 4.4 \text{ mm}$) was confirmed to be a function of the

bubble Reynolds number Re as shown in Fig. 2.1, while the C_T of the large bubbles ($d > 4.4$ mm) was a function of Eotvos number (Eo) in addition to the bubble Reynolds number (Re) as shown in Fig. 2.2.

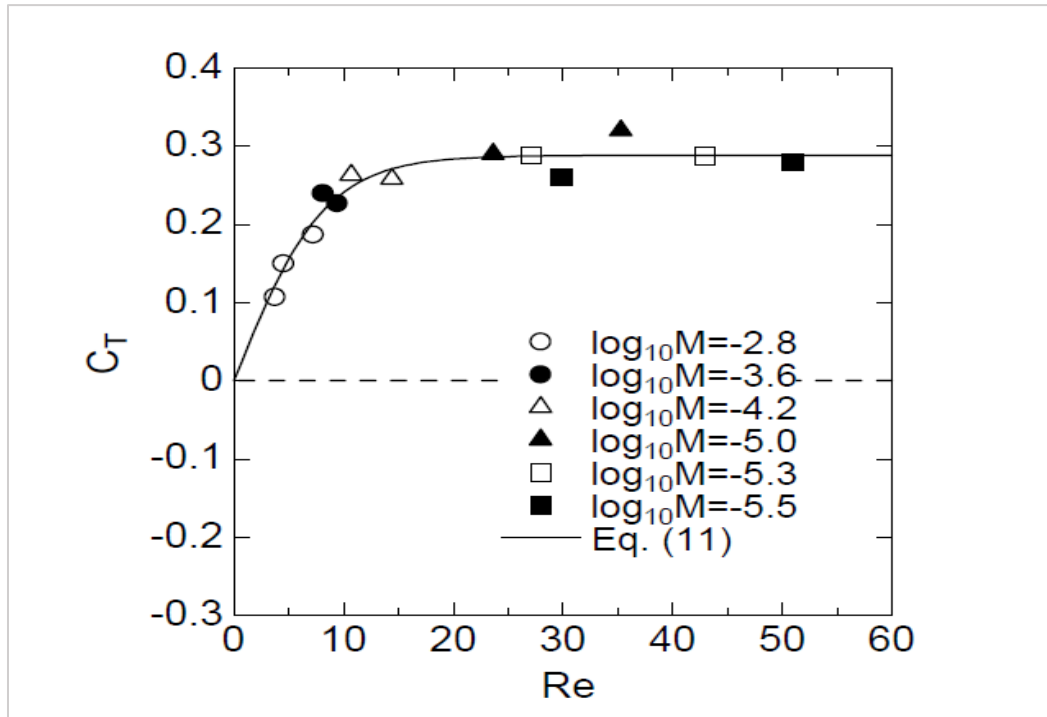


Figure 2.1: C_T for small bubbles

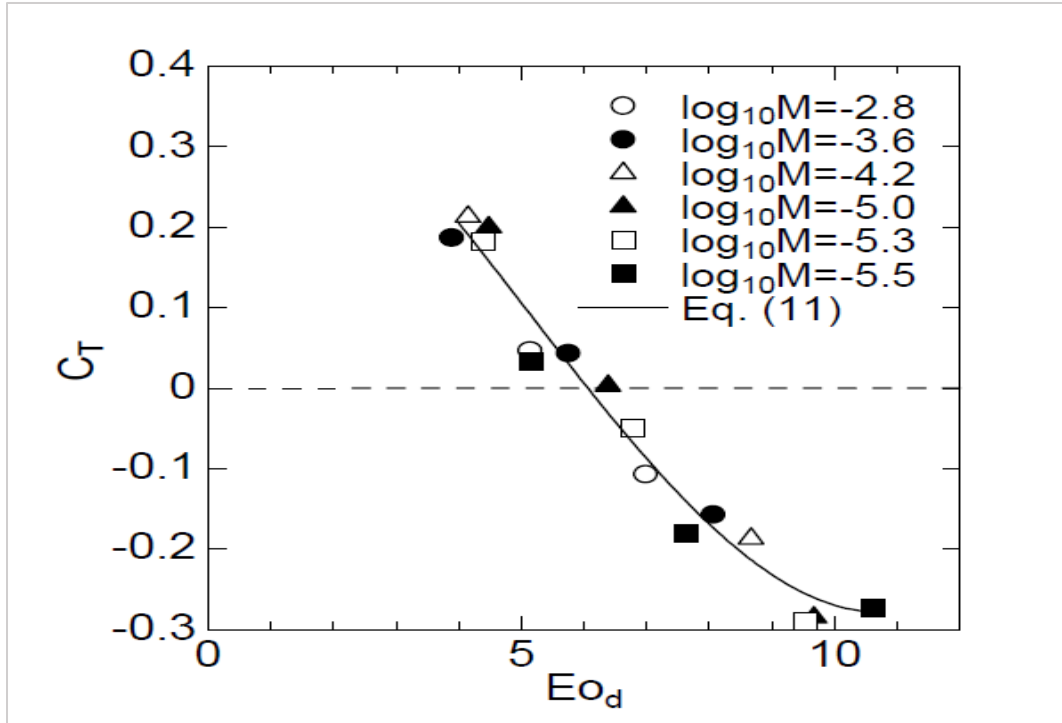


Figure 2.2: C_T for large bubbles

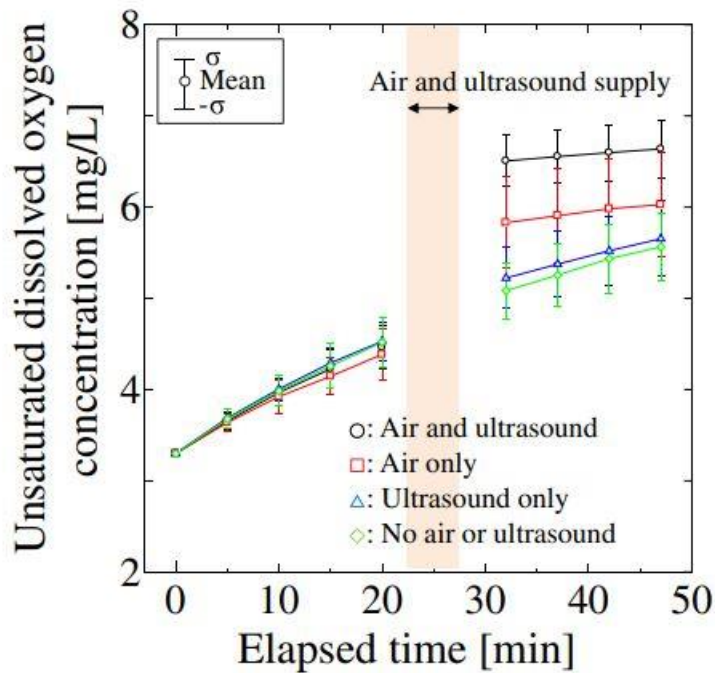
2.4 Liquid degassing

Lab studies conducted when considering aeration systems to obtain the dissolved oxygen measurements require an additional process that involves degassing of liquid, where dissolved oxygen must be removed from water in order to start the experiment with zero dissolved oxygen water. Several methods were experimented or discussed in the current work. The addition of Sodium Sulfite to the water is adopted to remove dissolved oxygen from water in all the experiments conducted in this work. Another method has been experimented but not adopted, which involves degassing of water by using vacuum based on Henry's law (Henry, 1803). Details of the first and second methods are discussed in detail in succeeding sections.

Another efficient method could be used in this subject utilizes ultrasonic waves. There are mainly two arrangements considered in ultrasonic degassing, these are batch and continuous arrangements (Eskin, 2017), (Eskin D., 2015). The continuous arrangement is more applicable

than batch arrangement since it can treat systems with high capacity as in the case of aeration systems. The operating flow rates for continuous ultrasonic system is about 1 liter/h (Guyurgina, 2016).

At the same time ultrasonic is used for aerating the liquids by applying an ultrasonic vibrator while dispersing air. This method shows promising results as shown from Hikaru (Hikaru Miura, 2015) and Ajay (Ajay Kumar, 2004). Figure 2.3 shows the results obtained by Hirkaru (Hikaru Miura, 2015), which shows that the dissolved oxygen concentration can increase to up to 40% when using ultrasonic along with dispersed air bubbles after 30 minutes from applying ultrasonic to the water.



2.3: Dissolved oxygen concentration in water with and without ultrasonic

The ultrasonic method is seeming very interesting method to increase the rate of oxygen transfer, and based on the literature, there is a possibility of significant increase in the standard oxygen transfer rate, therefore, this method can be added as a highly recommended for future research.

2.5 Mixing in the aeration tank

For the best operation of the aeration process, water must be brought into contact with air by dispersion of bubbles streams from air diffusers submerged at the bottom of the aeration tank (sub-surface diffusion). For this bubbly flow, the region that surrounds the bubble or the interface between the air and the water is considered the interfacial mass transfer area and this is mainly affected by the size of the bubble. Although, it is evident that small size bubbles have higher interfacial area per unit volume than coarse bubbles. But, the extent of mixing between the two phases has also very influential effects on the interfacial diffusion of mass in this region, since increase mixing by creating more waves in the water can entrain the bubbles to favorable turbulent flow conditions.

For isolated bubble rising in water at static or very low turbulence conditions, the bubble will rise leaving behind it a region of concentrated oxygen as shown in Fig. 2.4 (Dani, Guiraud, & Cockx, 2007). Figure 2.4 shows three scenarios; before, as, and after the bubble passes the captured image. There are light reflections effects in Fig. 2.4 (b), this is due to the bubble being reflecting the laser light. After the bubble passes, the disturbance due reflection is disappeared as shown from Fig. 2.4 (c). This figure shows that without enough mixing around the bubble, there will be low diffusion rate of oxygen from the high to the low concentration regions, and there will be poor

oxygen transfer rate. Therefore, oxygen transfer rate is strongly related to the level of mixing around the bubble.

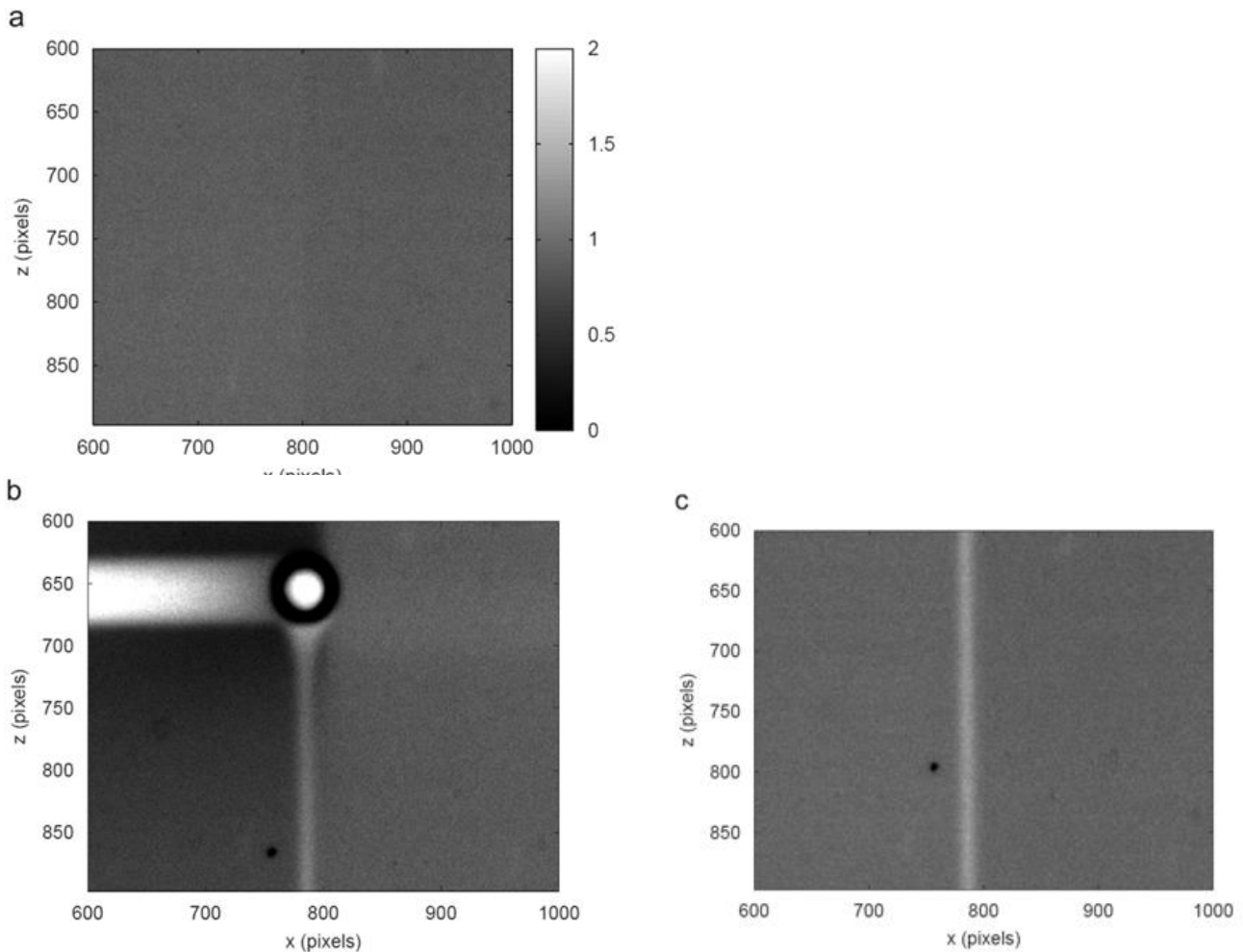


Figure 2.4: Dissolved oxygen concentration in liquid (mg/liter); *a. before the bubble passes, b. as the bubble passes, c. after the bubble passed*

Tank size and the effect of the diffusers distribution inside the aeration tank can also have noticeable effects on the oxygen transfer efficiency. (Bewtra & Nicholas, 1965) have studied experimentally the oxygen transfer during bubble ascent, which is depending mainly on the diffuser submergence, velocity of rise of air bubbles, diameter of the air bubbles, the air flow rates, tank geometry, and the location of the diffusers relative to one another and also relative to the tank.

They used both tube and sparger diffuser to obtain their data for tap water in a conventional aeration tank. Based on that, they concluded that the oxygen transfer rate increases with the tank width because a large percent of the air bubbles will reach the zone of downward moving water and entrained towards the bottom of the water tank. These entrained air bubbles will increase the resident time, and thus increasing the oxygen transfer rate. The case is opposite when increasing the tank width. This will lead to the conclusion that diffusers distribution inside the aeration tank will also affect the percentage of the entrained air bubbles and the oxygen transfer rate.

The effect of bubbles interaction on the water turbulence was studied by Lance (Lance & Bataille, 1991) and Behzadi (Behzadi, Issa, & Rusche, 2004). The distinguishing between real turbulence and bubble-induced turbulence was investigated for low volume fraction bubbly flow. It was concluded that for low volume fraction ($\alpha < 1\%$), the total turbulent kinetic energy is the sum of turbulent kinetic energy of bubbles motion without interactions. Above 1%, the turbulence is strongly attributed to the hydrodynamic interaction between the bubbles. Furthermore, Behzadi (Behzadi, Issa, & Rusche, 2004) predicted a threshold in which the dispersed phase turbulence cannot be ignored anymore, and a mixture of continuous and dispersed phases turbulence should be considered.

Based on that, creating self-mixing flow by utilizing the mixing-induced bubbly flow made some researchers to start thinking of some ways to agitate the bubbly flow in the aeration tank. (Alkhalidi, Alba'ba'a, & Amano, 2016) proposed a new method to admit the gas into the liquid for an aeration system by distributing the air alternatively to air diffusers submerged at the bottom of the water tank. This air diffusion method is called pulsating airflow method as opposed to the common continuous airflow method. This pulsating airflow method requires the use of more than one diffuser to achieve the alternating effect efficiently. Also, this alternating diffusion is generated

from diffusing the bubbles stream from both diffusers with some differential time. The method can be considered as self - agitation method due to creating additional mixing in the aeration tank by the wave induced bubbly flow. The results from these experimental studies for lab scale aeration systems have shown mixing can have significant effect on the aeration efficiency.

3. Method of approach

To improve any aeration system, we need to look at some important parameters, which represents the main factors affecting the efficiency of the aeration systems. These parameters are called the transfer parameters, and these are the oxygen transfer rate (OTR) and the oxygen transfer efficiency (OTE). Therefore, for any results that we are looking for here, it is expected to reflect the effect of the investigated case on any or both of these transfer parameters. The aeration efficiency (AE) is also important to consider here. Two approaches are followed to achieve the outcome of the current study: experimental and numerical (CFD) approaches.

3.1 Experimental approach

The experiments are conducted using plastic circular tanks with different sizes to contain the air-water system. Tap water under standard conditions is used throughout all the experiments. Each of these tanks are set up with all the requirements to accomplish the experimental approach.

Supplied air is used to aerate the water in the tank, where the flow rate of the supplied air is split equally by using a T – fitting. Then, each branch of airline will lead to a solenoid valve, which is controlled by a computer – programmable circuit. The control circuit is functioning as an on – off switch to generate the pulsating air flow and control the pulsating time. The experimental set up can be illustrated in Fig 3.1. It consists of the aeration tank, two air diffusers submerged at the bottom of the tank and three oxygen probes. The aeration tanks differ in size, ranging from 400 to 1200 liters. All the aeration tanks have constant diameter of 0.9 m. The dissolved oxygen (DO) probes installed at different elevations of the water tank. These DO probes are used to measure the dissolved oxygen concentration in the water with 1 Hz frequency. They can measure oxygen concentration up to 20 mg/liter within $\pm 2\%$ accuracy.

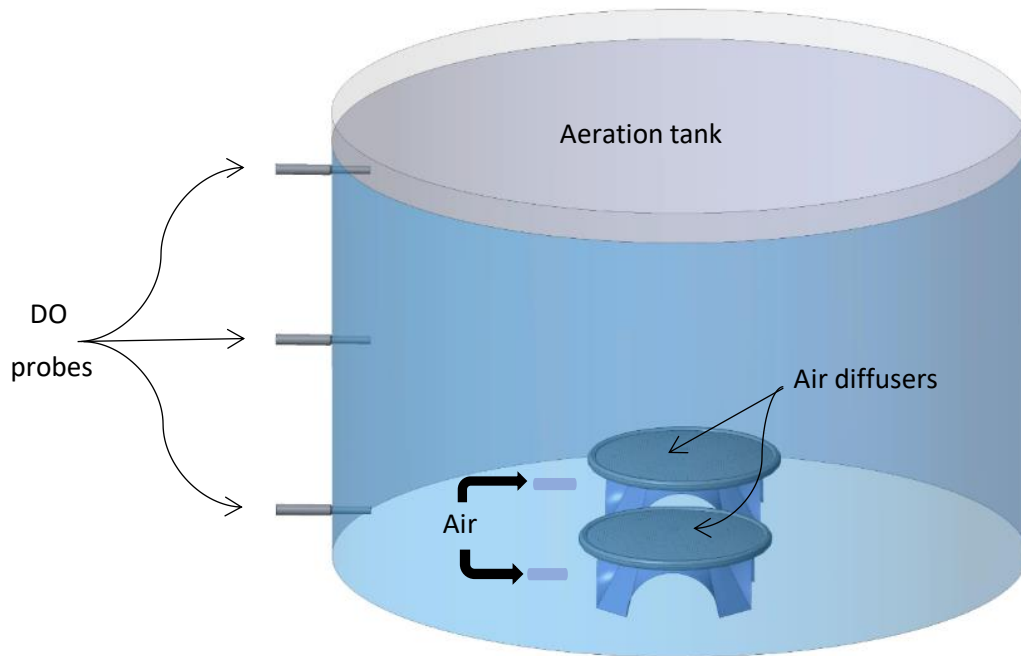


Figure 3.1: Experimental set up

The two diffusers submerged at the bottom of the water tank shown in Fig. 3.1 are used to diffuse the air into the water tank by using very fine pores. There are two kinds of set up used in this work as shown in Fig. 3.2 (a) and (b). Set up (a) shows membrane type diffusers, each of these diffusers contains 5000 pores of about 0.3 mm diameter. While set up (b) shows another type of diffusers called disk or porous diffusers. Both types are considered fine pore diffusers, and that makes them very efficient in the oxygen transfer rate, because fine pores generate fine bubbles, which means higher interface area. This leads to the fact that the oxygen transfer rate will increase since it is proportional to the interface or bubbles surface area.



Figure 3.2: Air diffusers; (a) Membrane, (b) Porous

3.2 Theory for the experimental approach

To obtain the transfer parameters, the volumetric mass transfer coefficient (K_{La}) should be determined first. This can be done by measuring the dissolved oxygen concentration in the aeration tank to obtain the time evolution of the dissolved oxygen concentration in the water. When measuring the dissolved oxygen concentration in the water, measurements should start with zero oxygen water, this means that the oxygen should be removed from the water before starting the experimental measurements. By adding sodium sulfite (Na_2SO_3) to the water, the later will react and converted to sodium sulfate (Na_2SO_4) leaving water with zero oxygen. An illustration of the degassing of water can be shown in figure 3.3. The use of Sodium Sulfite will affect the properties of the system (viscosity and surface tension) which can decrease the oxygen diffusion in water (Matthew McCartney, 2008). The viscosity and surface tension of the dispersed bubbles can be included by Schmidt and Weber numbers as:

$$SC = \frac{v}{D_{ji}} \quad (3.1)$$

$$We = \frac{\rho U^2 d_j}{\sigma} \quad (3.2)$$

However, in wastewater treatment plants which is the real case, there are different salts existing in wastewater. Typically, 200 to 300 mg/liter of salinity is added to the wastewater from city usage (Matthew McCartney, 2008). Adding the Sodium Sulfite can increase the water salinity to 100 mg/liter. Therefore, using sodium sulfite with water is considered closer to the real case than using tap water only.

Another degassing method can be used by applying vacuum to the air-water system. This method is based on Dalton's law, which states that the total pressure of the gas is equal to the sum of the partial pressure of the components that form this gas or can be given from the following equation:

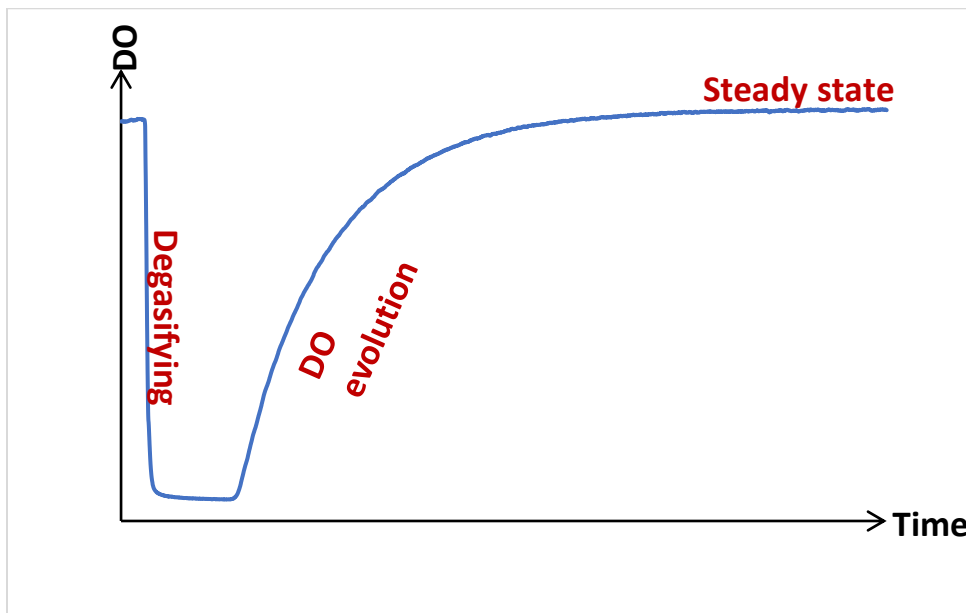


Figure 3.3: Dissolve oxygen concentration variation with time

$$P_{g_{tot}} = P_{g_1} + P_{g_2} + \dots + P_{g_n} \quad 3.3$$

For this case, the air is diffused into the water and since air is consisting of oxygen and nitrogen, then decreasing the air pressure to vacuum or zero absolute pressure will decrease the dissolved oxygen pressure to zero.

Then from the Henry's law, which states that the dissolved oxygen in the water is proportional to its partial pressure according to equation 3.4, the dissolved oxygen concentration of the oxygen in the water will decrease when the total pressure of the air decreases.

$$C_g = P_g / H \quad 3.4$$

The experimental set up for this method consists of a vacuum container with multiple holes as shown in figure 3.4. The water will enter this container through a 1.5 mm diameter nozzle; this small size nozzle is necessary to create small water droplets which will be more efficient in extracting the dissolved oxygen from the water under vacuum conditions.

This system was tested successfully, and it was able to really bring the dissolved oxygen concentration (DO) to a very low levels as can be shown in Fig. 3.5.

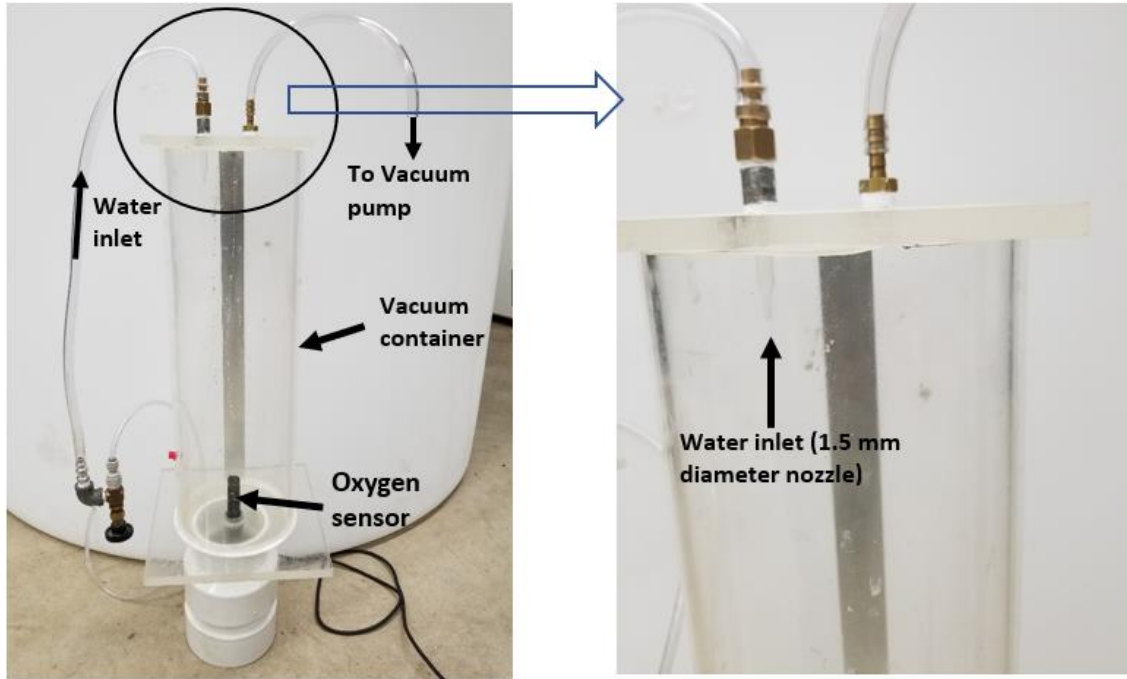


Figure 3.4: Vacuum degasification set up

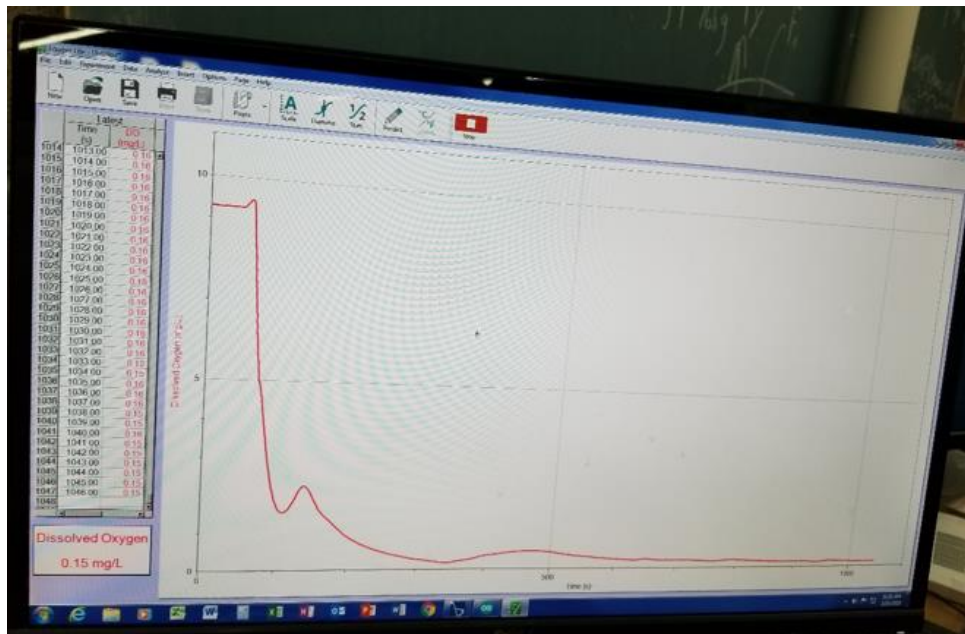


Figure 3.5: Data collection of the DO

The vacuum degasification is very interesting method since it employs no chemicals. However, the setup explained above is used for small scale system with very small flow rates (around 1 liter/h) which cannot be implemented for full scale aeration systems because it requires to transfer the water from small container to a full-scale tank. During this transfer process, the water will gain pressure and so as the oxygen dissolved in the water, which cause the oxygen concentration to rise again. To apply this method to a full-scale aeration system, higher capacity equipment should be used. Therefore, this system can be used a reference to future studies involving degassing methods using vacuum systems.

The degree of oxygen transfer process will be related to the transfer area and the extent of the diffusion process in the aeration tank, which can be determined by considering the mass flux of the oxygen is proportional to the difference of its concentration between the initial and steady state concentrations multiplied by the local mass transfer coefficient and the transfer area:

$$N = K_L A_j (C g_{\infty} - C g_{in}) \quad (3.5)$$

If we consider the bubble as the control volume, applying a mass balance will lead to:

$$V_j dC g / dt = N \quad (3.6)$$

Equating 3.5 and 3.6 to yield:

$$V_j dC g / dt = K_L A_j (C g_{\infty} - C g_{in}) \quad (3.7)$$

It is not easy, experimentally or theoretically, to determine the surface area of the bubble (A_b); therefore, it is more convenient to write $K_L A_j$ in equation 3.7 in terms of the volumetric mass transfer coefficient. This can be done from dividing equation 3.7 by V_j , and considering the overall volumetric mass coefficient ($K_L a$) resulting:

$$dC_g / dt = K_L a (C_{g\infty} - C_{g_{in}}) \quad (3.8)$$

For this case, the overall volumetric mass transfer coefficient ($K_L a$) can be determined by re – arranging and integrating equation 3.8. Thus, it can be obtained from:

$$K_L a = \frac{\ln((C_{g\infty} - C_{g_1}) / (C_{g\infty} - C_{g_2}))}{t} \quad (3.9)$$

Equation 3.9 is only used for the region between $C_{g_1} = 0.2 C_{g\infty}$ and $C_{g_2} = 0.8 C_{g\infty}$, where the trend of the time evolution of the oxygen concentration can be approximated to linear.

Then, the oxygen transfer rate (OTR) can be obtained from equation 3.10, where:

$$OTR = K_L a V (C_{g\infty} - C_{g_{in}}) \quad (3.10)$$

The oxygen transfer rate is very important because it shows how rapid the oxygen is transferred from the air to the water through the air bubble and it is depending on the overall volumetric mass transfer coefficient, the volume of the water in the aeration tank, and the oxygen concentration difference. Nonetheless, the oxygen transfer rate doesn't indicate the efficiency of the oxygen transfer in the system. In order to pinpoint that, another transfer parameter should be determined;

that is the oxygen transfer efficiency (OTE), which can be obtained from dividing OTR on the oxygen mass flow rate:

$$OTE = OTR/0.21 \dot{m}_{air} \quad (3.11)$$

Usually, measurements of the dissolved oxygen concentration are taken under standard conditions, which include tap water, ambient conditions and zero salinity. Therefore, standard oxygen transfer efficiency (SOTE) will be sought in this case.

The overall heat transfer coefficient given by equation 3.9 is based on the condition that the water temperature is 20 °C. For measurements undergone at different temperatures, equation 3.9 must be corrected using the following equation (ASCE, 1993):

$$K_L a_{20} = K_L a \theta^{(20-T)} \quad (3.12)$$

Where θ is constant and equal to 1.024.

3.3 Numerical approach

When working on the experimental approach, the apparatuses and the experimental set up necessary to complete the experiments and obtain the experimental results are very expensive or results cannot be expanded to include all the desired cases due to zone or equipment limitations. Therefore, at some point, computational fluid dynamics (CFD) approach becomes very necessary to investigate all the cases related to this work. In CFD, the aeration tank is considered as the computational domain where the air bubbles are formed and emerged from air diffusers located at the bottom of the aeration tank.

3.3.1 Volume fraction

The computational domain consists of air and water, which entails to model a two-phase flow, the volume fraction is defined as the volume occupied by each phase. Therefore, it becomes necessary to include the volume fraction in the governing equations of mass and momentum.

The mass conservation equation for each phase will be:

$$\frac{\partial \alpha_i \rho_i}{\partial t} + \nabla \cdot (\alpha_i \rho_i v_i) = 0 \quad (3.13)$$

The momentum conservation equation can be written as:

$$\frac{\partial \alpha_i \rho_i v_i}{\partial t} + \nabla \cdot (\alpha_i \rho_i v_i v_i) = -\nabla(\alpha_i p_i) + \nabla(\alpha_i \tau_i) + M_i + \alpha_i \rho_i g \quad (3.14)$$

Where $\sum_{i=1}^{\infty} \alpha_i = 1$

In addition to that, the source term M in the momentum equation is included in the momentum equation to account for all the hydrostatic forces in the liquid phase due to the bubble formation and dispersion. The definition of these hydrostatic forces plays an important role in predicting the forces exerted by the liquid phase onto the bubble.

3.3.2 Hydrostatic forces

The main forces affecting the bubble flow are the surface tension, lift, and drag; where the lift accounts for the inertial forces due to the interactions between the adjacent bubbles; the drag accounts for the viscous effect of the liquid on the rising bubble. The surface tension force will act

to retain the spherical bubble shape. Therefore, all these forces should be included in the CFD model to define the computational problem accurately.

The drag coefficient can be obtained from equation 2.10 (Tomiyama, Kataoka, Zun, & Sakaguchi, 1998), which is classified according to the degree of contamination or the purity of water. Where tap water is considered contaminated, and carefully distilled water is considered pure, while slightly contaminated water refers to the purity in between. Tap water is used for this current case and therefore C_D can be obtained from:

$$C_D = \max [\min(24/Re(1 + 0.15 Re^{0.687}), 72/Re), 8Eo/3(Eo + 4)] \quad (3.15)$$

Where $Eo = (\rho_i - \rho_j)gl/\sigma$

Also, another correlation is used for determining the drag coefficient for Reynolds number less than 1000. This is obtained from Schiller (Schiller & Naumann, A., 1933):

$$C_D = \frac{24(1 + 0.15Re^{0.687})}{Re} \quad (3.16)$$

Equations 3.15 and 3.16 are both used for comparison, the results were similar. This entails that both equations can be used for the current study. Equation 3.15 can be considered for more general cases since it can be used for any Reynolds number.

The lift coefficient is depending on the Eotvos number, and since the Eotvos number is proportional to the bubble size, then there will be more than one relation to account for each bubble size, and according to the following relations (Tomiyama, Tamai, Zun, & Hosokawa, 2002):

$$C_L = \begin{cases} 0.28 \tanh(0.121 \max[Re, 7.374]) & Eo < 4 \\ 0.00105 Eo^3 - 0.0159 Eo^2 - 0.0204 Eo + 0.474 & 4 \leq Eo \leq 10 \\ -0.27 & Eo > 10 \end{cases} \quad (3.17)$$

The Reynolds number in all the equations above is determined based on the bubble diameter and the slip velocity. This can be given by:

$$Re = \frac{\rho_i (U_i - U_j) d_j}{\mu_i} \quad (3.18)$$

For flow in multiphase mixtures, the slip between the phases introduces additional terms in the transport and momentum equations. Therefore, the slip or characteristic velocity ($U_i - U_j$) is modelled based on the drag coefficient and body forces. The drag coefficient is calculated from equation 3.16 and the body forces are the forces acting at the air – water interface which are calculated based on the gravity and relative motion of the air – water mixture (Khan M. P., 2013).

3.3.3 Henry's law

When the two phases of the system are in equilibrium, there will be no mass transferred from one phase to the other phase. In order for the system to experience interphase mass transfer, the two phases must be in unstable conditions. That means, there should be a difference in the concentration of the solute component between the two phases. This concentration gradient can influence the rate of the interphase mass transfer, the higher the difference the higher mass transfer according to equations 3.6 and 3.10. At all stages of oxygen diffusion process in water, there is a tendency for oxygen to move into the water to achieve equilibrium between the two fluids. The

equilibrium will be achieved faster at the interface but will require more time to be established in the bulk water. When the oxygen concentration in the bulk water reaches a constant value then, equilibrium condition is satisfied in the bulk water. Therefore, it will be necessary to define the equilibrium constant based on the solubility of oxygen in bulk water and its partial pressure in air to determine the degree of the mass transfer process. Since, the air and the water are existed in one system, therefore, gas molecules will transfer from the air to the water, and for this case the linear relation of Henry's law can be used, which states that the gas concentration in the liquid phase is proportional to its partial pressure in the gas phase. For any aeration system, the oxygen transfer is the process we are interesting to observe, where the oxygen will transfer from the air bubbles to the water. Therefore, the solubility can be obtained from:

$$X_{O_2} = P_{O_2}/H_{O_2} \quad (3.19)$$

Where:

H_{O_2} is Henry's law constant and has a value of 4.26×10^9 Pa at 298 K and atmospheric pressure.

X_{O_2} is the concentration of Oxygen in the water, mol O_2 /mol H_2O .

P_{O_2} is the partial pressure of the Oxygen in air (pa).

3.3.4 Mass transfer coefficient

For both experimental and CFD approaches, the mass transfer coefficient plays very important role in any process involving mass transfer between gases and liquids. The mass transfer coefficient can be defined as the resistant the mass experiences as it transfers from the gas phase to the liquid phase through the gas – liquid interface. Since the current case involves the transfer of oxygen molecules from the air to the water, then this gas – liquid interface can be represented by the air bubble.

For the experimental approach, the overall volumetric mass transfer coefficient (K_{La}) was considered instead of the mass transfer coefficient (K_L), which was determined directly from the measurements of the dissolved oxygen concentration in the water, but for the CFD approach, it should be defined according to the flow conditions. One of the key factors affecting the mass transfer coefficient is the agitation intensity in the aeration tank. For this case, the mass transfer coefficient is correlated based on the convection and diffusion effect. This effect can be interpreted in terms of the non - dimensional Sherwood number, then Higbie – Poissonesq correlation (Higbie, 1935) can be used for this case;

$$Sh = 2 + \sqrt{4Re * Sc / \pi} \quad (3.20)$$

The mass transfer coefficient is obtained from:

$$K_L = Sh \frac{D_{ji}}{d_j} \quad (3.21)$$

3.3.5 CFD-Experiment preliminary study

Before adopting any CFD results, it is important to see how accurate these CFD results are. Therefore, results of volume fractions of the air – water bubbly flow were studied using the CFD method as a first step to establish the CFD method for different aeration cases. Since CFD is a prediction tool, it becomes necessary to validate these results from CFD with the actual or the experimental case. The experimental set up used for this study is the same one shown in figure 3.1, which consists of a tank filled with water and there are two diffusers to diffuse the air in a pulsating order. High speed camera with 2000 frames per second speed was used to capture the rise of

bubbles plume in the water. In order to accurately model the same experimental case in CFD, it requires to mesh each membrane punch in the aeration diffusers individually. Since, there are 5000 punches for each of the two diffusers, it will be very difficult to reach an accurate solution because it requires too much meshing, hence too much computation time. Therefore, the assumption of treating each air diffusers as porous media will be necessary, since it will model the same diffusers with the same scales used in the experimental case without the requirement for meshing individual punches. The porous media model is very useful tool for cases that experience too much computation time because it requires too much meshing. This model can be used for different applications such as filters, membranes, porous plates and tube banks. When using porous media model, the pressure drop experienced by the fluid as it flows through the porous media becomes very important, because this pressure drop will predict the inertial and viscous coefficients. These coefficients need to be added as scalars to create an additional momentum source tensor term in the momentum equation. The pressure drop can be either measured by conducting experimental work or using a theoretical correlation. For the current case, Darcy – Weisbach relation is used which can be given by:

$$\frac{\Delta P}{L} = \frac{32\mu V}{D^2} \quad (3.22)$$

Figures 3.6 and 3.7 show the bubbles upward flow in the water for both experimental and CFD cases at 0.5 and 1 second physical time. A comparison of the bubbles average rising velocity between the two cases shows that the CFD average velocity is less at 0.5 second, then it becomes higher at 1 second. This could be attributed to the mesh resolution, because the mesh size is large compared to the bubbles size. To bring the discretized cells size down to the bubble size, it requires

very fine mesh which cause very high computation time. Therefore, there will be more room to better rendering the CFD average velocity and bring it closer to the bubble average velocity acquired from the experimental case.

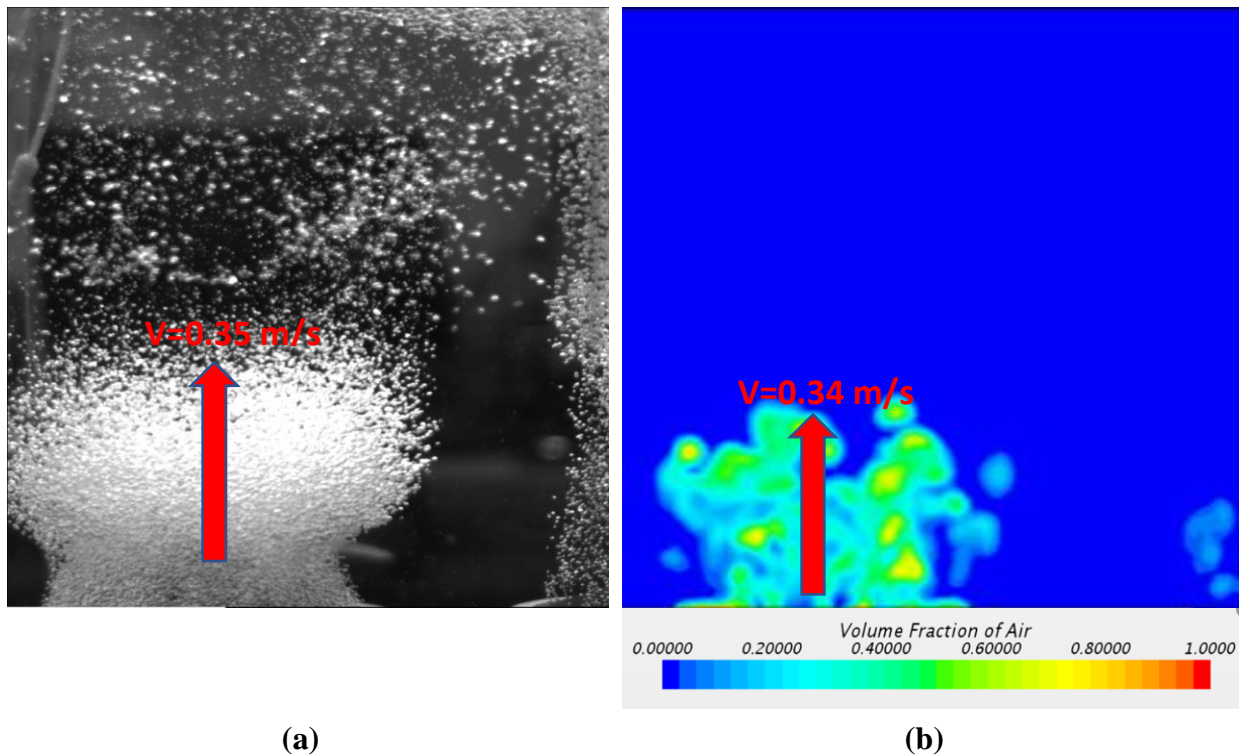


Figure 3.6: Bubbles average rising velocity at 0.5 second; a) Experiment, b) CFD

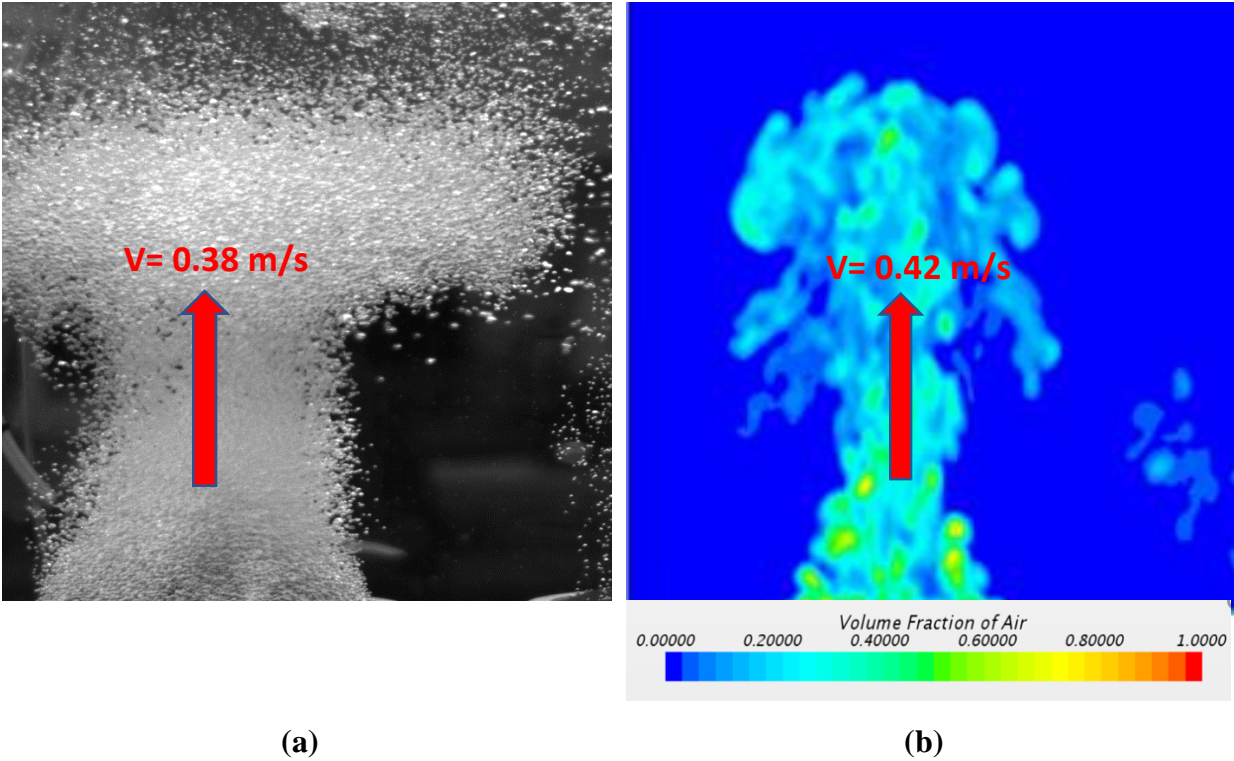


Figure 3.7: Bubbles average rising velocity at 1 second; a) Experiment, b) CFD

3.4 Use of image processing technique

Another approach to compare and validate the CFD results with the experimental results by using image processing is considered. This approach was performed by creating a MATLAB code to determine the fraction of the air bubbles for both CFD and experiment. Four cases were considered here based on the physical time. These cases were 0.5, 1, 1.5, and 2 seconds. Figures 3.8 to 3.11 show the results obtained from the image processing of the physical time cases discussed here. By comparison, it was found that the difference in the density of bubbles in experiment is greater than CFD. This difference can be as low as 6% for the 1 second cases and as high as 34% for the 2 seconds case. This high difference for some of the cases could be the results

of mesh resolution, and also, the MATLAB code was not very successful to separate some of the unwanted noise in the pictures which can be clearly noted in the 1.5 and 2 seconds.

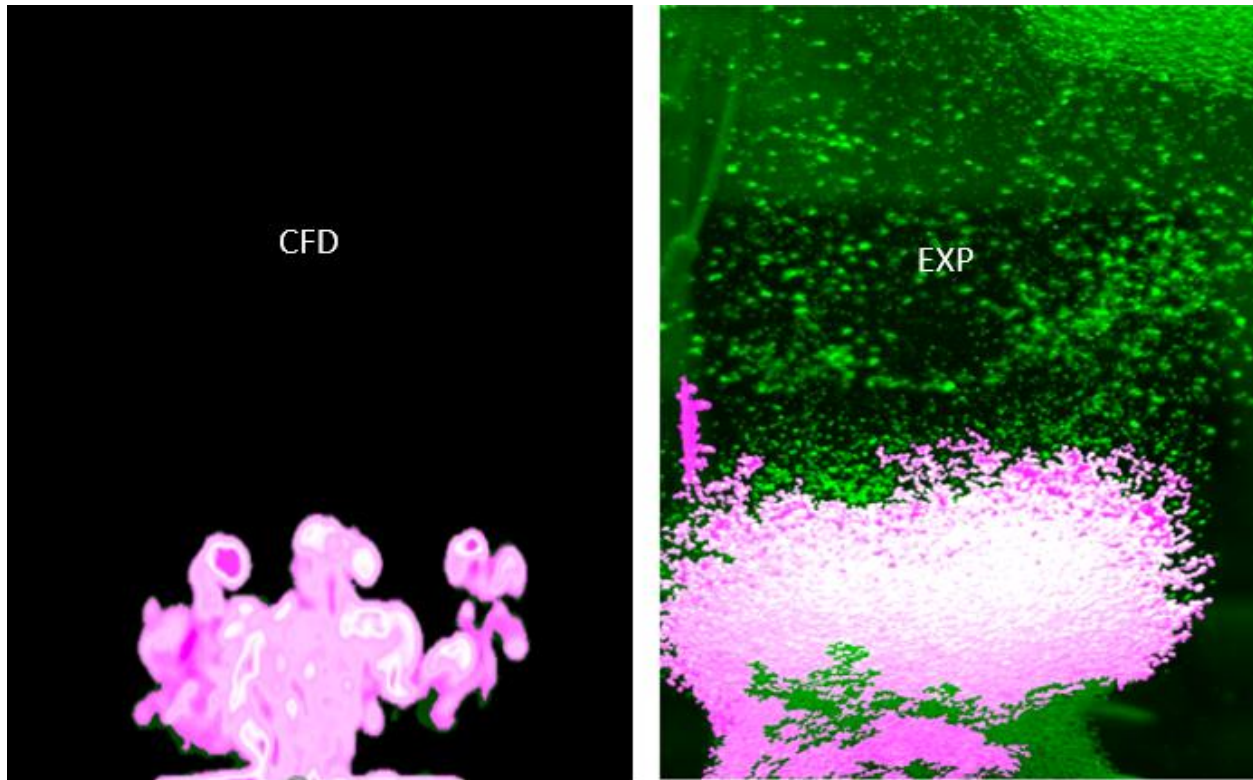


Figure 3.8: images processed for CFD and experiment cases at 0.5 second physical time

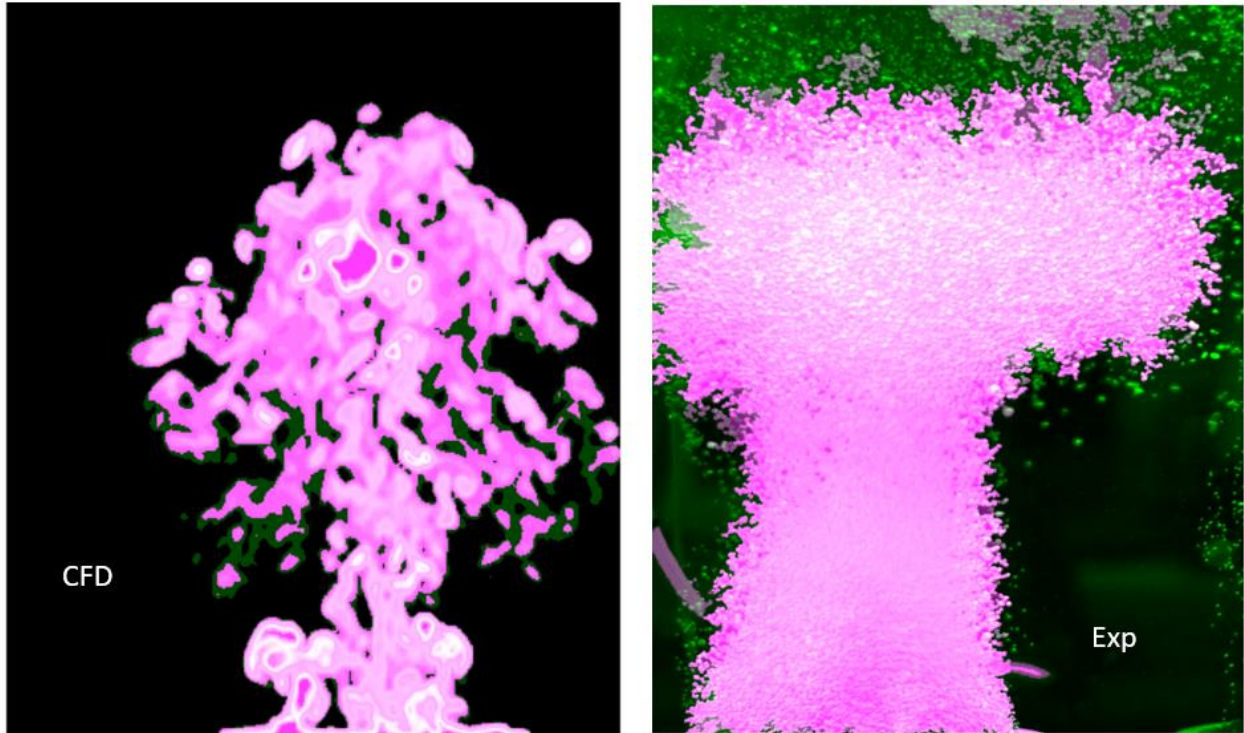


Figure 3.9: images processed for CFD and experiment cases at 1 second physical time

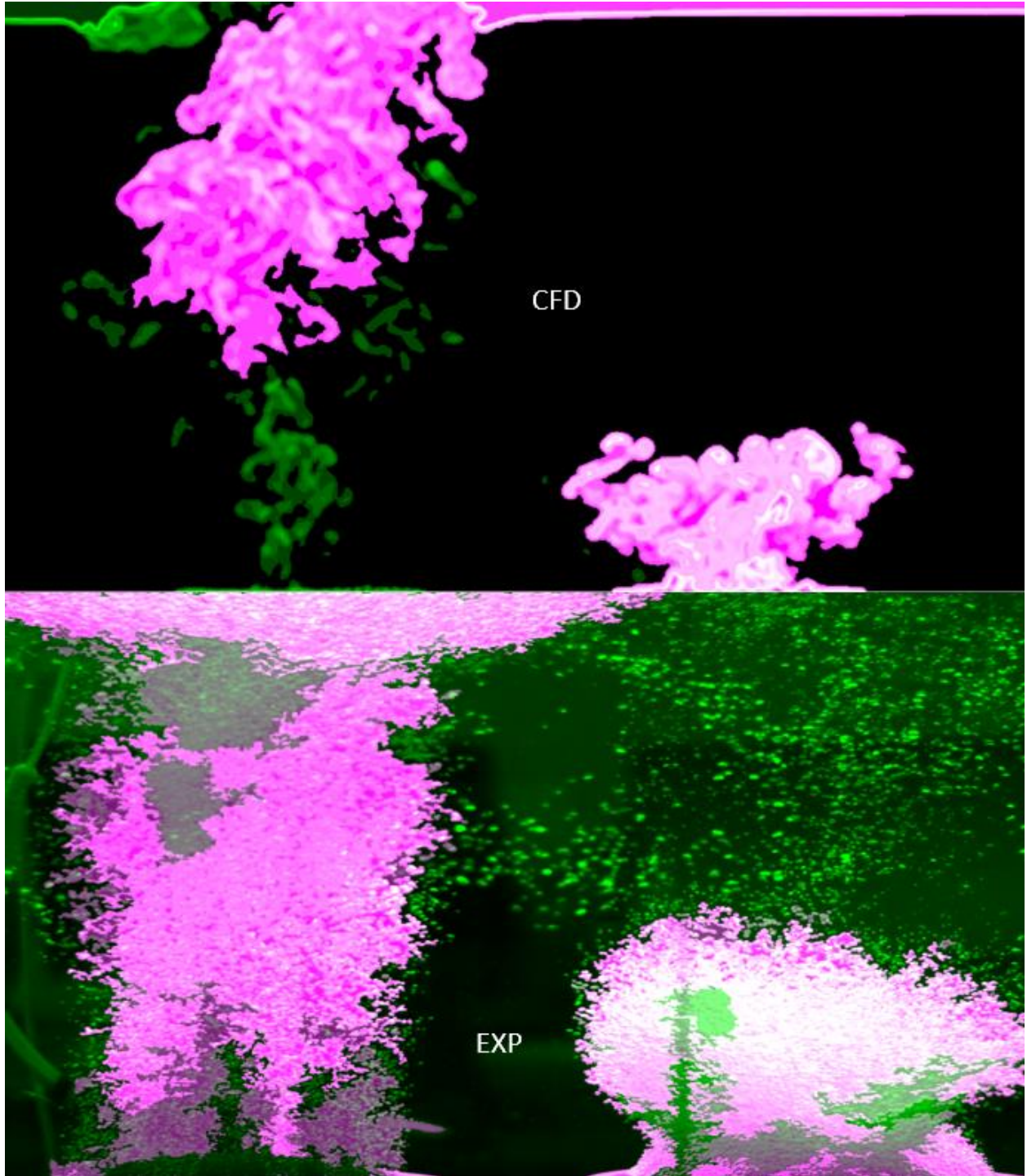


Figure 3.10: images processed for CFD and experiment cases at 1.5 second physical time

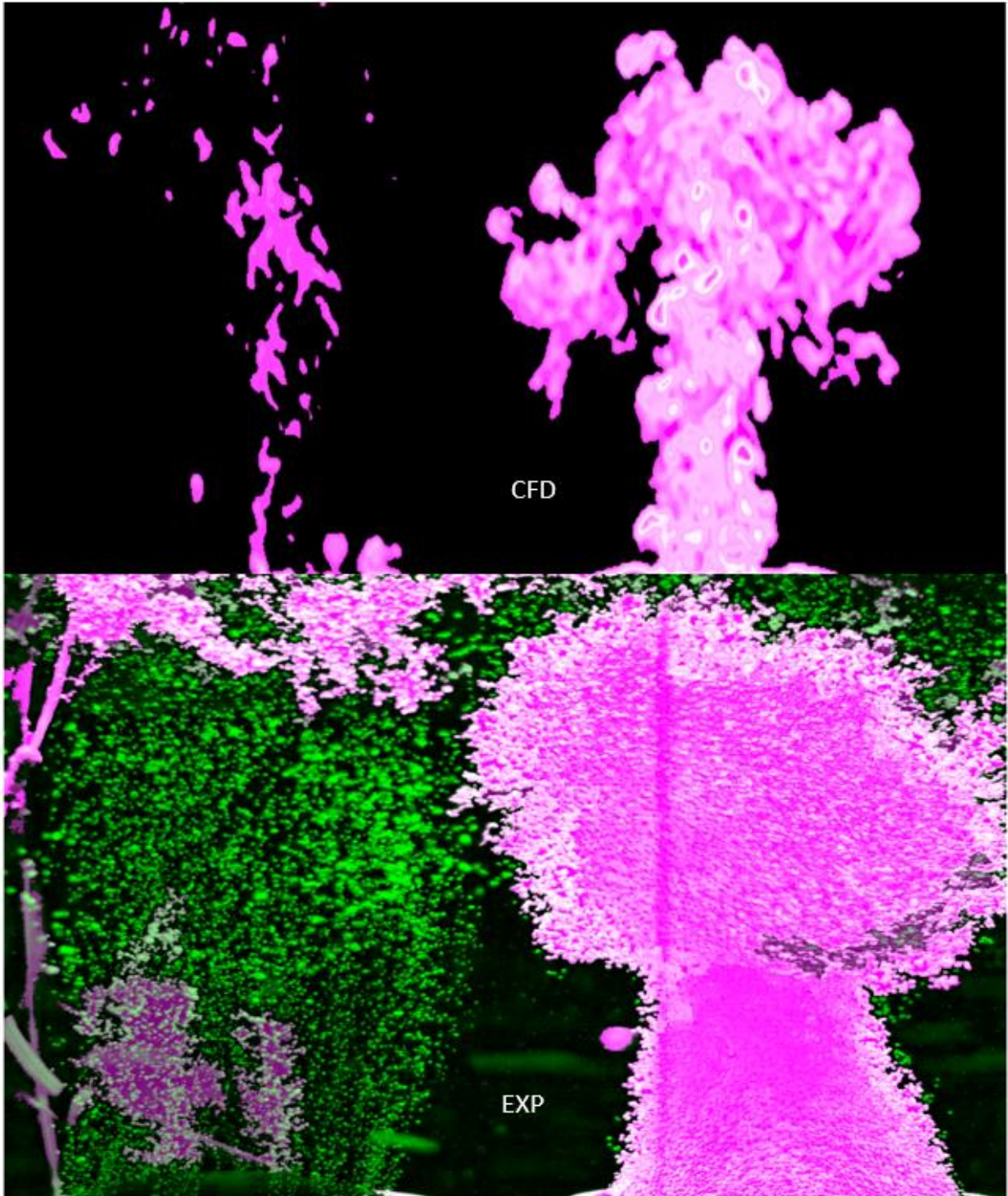


Figure 3.11: images processed for CFD and experiment cases at 2 second physical time

4. Experimental studies on aeration

Several experimental studies were conducted to see the impact on the aeration efficiency. These studies involve setting up aeration systems and perform experimental measurements to measure the oxygen dissolved in the water and determine the oxygen transfer rate from these measurements. Most of the experimental measurements are conducted based on the methodology discussed in chapter 3.

4.1 Aeration study using pulsating air flow

This work is based on the fact that creating more mixing within the aeration tank can improve the rate of oxygen transfer from inside the air bubble to the water surrounding the bubble (Dani, Guiraud, & Cockx, 2007). The experimental set up for this work can be illustrated by figure 4.1.

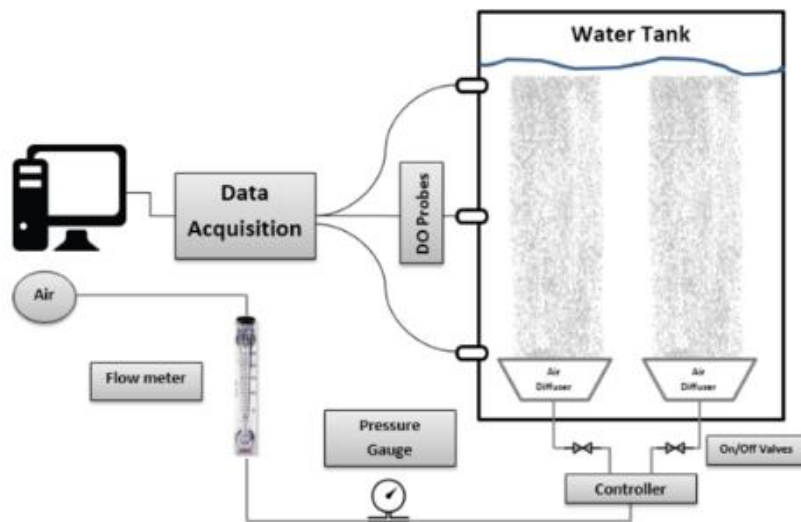


Figure 4.1: System set up

New air diffusion method (pulsating) through submerged diffusers (Alkhalidi, Alba'ba'a, & Amano, 2016) was found to be effective in improving the oxygen transfer efficiency. This technique can be applied by supplying the air to the two aeration diffusers used for this case alternatively. This is accomplished by using a programmable control circuit (figure 4.2), where the time that is set for the supplied air to flow into any of the two diffusers can be controlled by using the programmable control circuit.

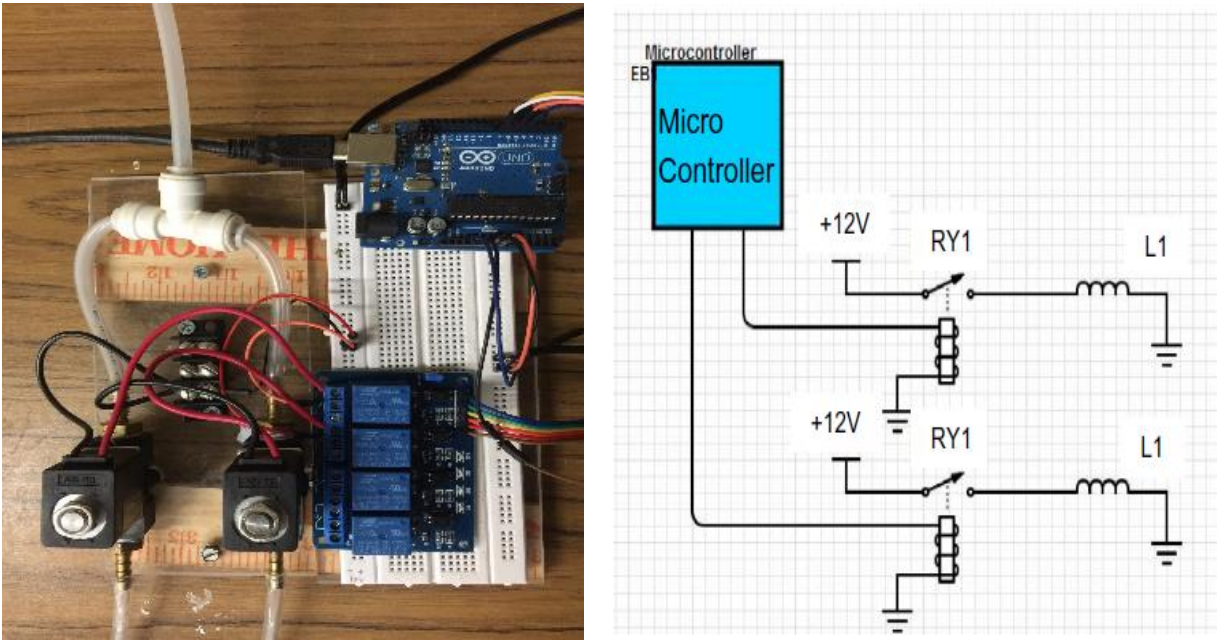


Figure 4.2: Control circuit

A ratio parameter between airflow to tank size, called Amano Alkhafaji Alkhalidi (AAA), see equation 4.1, is introduced for best data rendering.

$$AAA = 4Q / (\pi D^2 H) \quad (4.1)$$

The results of the SOTE were mainly obtained for air flow rate ranges from 14 to 70 L/min and the water column height is 0.64 m. The air was diffused into the water tank by using continuous

and pulsating air flow. Therefore, the results were also obtained for both cases of continuous and pulsating air flow.

Figure 4.3 shows the results of the standard oxygen transfer efficiency (SOTE) for both pulsating and continuous air flow. Four different cases were considered, which are continuous, 0.5, 1.5, and 2.5 seconds pulsating time, for values of AAA ranging between 0.03 – 0.16 min^{-1} .

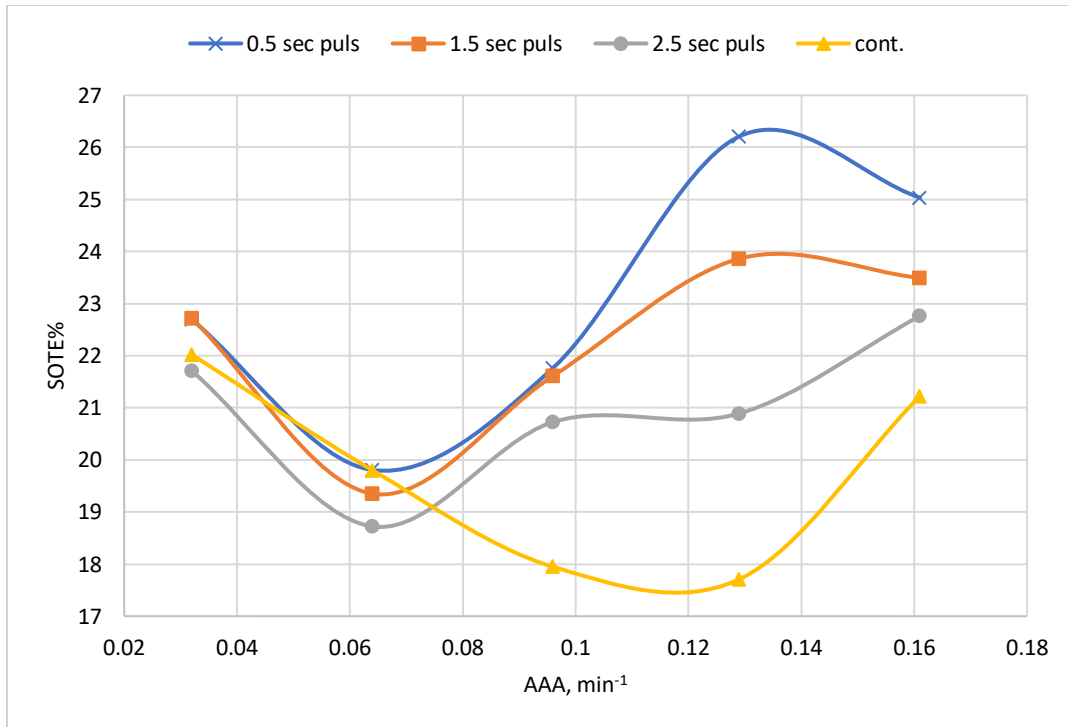


Figure 4.3: SOTE % variation with AAA

Figure 4.4 shows the normalized SOTE results, i.e., it represents the Standard oxygen transfer efficiency of the pulsating flow of the 0.5, 1.5, 2.5 seconds to that of the continuous flow when the flow rates ranges between 14 to 70 L/min, such that the range of the parameter AAA will be from 0.03 to 0.16 min^{-1} .

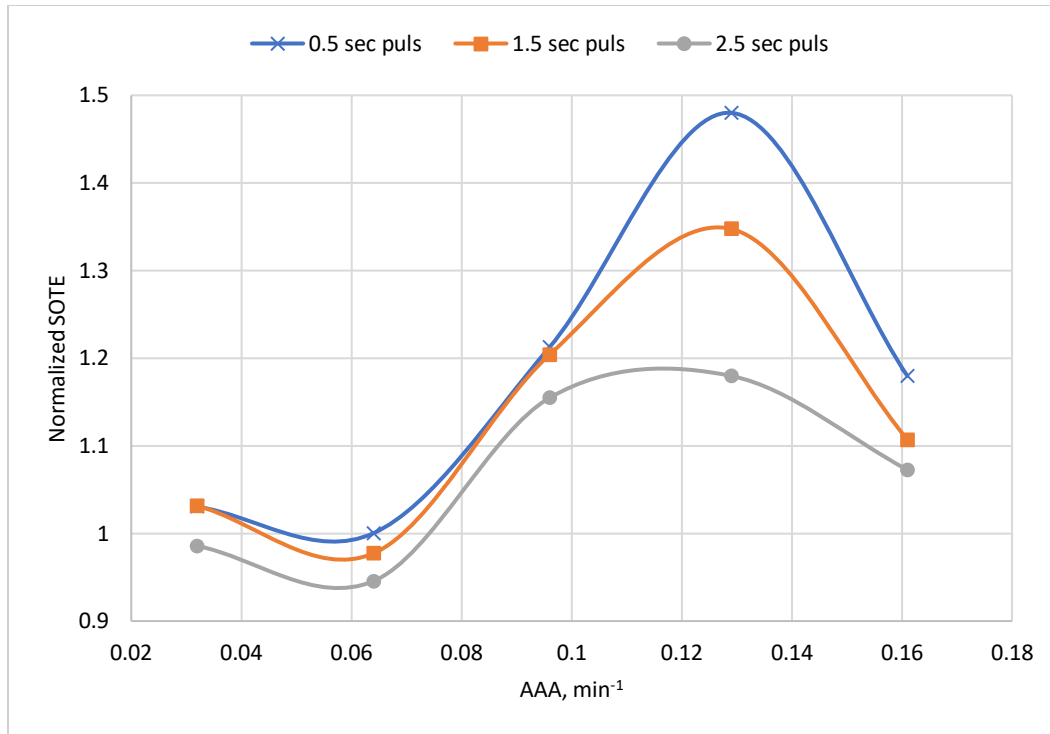


Figure 4.4: Normalized SOTE variation with AAA

The results of the standard oxygen transfer efficiency (SOTE) for pulsating air flow were clearly better than that of continuous air flow for both water column heights.

It can be seen from figures 4.3 and 4.4 that all the cases show similar behavior when the parameter AAA ranges from about 0.03 to 0.07 min⁻¹. All the pulsating flow cases start trending better than the continuous or the non – pulsating flow case beyond 0.07 min⁻¹. Also, it can be seen that the maximum SOTE is found at approximately 0.13 min⁻¹ (42 L/min), when the pulsating time is 0.5 seconds. Generally, the best results of the SOTE can be obtained when the pulsating time is 0.5 seconds.

4.1.1 Conclusions

Normal operation of aeration systems involves diffusing the air from the submerged diffusers continuously (non-pulsating). Standard oxygen transfer efficiency (SOTE) results of

pulsating air flow were obtained and compared with that of continuous air flow. It is concluded from the results obtained that the SOTE of pulsating flow is better than that of continuous air flow, considering a water column height of $H= 0.64$ m.

A parameter (AAA) was introduced to this work for better rendering of the results when considering more air flow rates and water volumes, or water column heights, since air flow and water volume are included within this parameter.

The effect of pulsating air flow starts to show up after AAA around 0.07 min^{-1} , and reaches maximum at 0.13 min^{-1} , particularly for the case of 0.5 seconds pulsating time, at which the SOTE is significantly more than that of continuous flow, about 50% more. When AAA starts increasing beyond 0.13 min^{-1} , the effect of pulsating air flow seems to diminish and pulsating air flow results tend to approach the continuous air flow results. This entails the conclusion that, at certain high flow rate, it is expected that pulsating and continuous air flow methods are affecting at a same strength on the SOTE. Therefore, there is no significance from using pulsating air flow method at very higher flow rates.

These improvements in the oxygen transfer efficiency at this water column height when using the pulsating air flow can be utilized in industry to minimize the energy cost of aeration. The increase in aeration efficiency when following this design will help towards decreasing the capacity of the air compressors which will not only reduce the energy cost but also the space required to contain the aeration equipment such as water reservoirs, diffusers and piping.

4.2 Effect of water column height

The effect of water column height on the oxygen transfer efficiency was investigated experimentally in this part. Despite being considered as a complementary part of section 4.1, but this work can point out to several important factors, which will be discussed based on the obtained

results. The experimental system set up and components used for this work is similar to the experimental set up shown in section 4.1, but, in order to achieve the outcome of this study, which is the effect of the water column height on the aeration efficiency, different water column heights should be considered. This means the use of tanks with different sizes but keeping all the tanks at constant diameter.

4.2.1 Effect of water column on the standard oxygen transfer efficiency

The effect of pulsating air flow is based on creating a wavy flow in the aeration tank, which is used similarly as in section 4.1. However, this effect will not be the same, if the water column height is changed. Therefore, the aim of this study is to see how the water column affects the oxygen transfer efficiency when using pulsating air flow. Three water columns heights are considered here, these are 0.6, 1.2 and 1.8 m.

Similar to the work discussed in section 4.1, the results of the standard oxygen transfer efficiency (SOTE) were obtained at different pulsating times and different flow rates. The SOTE is the transfer parameter that reflects the effectiveness of the aeration process. Therefore, the goal of the current part is to obtain the SOTE results for each water column at different pulsating times. Three pulsating times are considered; 0.5, 1.5 and 2.5 seconds. Increasing the water column height entails considering higher water tank volumes. On the other hand, increasing the water column height above the air membrane surface requires an increase in the supplied air pressure to overcome the increased hydrostatic pressure. But the flow rate is kept constant for all the cases discussed in this chapter. The AAA parameter, previously defined in section 4.1, will be used again to compare the SOTE results for different water column heights in the first part of the results discussed in this section (figures 4.5 to 4.7). The second part (figures 4.8 to 4.10) relates the SOTE to the flow rate at different pulsating times.

First, the SOTE investigation was carried out for each water column at different pulsating times, SOTE results will be compared to different water columns at each pulsating time. Figures 4.5, 4.6, and 4.7 show the SOTE variation with AAA for 0.6, 1.2 and 1.8 m water columns respectively.

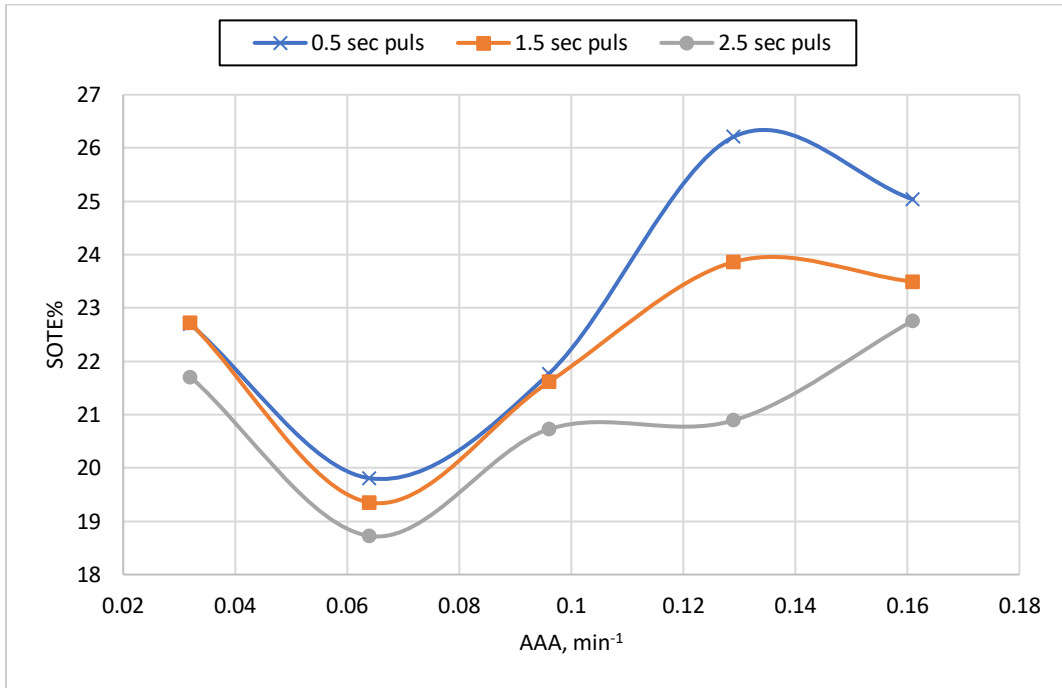


Figure 4.5: SOTE variation with AAA parameter for 0.6 m water column

Relatively similar behavior for all pulsating times can be noted from figure 4.5, where the SOTE decreases as AAA increases from 0.03 to 0.064 min⁻¹. The SOTE keeps increasing between 0.064 and 0.13 min⁻¹. Beyond 0.13 min⁻¹, the SOTE decreases again for all the pulsating time cases except the 2.5 seconds pulsating time case, where the SOTE increases.

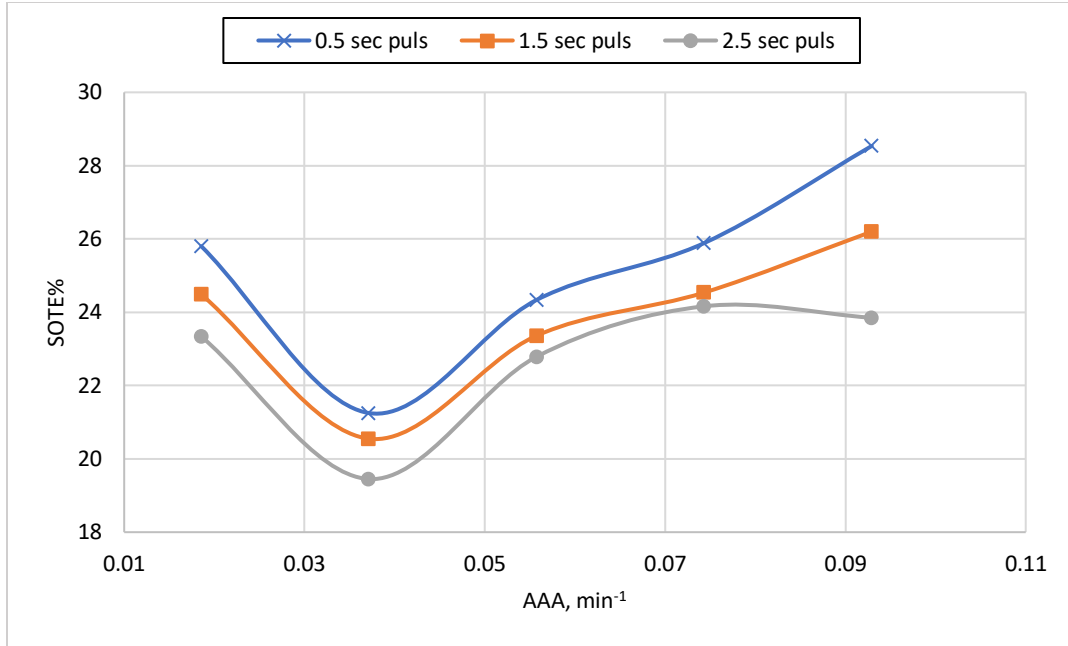


Figure 4.6: SOTE variation with AAA for 1.2 m water column

Figure 4.6 shows the SOTE variation with AAA when the water column equal to 1.2 m. This figure gives similar behavior to that of figure 4.5, except for the region when AAA ranges between 0.074 and 0.093 min⁻¹. The SOTE is increasing for the 0.5 and 1.5 seconds cases, but it decreases for the 2.5 seconds pulsating time.

The last figure to discuss in the first part of the results is figure 4.7, which is the case when the water column is 1.8 m. In this figure, the SOTE follows a similar trend as in figures 4.5 and 4.6 between 0.012 and 0.046 min⁻¹, except the case when the pulsating time is 2.5 seconds. Beyond 0.046 min⁻¹, the SOTE is decreasing for all pulsating times.

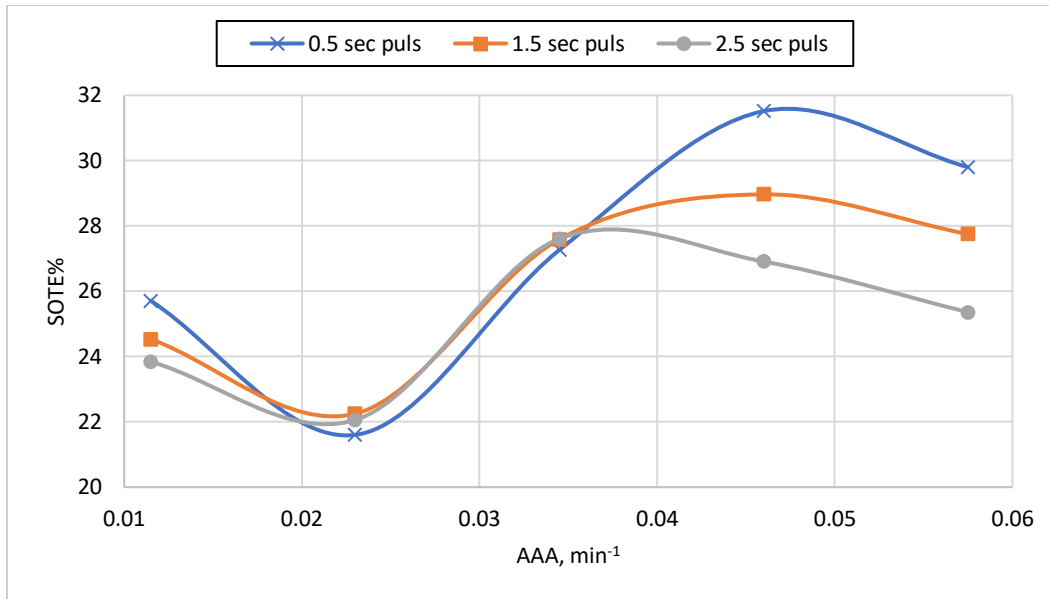


Figure 4.7: SOTE variation with AAA for 1.8 m water column

Figures 4.8, 4.9, and 4.10 show the SOTE variation with flow rate for the three water columns considered here when the pulsating time is 0.5, 1.5, and 2.5 seconds, respectively. When comparing Figures 4.8 through 4.10, they clearly show similar trends when the flow rate increases from 14 to 42 L/min. After that, the SOTE trend tends to be less steep for the higher water column as the pulsating time increases. While, the behavior is opposite for the lower water column. Also, the SOTE drops to minimum at 28 L/min. The same explanation used for the last part is applied here, that is the SOTE is inversely proportional to the oxygen flow rate. Therefore, the SOTE drops at 28 L/min then it experiences a continuous increase due to the enhanced mixing rendered by the increased air flow rate.

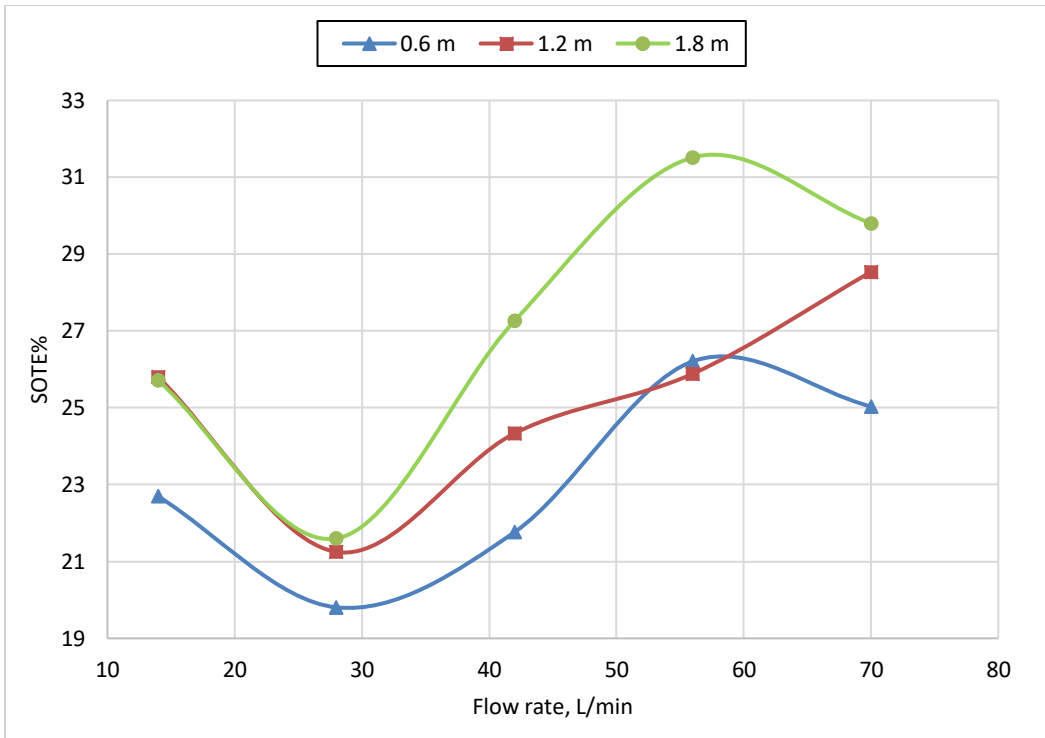


Figure 4.8: SOTE variation with flow rate at 0.5 sec pulsating time

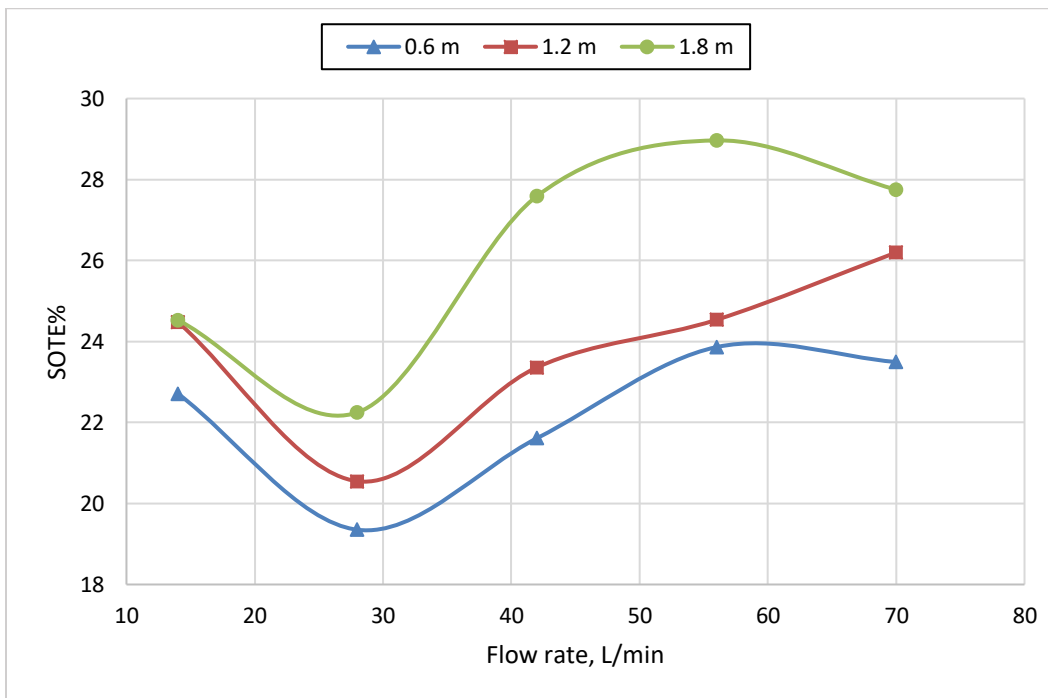


Figure 4.9: SOTE variation with flow rate at 1.5 sec pulsating time

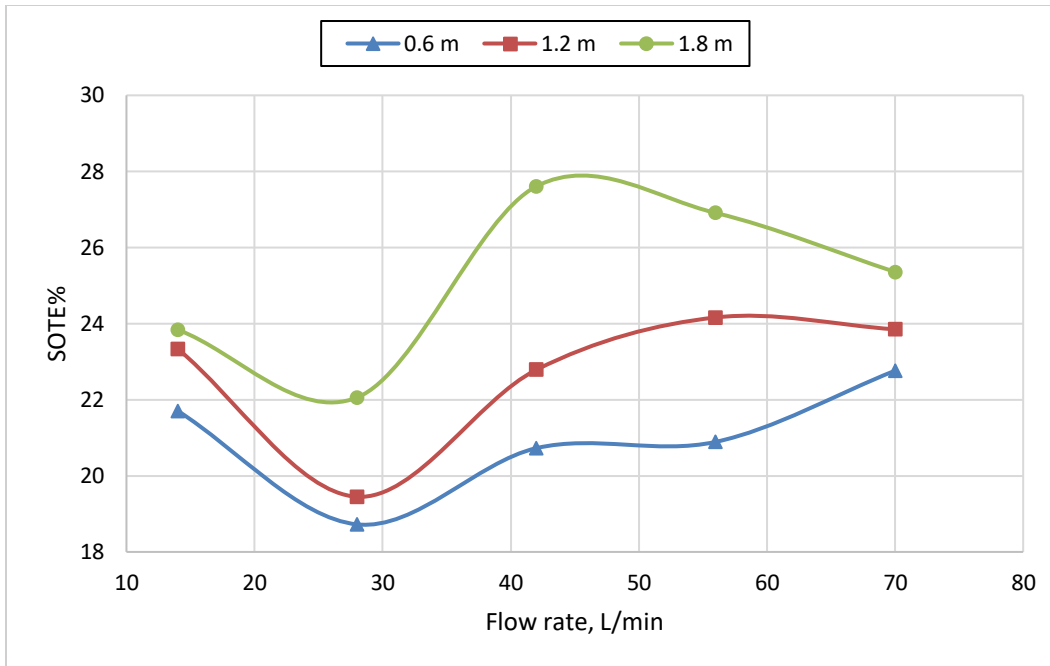


Figure 4.10: SOTE variation with flow rate at 2.5 sec pulsating time

Based on Figures 4.8 through 4.10, it is noted that, the higher SOTE can be considered to occur when using the higher water column (1.8 m). The lowest SOTE is noted when using the lowest water column 0.6 m. However, it is clearly evident from figures 4.8, 4.9, and 4.10 that, the SOTE trend is increasing for the lowest water column while it is decreasing for the highest water column at higher flow rates and vice versa at lower flow rates. This means that the waves created in the lower water column case (0.6 m) can be considered to have a greater effect than those created in the highest water column (1.8 m) at higher flow rates. This behavior is particularly observed when the pulsating time is 2.5 seconds, where all the SOTE results are tending to approach each other. Also, it is noted that, in the case of the 1.2 m water column, the SOTE always represents a median between that of the higher and the lower water column for all ranges of flow rates and at any pulsating time.

SOTE measurements uncertainty analysis was performed for the 1.2 m water column height. The uncertainty of the aforementioned case measurements is ranging between ± 3.9 and ± 0.05 % as shown from figure 4.11 and Table 4.1.

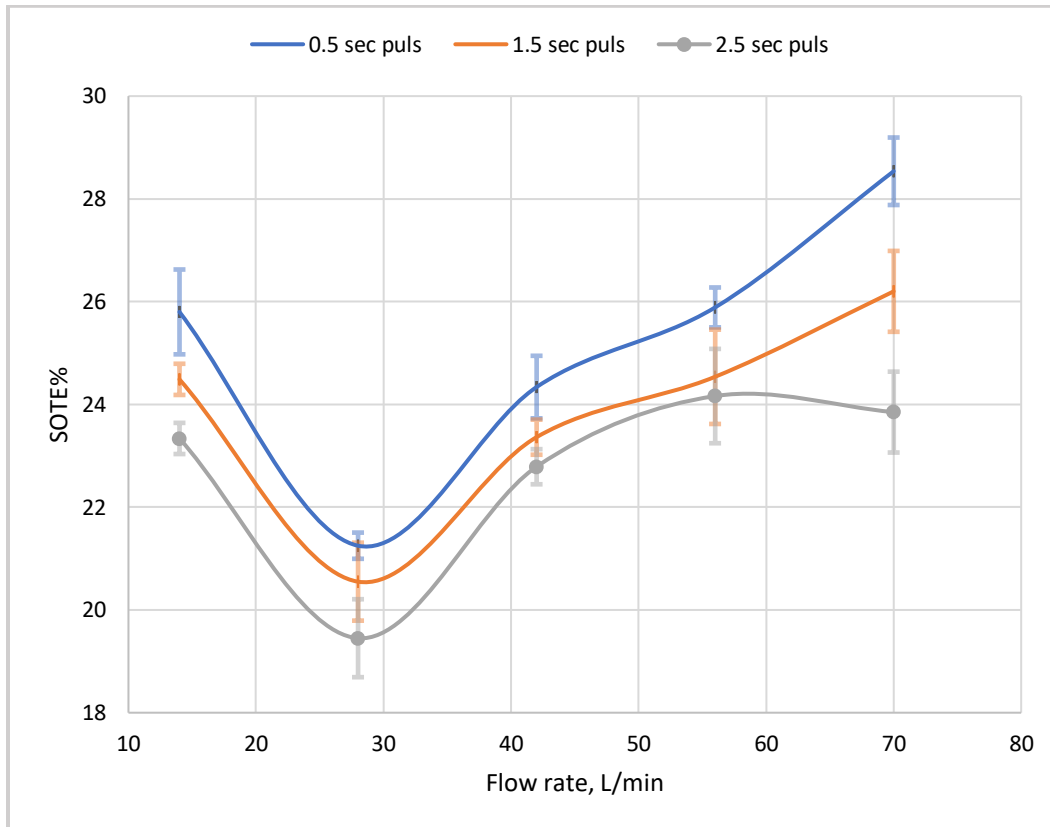


Figure 4.11: Measurement uncertainty of SOTE for the 1.2 m water column

Table 4.1: Measurement uncertainty of SOTE for the 1.2 m water column

		Pulsating time (seconds)		
		0.5	1.5	2.5
Flow rate (L/min)	14	± 0.032	± 0.023	± 0.013
	28	± 0.012	± 0.002	± 0.039
	42	± 0.025	± 0.0005	± 0.015
	56	± 0.015	± 0.035	± 0.038
	70	± 0.023	± 0.021	± 0.033

It was noted that the SOTE results for the 1.8 m water column is the highest among all the water columns. The lowest SOTE results are obtained with the 0.6 m water column. An intermediate behavior is observed when considering the 1.2 m water column. Also, the highest SOTE can be found when the pulsating time is 0.5 seconds, this applies to all the water column cases. The higher SOTE when using the higher water column can be attributed to the rising velocity of the bubbles, which becomes low compared with the lower water column. In this case, the bubbles will stay longer in the water and the oxygen transfer process from the bubble to the water will take longer time. Therefore, better oxygen transfer rate is experienced as the water column becomes higher. On the other hand, another important factor that has been observed to affect the results, particularly for the lower water column, that is the effect of the air flow rate. The SOTE results tend to trend better than that of the higher water column at higher flow rates. Therefore, there can be a better potential for improvement when considering lower water column with higher flow rates.

4.2.2 Conclusions

Investigating the effect of water column height is very important due to its significance in the actual aeration systems and also in altering the rate of oxygen transfer as was shown from the results of standard oxygen transfer efficiency (SOTE), where we can conclude that SOTE results of the 1.8 m water column are the highest among all the water columns. The lowest SOTE results are obtained with the 0.6 m water column. An intermediate behavior is observed when considering the 1.2 m water column. In addition, the highest SOTE can be found when the pulsating time is 0.5 seconds, this applies to all the water column cases. The higher SOTE obtained when using the higher water column can be attributed to the rising velocity of the bubbles, which becomes low compared with the lower water column. In this case, the bubbles will stay longer in the water, and the oxygen transfer process from the bubble to the water will take longer time. Therefore, better oxygen transfer rate is experienced as the water column becomes higher. On the other hand, another important factor that has been observed to affect the results, particularly for the lower water column, that is the effect of the airflow rate. The SOTE results tend to trend better than that of the higher water column at higher flow rates. Therefore, there can be a better potential for improvement when considering lower water column with higher flow rates.

4.3 Froude number

The previous results from section 4.2 showed the tendency for improvement when the water column becomes lower because the surface waves becomes higher. This effect can be discussed generally in terms of the Froude number. Froude number can be defined as the ratio of the inertial to gravitational forces and is given by;

$$Fr = \frac{V}{\sqrt{gH}} \quad (4.1)$$

Figures 4.12 and 4.13 show the height of the wave developed on the water surface which can be used as an illustration for the relationship between Froude number and the height of the surface waves. The experimental correlation given by (Chow, 1959) can be used for the current case. This equation correlates the ratio of the depth of the surface wave to the depth of the water surface or water column to the Froude number according to:

$$\frac{H_2}{H_1} = \frac{\sqrt{1 + 8Fr} - 1}{2} \tag{4.2}$$

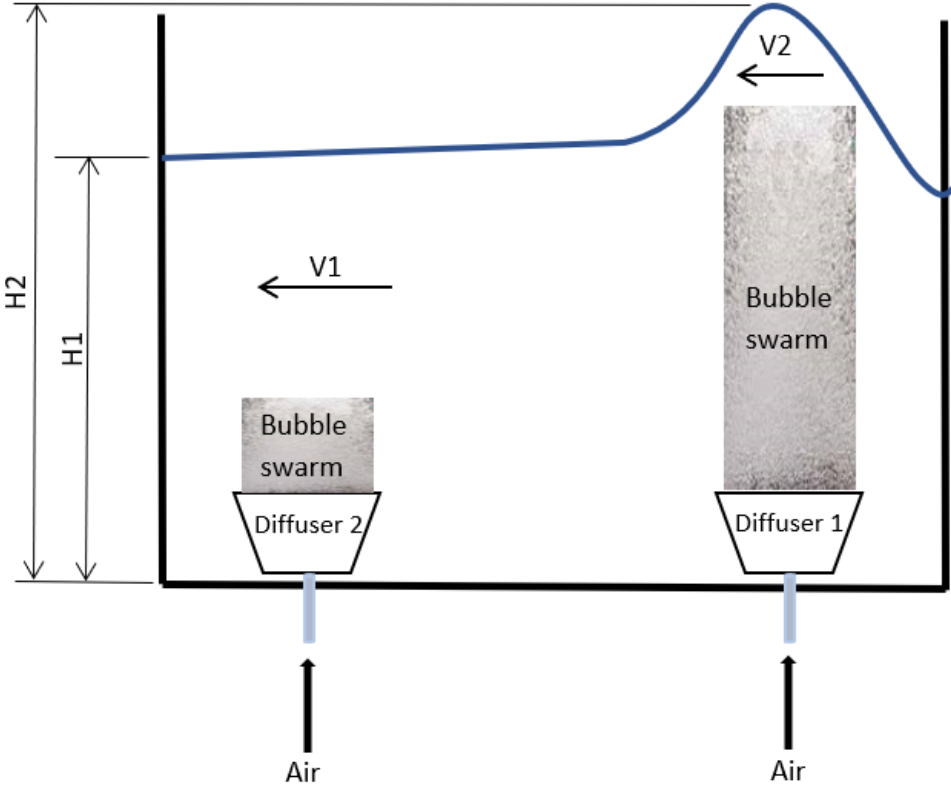


Figure 4.12: Schematic illustration of waves (pulsating flow)

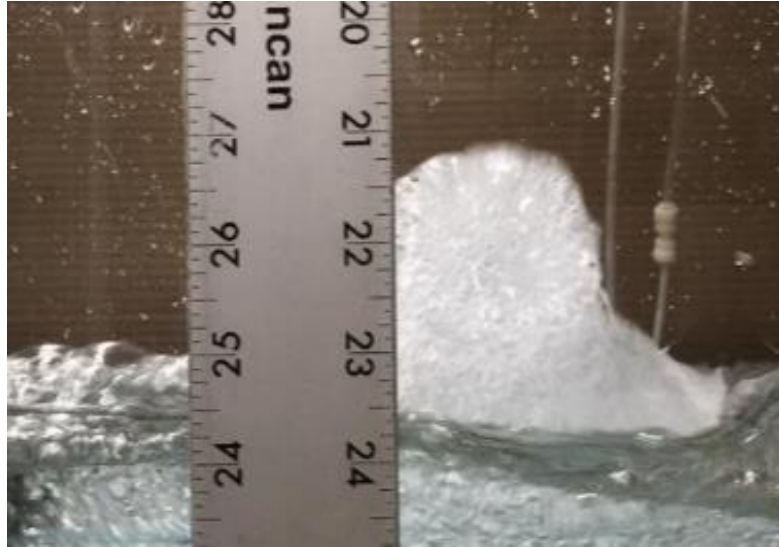


Figure 4.13: Surface wave with 1.14 Froude number

After applying equation 4.2 to the surface waves generated for each of the water column height cases discussed in section 4.2, the values of Froude number are 1.14, 1.06 and 1.02 for the 0.6, 1.2, 1.8 m respectively, as shown in figure 4.14.

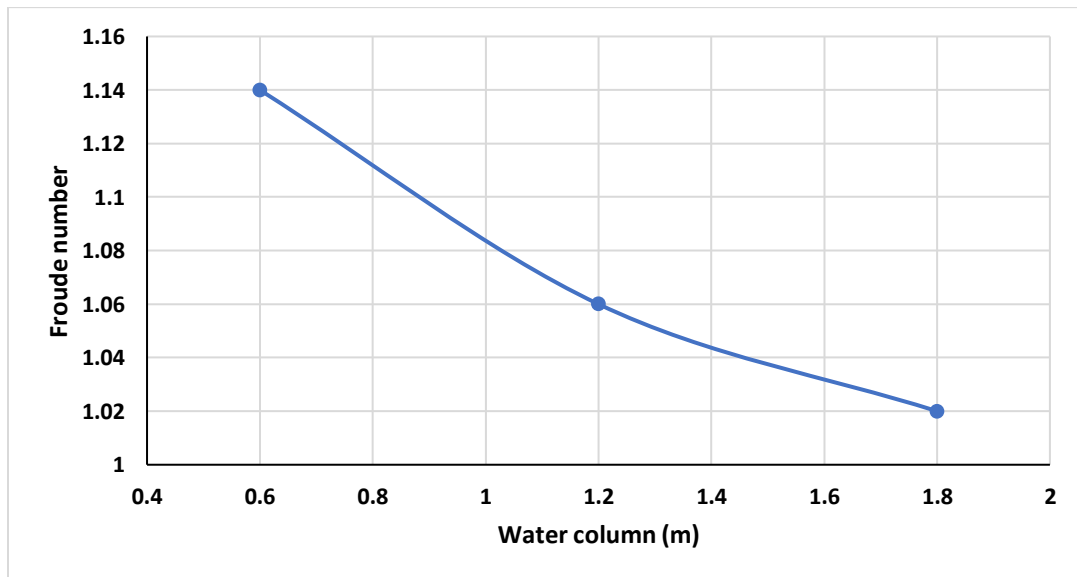


Figure 4.14: Froude number vs water column

4.4 Aeration from ceramic diffusers and comparison with membrane diffusers

Some wastewater treatment plants are using porous materials instead of rubber membranes to diffuse the air to the wastewater. Ceramic diffusers which are made of porous materials have the advantage of generating very fine bubbles. Since the energy crisis in 1970s, interests in fine pore diffusers have been increased due to the high oxygen transfer efficiency obtained when pores diameter is decreased.

In the current section, ceramic discs are used instead of the rubber membranes that have been used in the previous sections. The diameter of each disc is the same as that of the rubber membrane, but these are made of porous material and therefore they have very fine pores which are even finer than rubber membrane pores.

Different water columns are considered here. In addition to the SOTE results, standard aeration efficiency (SAE) results will also be obtained since using different diffusers can affect the pressure drop across the diffuser which in turn affect the aeration efficiency.

When comparing between the two diffusers types considered here, we are considering several factors such as flow rate, water column, pulsating time, and dynamic wet pressure. The porosity and permeability were not available at the time of conducting this study. Communications were conducted with one of the largest distributors of diffusion systems (Xylem) to provide the permeability and porosity but these were not available because the dynamic wet pressure (DWP) is more important in industry, since it can gives the difference in pressure drop between aeration diffusers. Therefore, this comparison can be performed to reflect the industrial necessity for evaluating two diffusion systems to see which one is more efficient based on the SOTE and SAE results. The provided DWP from Xylem was used in this study as the parameter that is used as a

measure for pressure drop, which will be reflected in the SAE results as it will be shown in the SAE results.

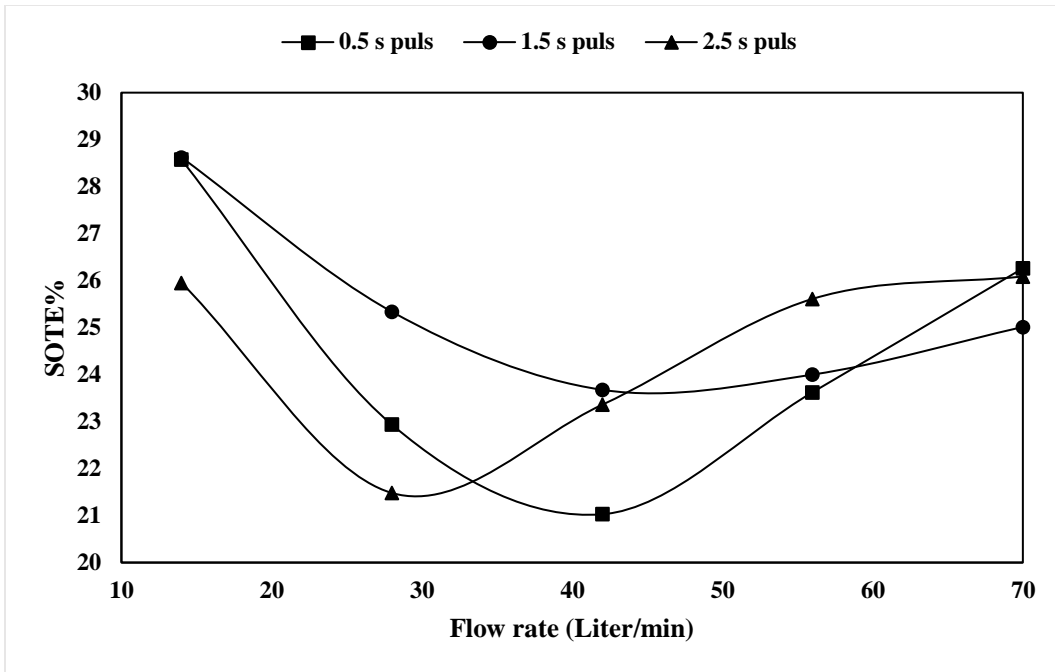
In addition to that, the SOTE results of the ceramic diffusers were presented too, to show the effect of pulsating time and water column on the SOTE.

4.4.1 Standard oxygen transfer efficiency

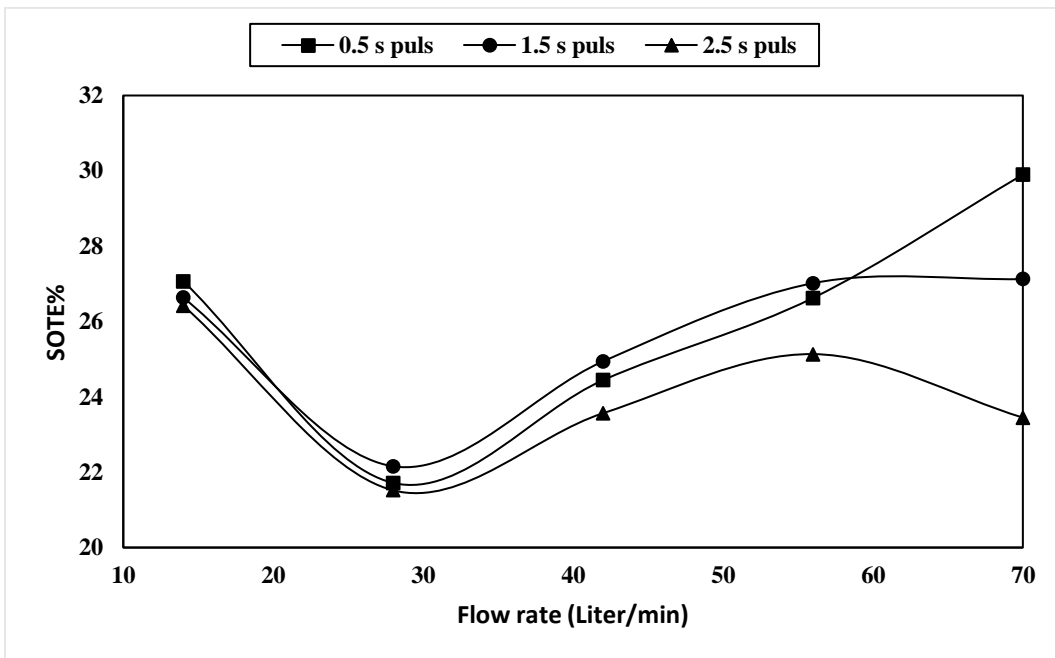
Similar to the rubber membrane diffusers discussed in previous sections, experimental measurements are conducted to find the standard oxygen transfer efficiency (SOTE) by using the same methodology discussed in chapter 3.

Results of the SOTE were obtained for the ceramic disc diffusers and compared with the previously obtained results of the membrane diffusers.

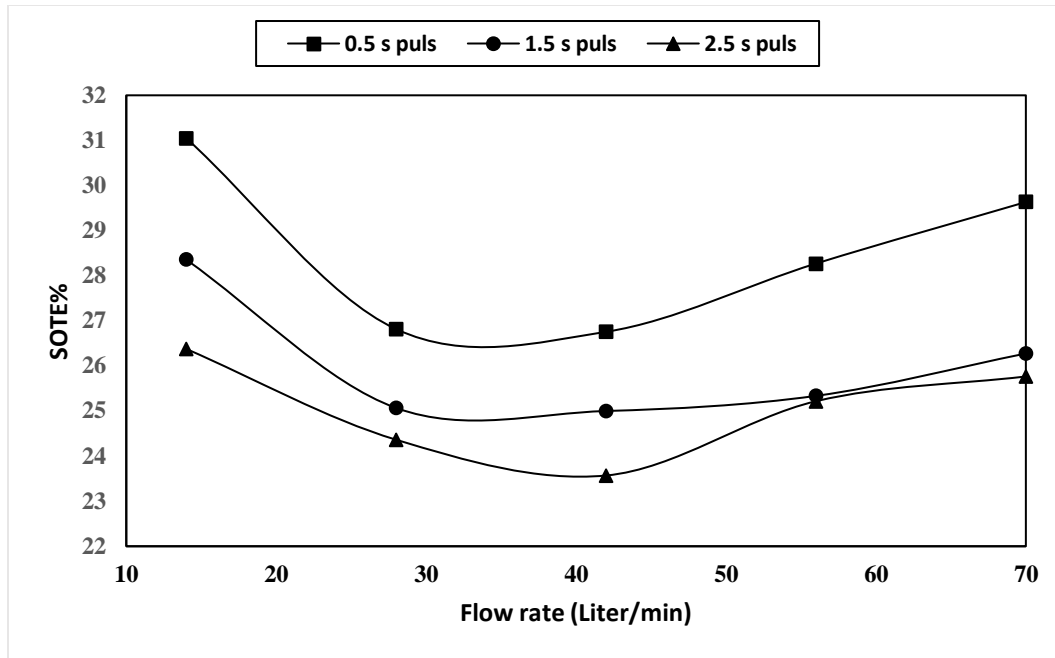
Figures 4.15 to 4.17 show the SOTE variation with flow rate for the ceramic results. Each figure is corresponding to a water column case. These results show the effect of pulsating time on the SOTE results for the ceramic case only. The results do not show significant difference between pulsating time cases for 0.6 and 1.2 m water columns. But, when the water column is 1.8 m (figure 4.17), the results clearly show that 0.5 s is the highest results and then 1.5 s and the lowest results can be seen when the pulsating time is 2.5 s, which is similar to what previous cases showed.



4.15: SOTE variation with flow rate for 0.6 m water column



4.16: SOTE variation with flow rate for 1.2 m water column



4.17: SOTE variation with flow rate for 1.8 m water column

In comparing with the membrane results, all the results were investigated for three water columns; 0.6, 1.2 and 1.8 m and three pulsating times; 0.5, 1.5 and 2.5 seconds. These results were shown for flow rates from 14 to 70 L/min by figures 4.18 to 4.26, and this is the range of flow rate considered for all the results in this study.

Figures 4.18, 4.19, and 4.20 show the SOTE results of the ceramic and the membrane diffusers for 0.6 m water column at 0.5, 1.5, and 2.5 second pulsating time respectively. As expected, based on the theory and practice, the SOTE decreased and then increased when the flow rate increased from 14 to 70 L/min. The ceramic diffuser results show higher SOTE at lower flow rates. Then, results take different behavior depending on the pulsating time.

Figures 4.21, 4.22, and 4.23 show the SOTE results when the water column is 1.2 m and the pulsating time at 0.5, 1.5, and 2.5 seconds respectively. Similar to the previous cases, the SOTE decreased and then increased when the flow rate increased from 14 to 70 L/min. But the difference

here is that both ceramic and membrane diffusers show very similar behavior, where the higher SOTE can be seen at higher flow rates except for the 2.5 seconds pulsating time, where it shows the higher SOTE at 14 L/min for the ceramic diffuser's case. In this case, the ceramic diffuser can be considered to give higher SOTE results for all the range of flow rates, except a small drop at 70 L/min when the pulsating time is 2.5 seconds.

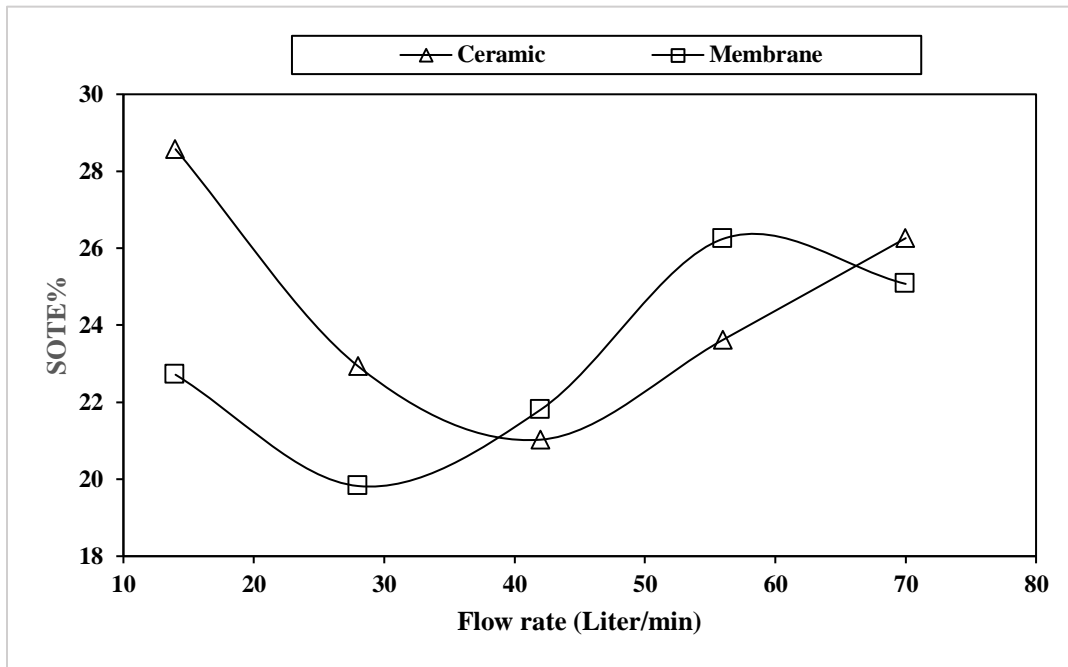


Figure 4.18: SOTE variation with flow rate for 0.6 m water column and 0.5 S pulsating time

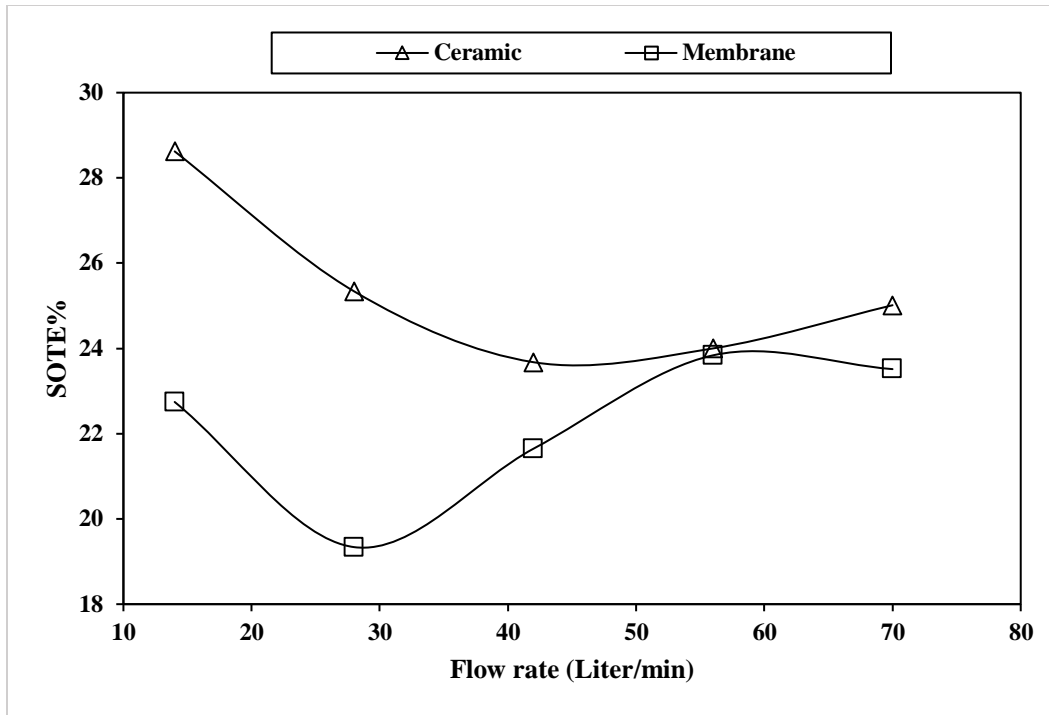


Figure 4.19: SOTE variation with flow rate for 0.6 m water column and 1.5 S pulsating time

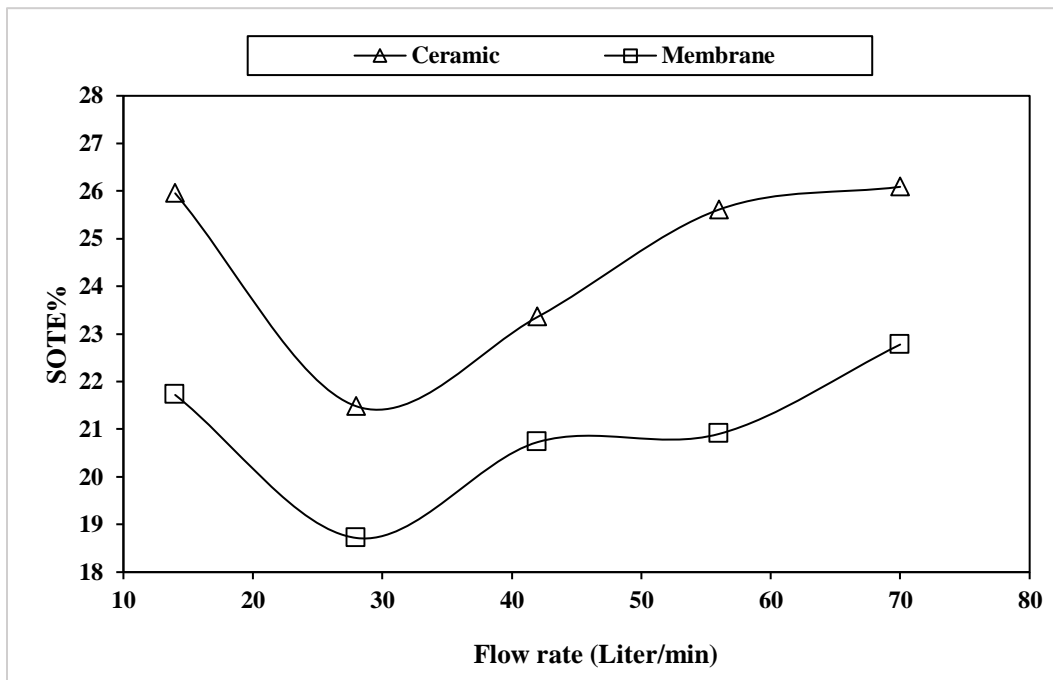


Figure 4.20: SOTE variation with flow rate for 0.6 m water column and 2.5 S pulsating time

Figures 4.24, 4.25, and 4.26 show the SOTE variation with flow rate for 1.8 m water column when the pulsating time at 0.5, 1.2, and 2.5 seconds, respectively. The results are showing the SOTE first decreases and then increases when the flow rate increase from 14 to 42 L/min, which is not different from the previous cases in this specific flow rate range. Also, it is important to note that the ceramic SOTE results drop lower than that of the membrane when the flow rate increases beyond about 30 L/min, and this can be noted to depend on the pulsating time.

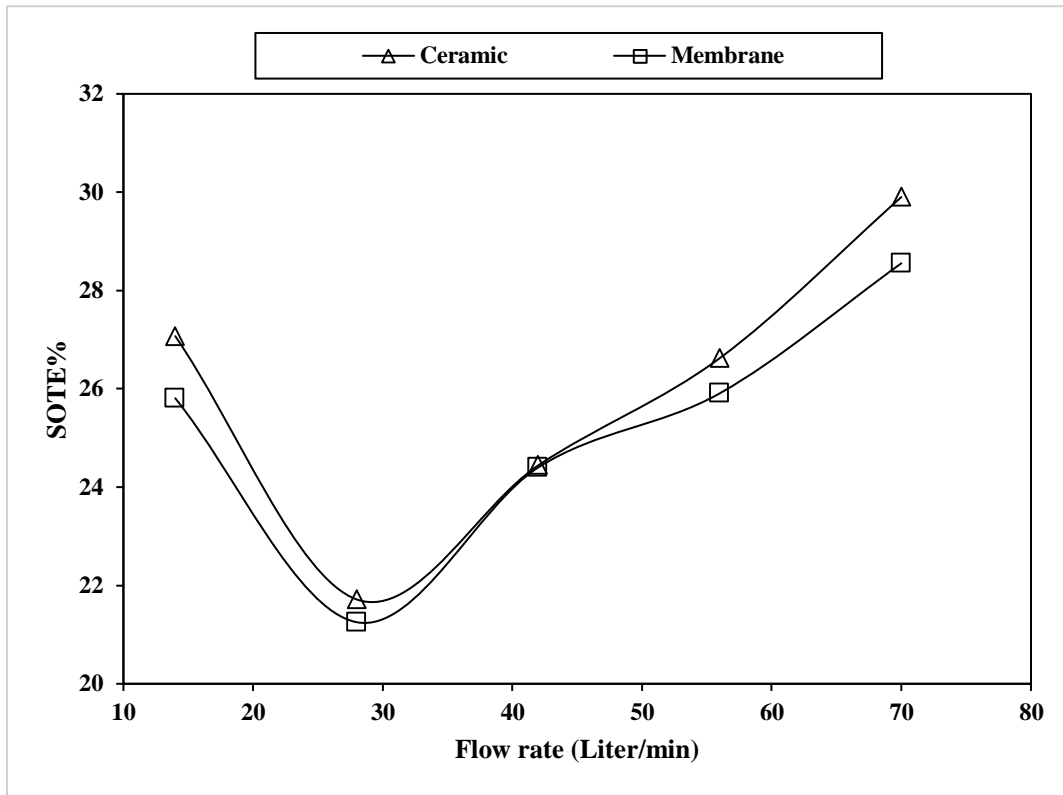


Figure 4.21: SOTE variation with flow rate for 1.2 m water column and 0.5 S pulsating time

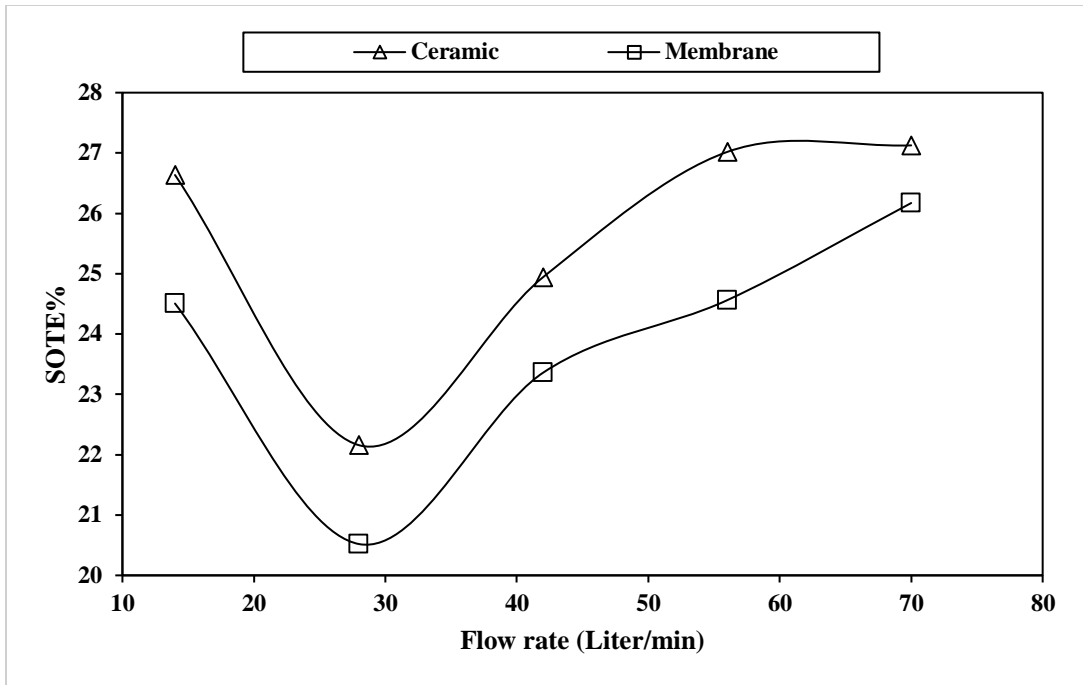


Figure 4.22: SOTE variation with flow rate for 1.2 m water column and 1.5 S pulsating time

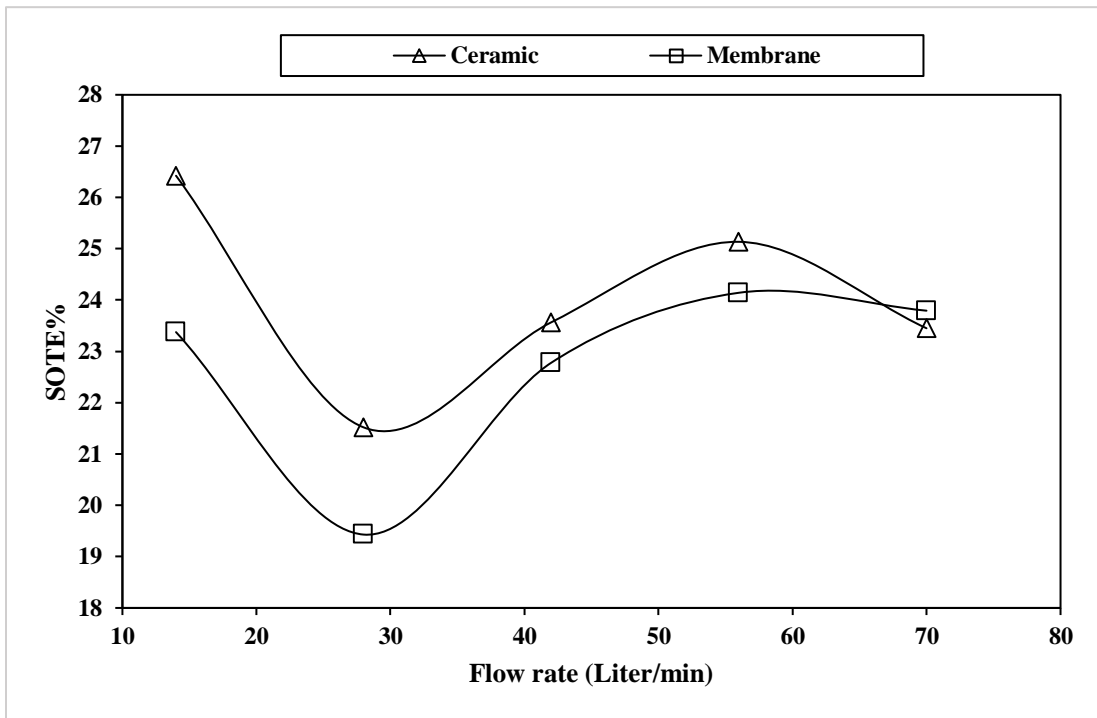


Figure 4.23: SOTE variation with flow rate for 1.2 m water column and 2.5 S pulsating time

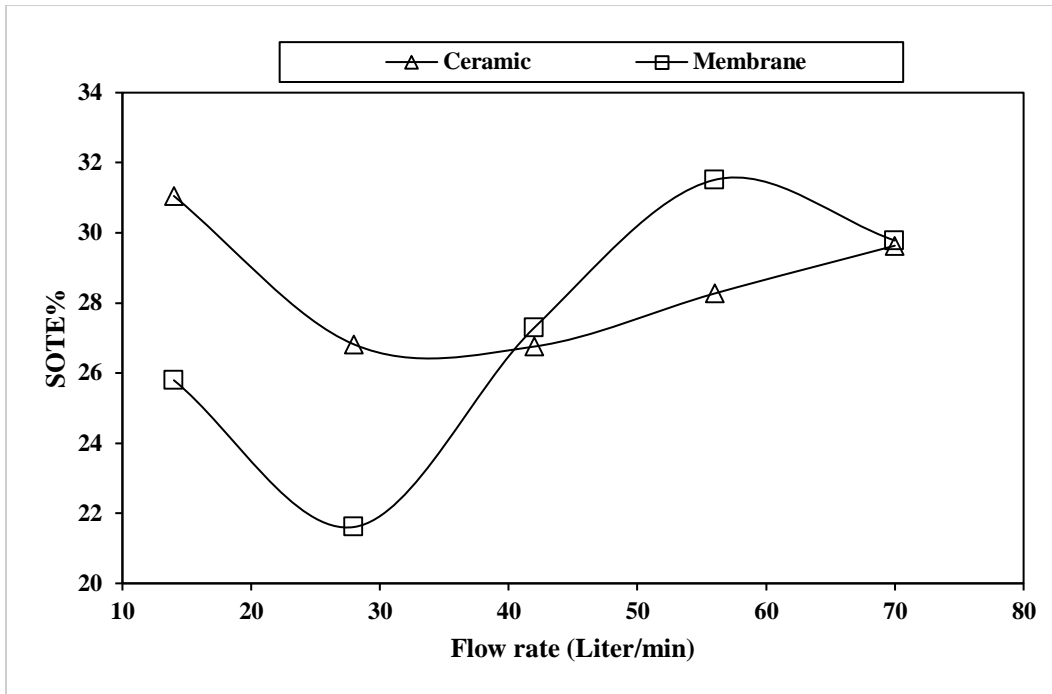


Figure 4.24: SOTE variation with flow rate for 1.8 m water column and 0.5 S pulsating time

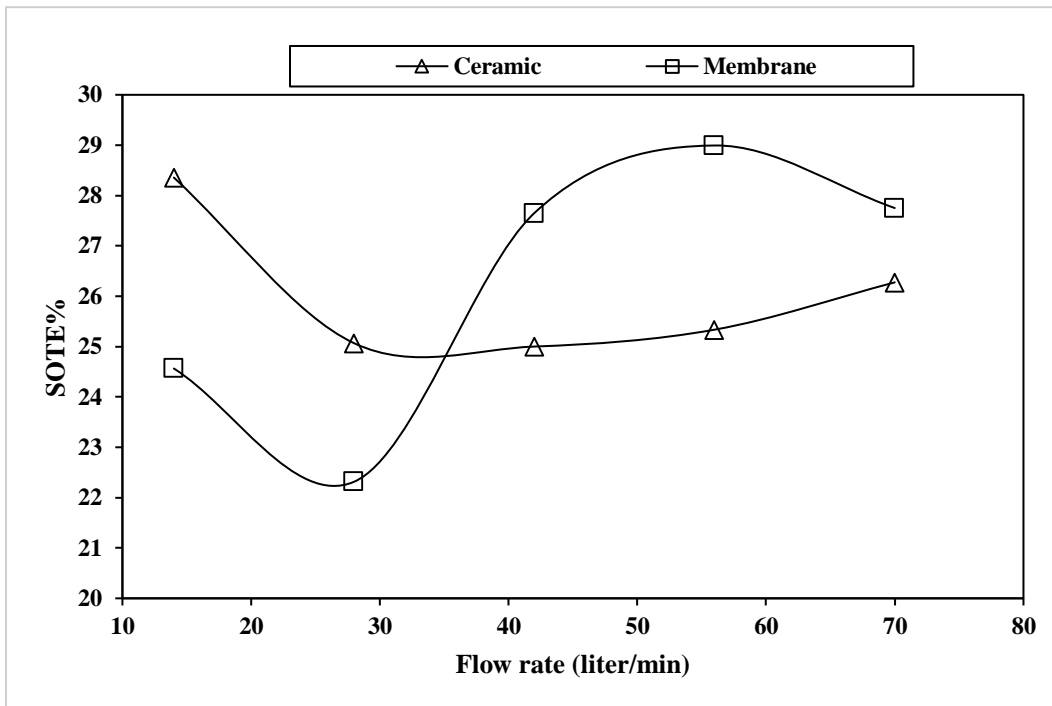


Figure 4.25: SOTE variation with flow rate for 1.8 m water column and 1.5 S pulsating time

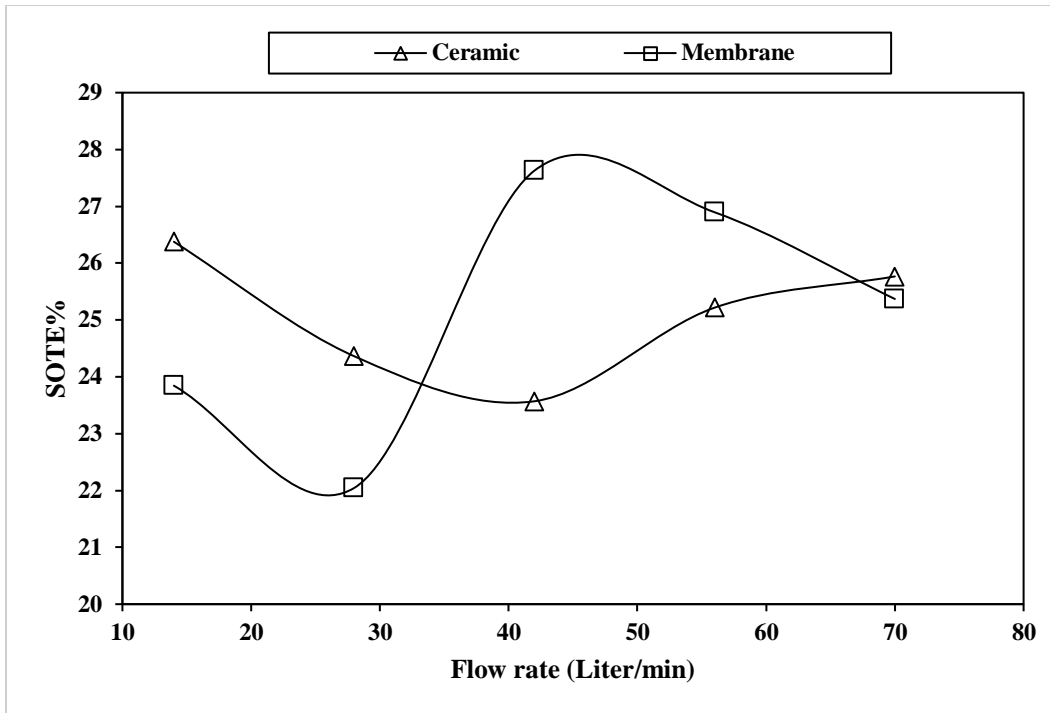


Figure 4.26: SOTE variation with flow rate for 1.8 m water column and 2.5 S pulsating time

In general, when looking at the SOTE results of all water columns cases, those of the ceramic diffuser are higher than those of the membrane diffuser at lower flow rates. At higher flow rates, this behavior is not always the same. Some of the results, specifically the 1.8 m water column, the SOTE of the ceramic diffuser, falls below that of the membrane diffuser.

4.4.2 Standard aeration efficiency

The standard oxygen transfer efficiency (SOTE) shows the effectiveness of the oxygen transfer process but it does not show the energy lost due to the pressure drop experienced by the air when it flows into the ceramic or the membrane diffuser and then through the water until it reaches to the water surface. However, the standard aeration efficiency (SAE) can be considered here to render this effect. For this purpose, the results of the SAE are investigated in a similar way to that used for the SOTE part.

The standard aeration efficiency (SAE) can be obtained from:

$$SAE = \frac{SOTR}{P} \quad (4.3)$$

In equation 4.3, the power (P) is the power delivered to compress the air at a certain pressure to overcome the pressure drop across the aeration diffuser and also the hydrostatic pressure above the surface of the diffuser. To determine the pressure drop across the diffuser, as discussed in section 3.3.5, there are two ways, either following the theoretical method or using experimental data. For this case, experimental data of the dynamic wet pressure are used, these data obtained from Xylem water solution and water technology company as tabulated in table 4.2.

Figures 4.27 through 4.35 show the SAE results. The results show a similar trend to the SOTE results, but since the aeration efficiency is inverse proportional to the power and in turn to the flow rate of the air, the results tend to be less steep as the flow rate increases.

Table 4.2: Dynamic wet pressure

Air Rate (L/min)	9” Membrane DWP (mm)	9” Ceramic DWP (mm)
28	279.4	159
56	368.3	185.7
84	444.5	203.2

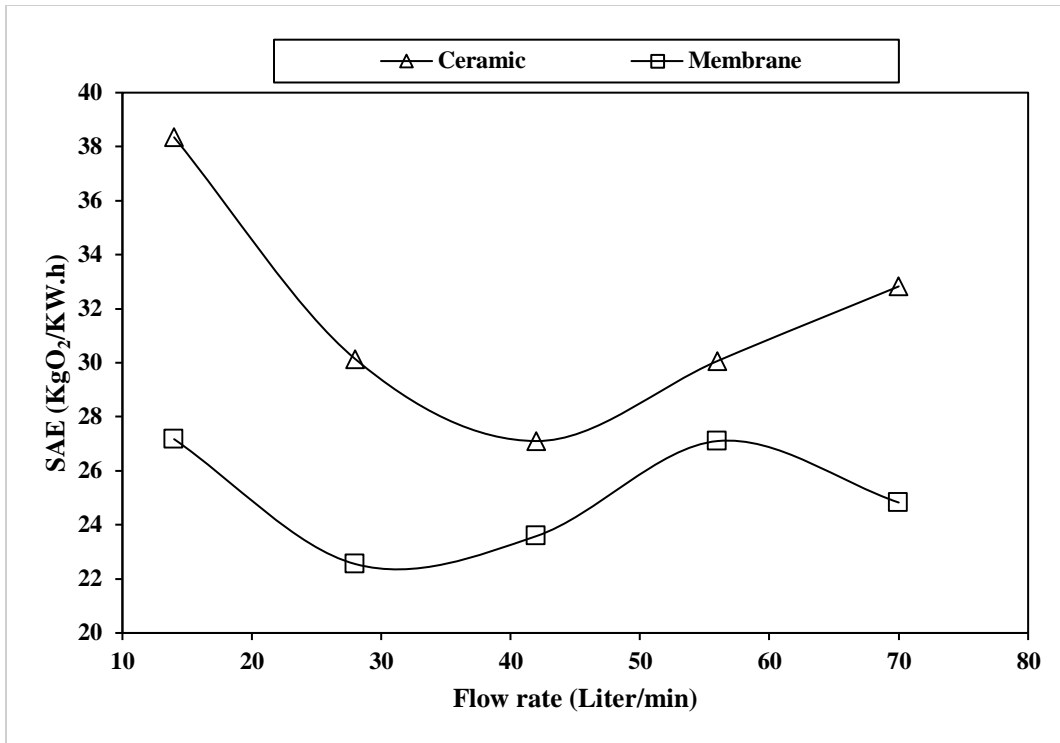


Figure 4.27: SAE variation with flow rate for 0.6 m water column and 0.5 S pulsating time

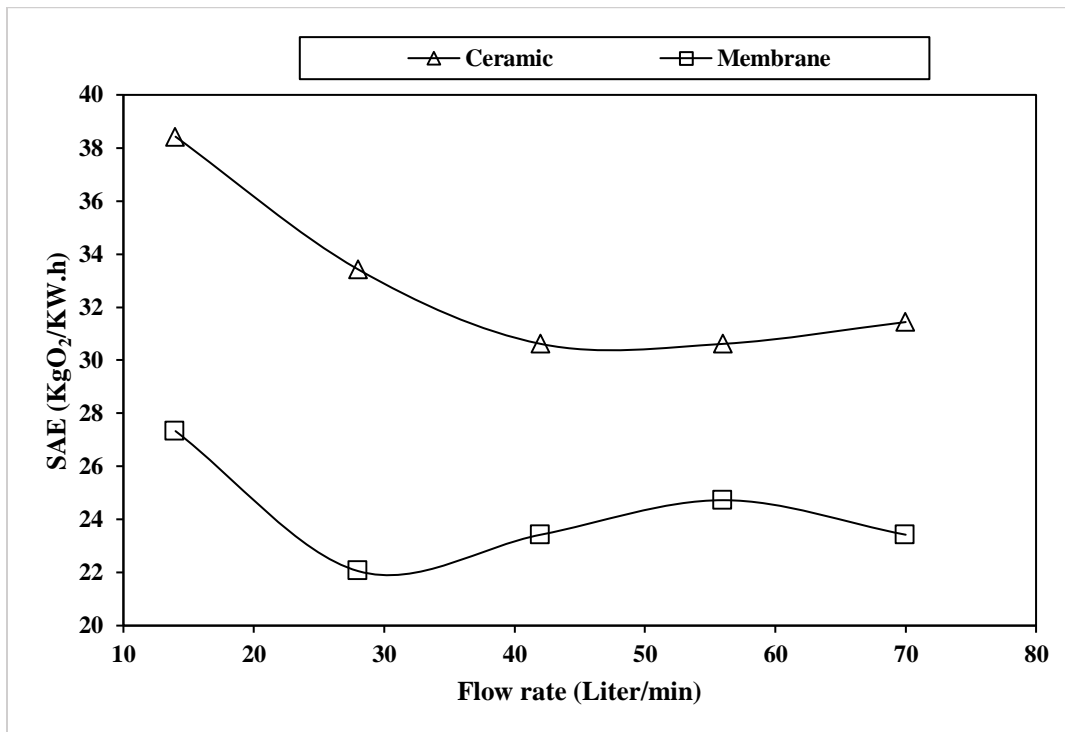


Figure 4.28: SAE variation with flow rate for 0.6 m water column and 1.5 S pulsating time

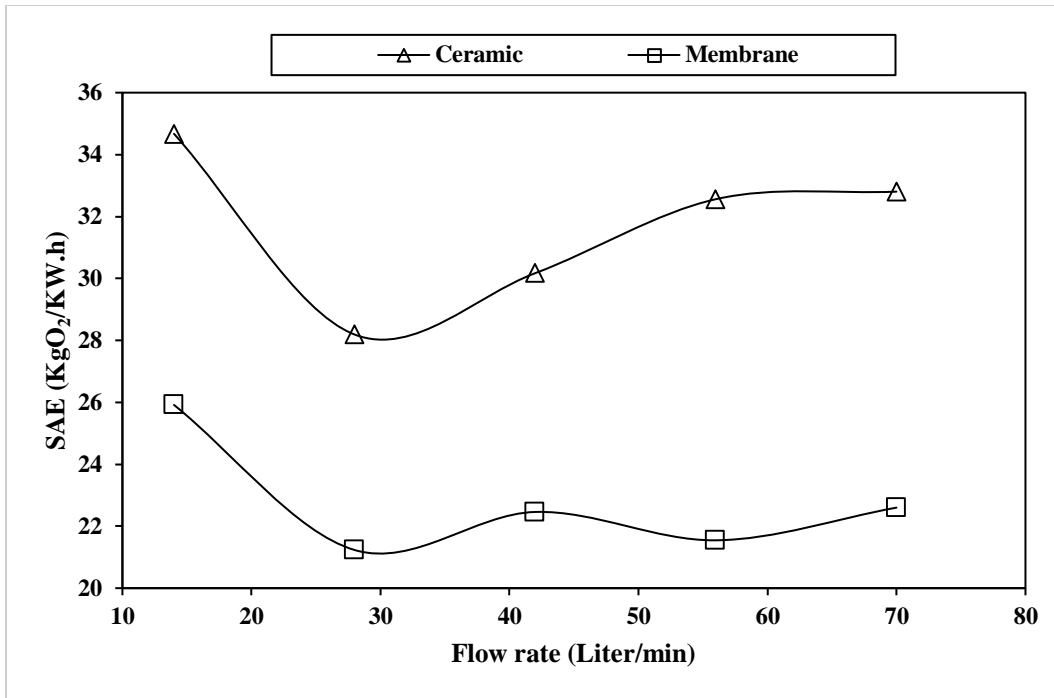


Figure 4.29: SAE variation with flow rate for 0.6 m water column and 2.5 S pulsating time

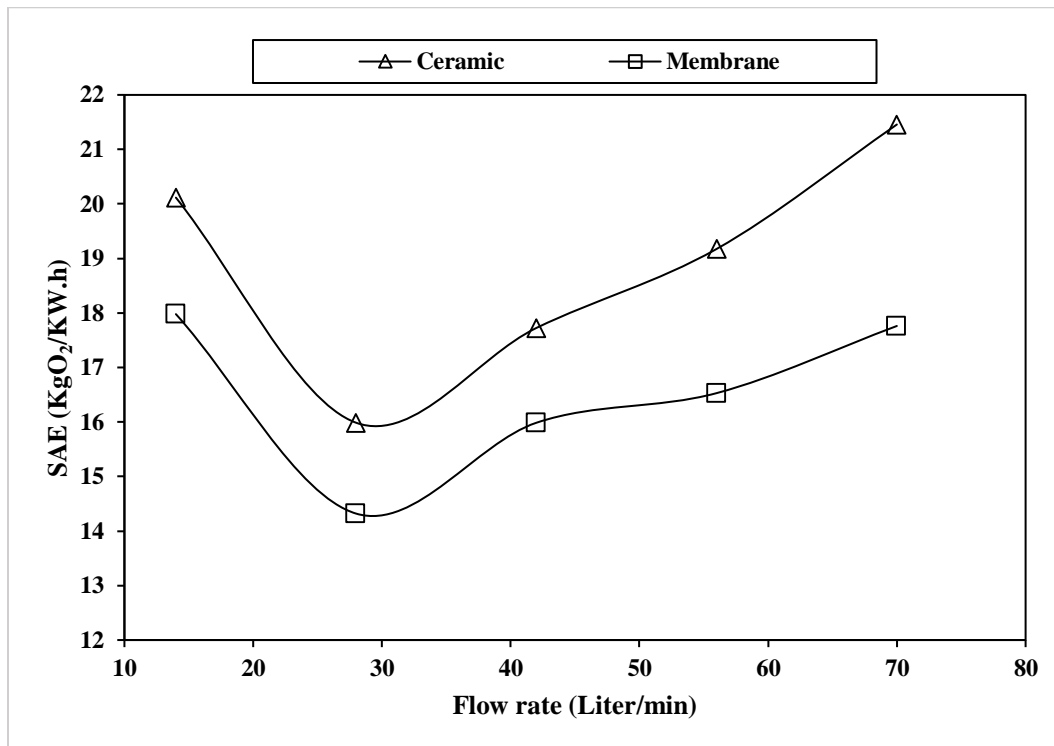


Figure 4.30: SAE variation with flow rate for 1.2 m water column and 0.5 S pulsating time

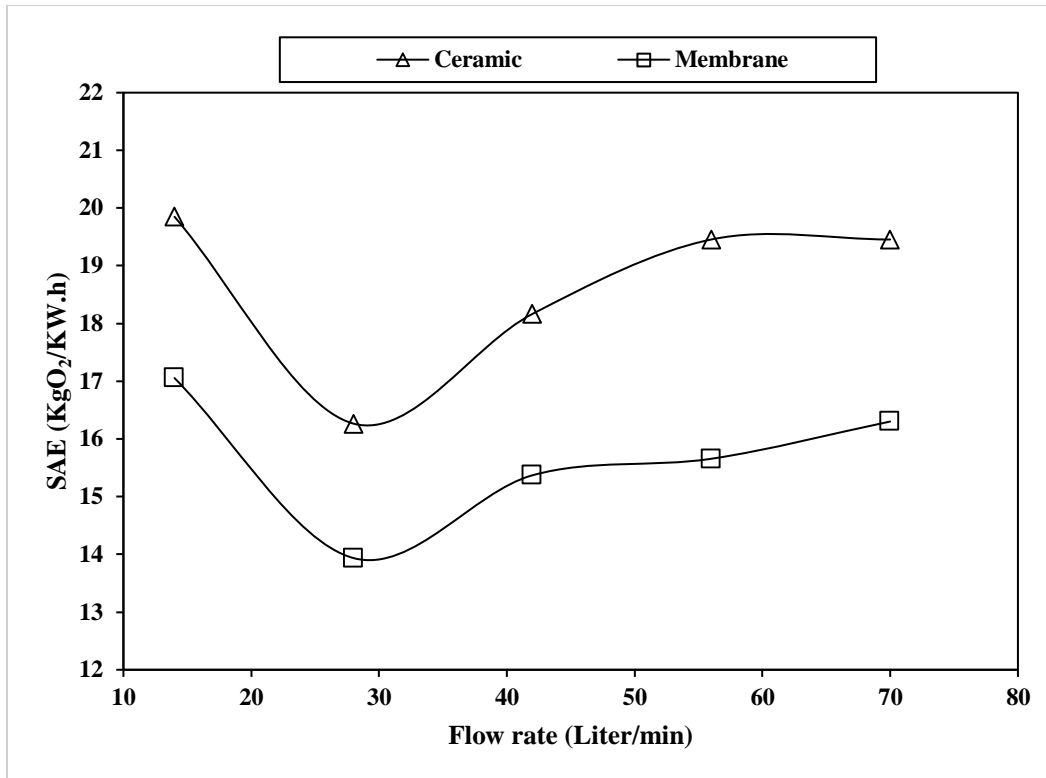


Figure 4.31: SAE variation with flow rate for 1.2 m water column and 1.5 S pulsating time

Also, the aeration efficiency is inverse proportional to the power consumed on supplying air to the aeration tank, this entails higher aeration efficiency for systems that are experiencing lower pressure drop. The lowest pressure drop is occurred when the water column height is the lowest. Therefore, the aeration efficiency could be the highest when looking at the 0.6 m water column's case.

In general, when observing figures 4.27 to 4.35, the best SAE results can be seen when the water column is 0.6 m, and then the 1.2 m water column follows. While the lowest SAE results can be seen on the highest water column, or the 1.8 m water column. In this case, the SAE results of the ceramic diffuser are falling below that of the membrane diffuser on some or most of the high flow rates' region.

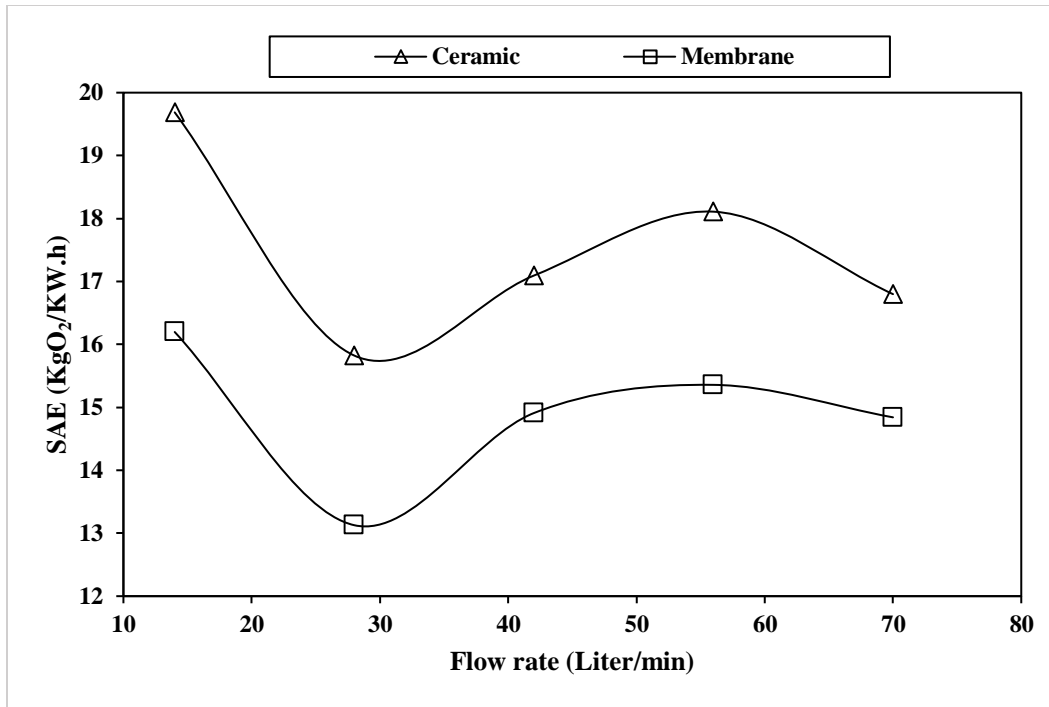


Figure 4.32: SAE variation with flow rate for 1.2 m water column and 2.5 S pulsating time

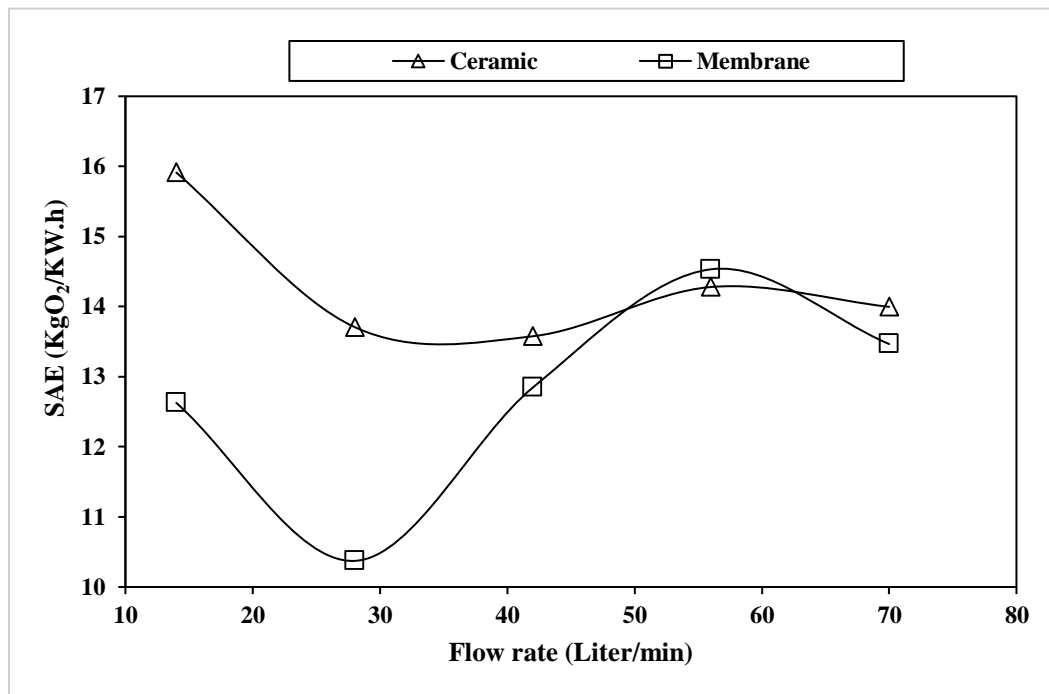


Figure 4.33: SAE variation with flow rate for 1.8 m water column and 0.5 S pulsating time

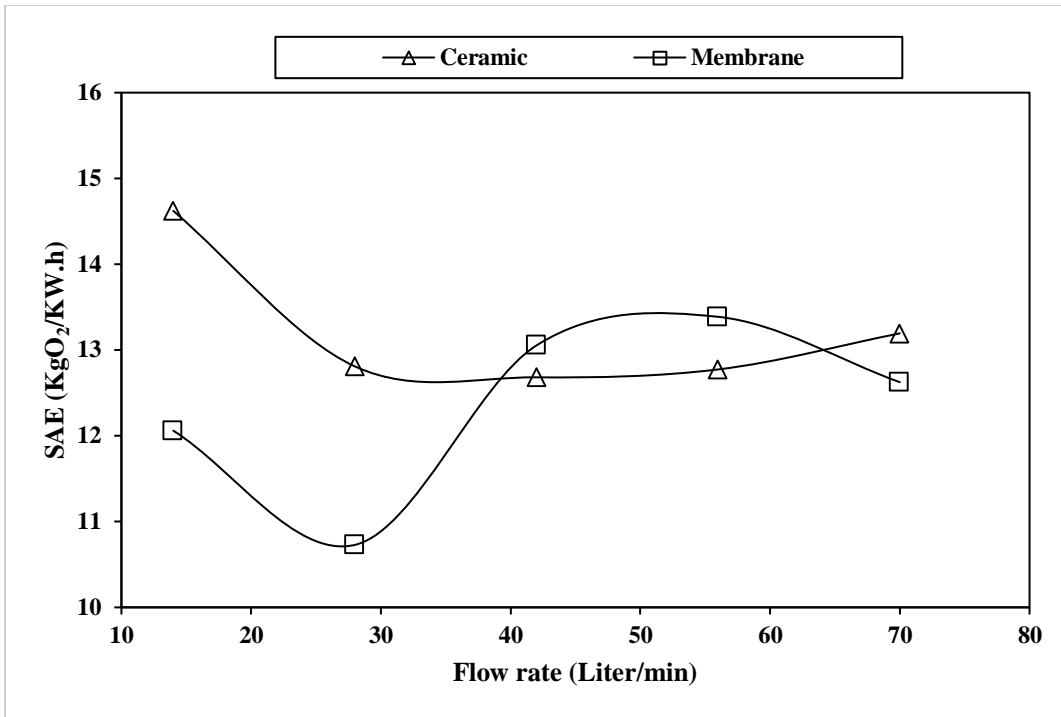


Figure 4.34: SAE variation with flow rate for 1.8 m water column and 1.5 S pulsating time

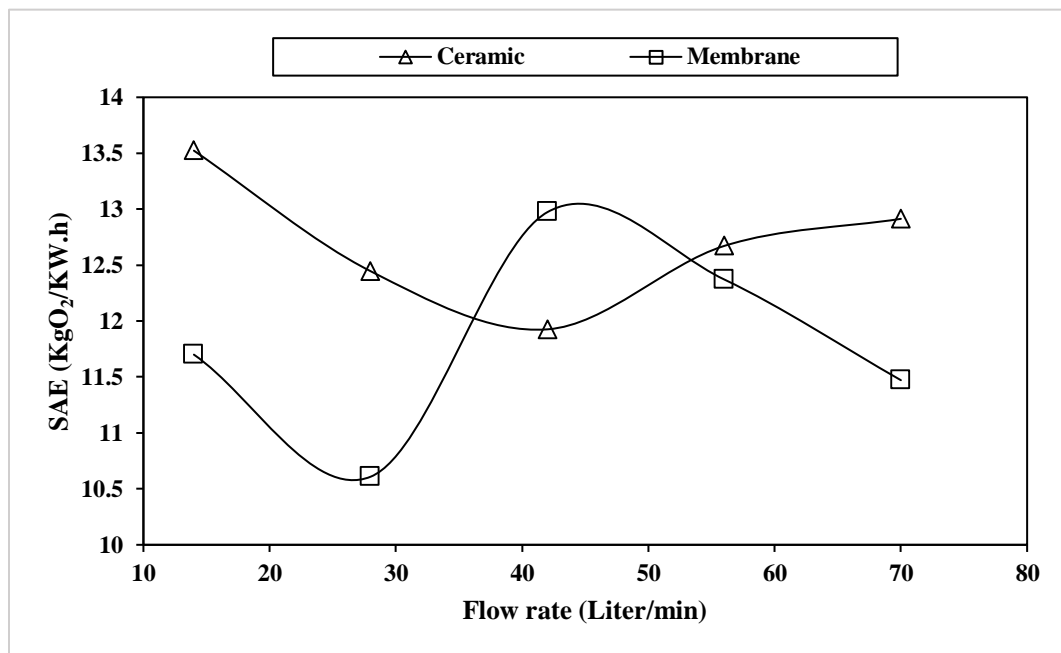


Figure 4.35: SAE variation with flow rate for 1.8 m water column and 2.5 S pulsating time

Table 4.3 shows the percentage of the error collected from the experimental measurements. The maximum error was recorded for the 0.6 m water column, 1.5 seconds pulsating time, and 56 L/min, which was 6% (SOTE $\approx 25.23 \pm 1.5$) and the minimum error is 0.2% (SOTE $\approx 26.46 \pm 0.05$). This means that measurement error can be considered within the test tolerance. Although test tolerance can vary based on the measurement's conditions, for example, measurements conducted in tap water differ from those in wastewater (real case).

Table 4.3: Percentage of experimental error

Water column (H), m	Pulsating time, Sec	Flow rate (Q), L/min				
		14	28	42	56	70
0.6	0.5	3.4	2	0.6	1.2	1.6
	1.5	2.4	1	0.8	6	1
	2.5	1.5	2.1	5.2	1.6	2.1
1.2	0.5	1.8	0.8	1.5	1.7	0.8
	1.5	2.1	1.2	0.5	3.4	1.8
	2.5	0.2	4.4	1.7	1	3.7
1.8	0.5	2.2	0.3	0.7	2.7	2.8
	1.5	1.4	1.3	0.6	2.1	1.9
	2.5	0.9	2.5	1.2	0.9	3.5

4.4.3 Conclusions

This work presents the evaluation results for two types of aeration diffusers based on two critical parameters for any aeration application. These parameters are the standard oxygen transfer

efficiency (SOTE) and the standard aeration efficiency (SAE).

It was discovered that the SOTE results of the ceramic diffusers are better at lower flow rates than higher flow rates. In other words, the waves created by increasing the flow rate is not affecting as much as that of the membrane diffusers. This is attributed to the finer bubbles generated at the ceramic diffuser surface, those are usually rising slower towards the surface of the water and contribute less to mixing, which causes surface waves with less energy.

On the other hand, since the pressure drop experienced by the air as it flows through the diffusers is not the same on both kinds of diffusers, the SAE results are significant to consider for this study. The SAE is inverse proportional to the air flow rate. Therefore, the results of the SAE are decreasing as the flow rate increases. It is shown through this study that a higher water column (1.8 m) is more effective for SOTE enhancement, which applies limitations to the use of the ceramic diffuser at higher water columns and higher flow rates. In this case, the use of membrane diffusers can be more efficient.

In particular, the ceramic diffusers show better performance than the membrane diffuser when the water column is 0.6 m, where the SAE can increase up to 35% higher than that of the membrane diffusers.

Also, it can be concluded that the ceramic diffuser results do not show a strong dependency on the surface waves created due to the pulsating effect, which opposed the membrane diffuser results, and therefore, it can be approximated to the continuous airflow case discussed in section 4.1.

4.5 Cyclone study

Another study was conducted to create a cyclone or vortex by allowing the air flow to be injected to create horizontal rotation, this means the air will be injected in horizontal direction rather

than the normal vertical direction. For this purpose, two PVC pipes are perforated so that each one is injecting air bubbles horizontally but on opposite directions. The holes diameter and number in each pipe are arbitrary selected since the purpose of this study is to see if a vortex can be created, which could increase the mixing in the water due to the water rotation.

The experimental set up is shown in figure 4.36, which consists of two hollow PVC pipes perforated and installed so that they diffuse air bubbles in opposite and horizontal direction. These are installed in a transparent water tank to visualize the motion of the bubbles as they emerge from the pipes and rising to the water surface.

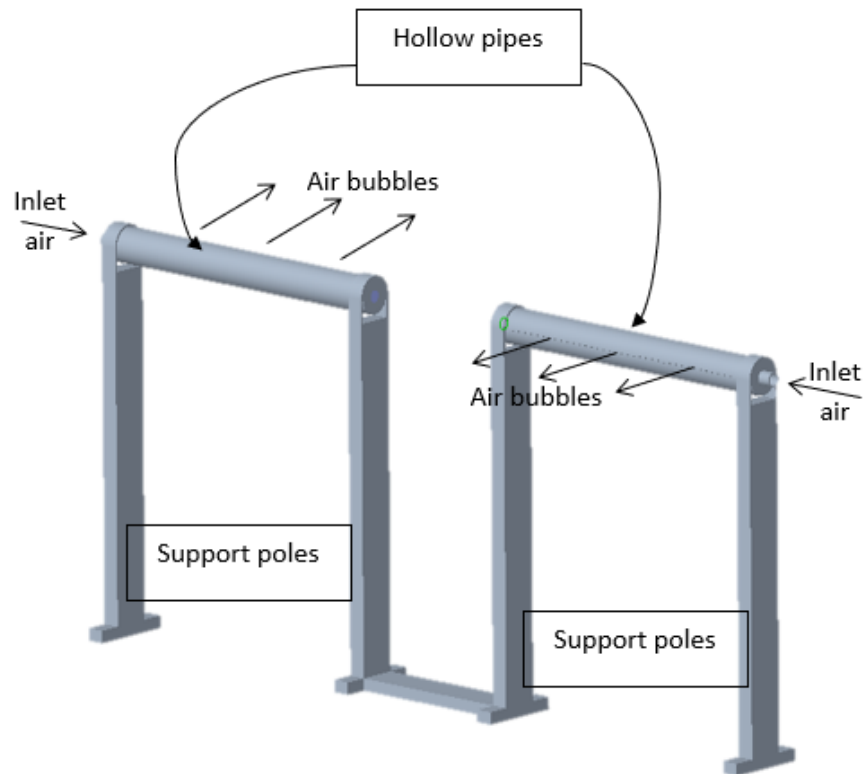


Figure 4.36: experimental set up

It was noted from the bubbles motion visualization that there is no vortex generated at all and once emerged from the pipe's holes, the bubbles take a direct upward route towards the water surface.

Based on that and observation, it is required that the momentum of the air exiting the pipe holes must be greater than the hydrostatic force acting on the bubble in order for the bubble to overcome the hydrostatic force and move horizontally before it rises upward. Other than that, the bubble will rise vertically once it is injected into the water. Therefore, there will be no swirl effect expected from this design. On the contrary, this design might be more deficient to aeration systems since there is a great chance that the bubble would grow in size after attaching for long time to the pipe surface before it is released into the water.

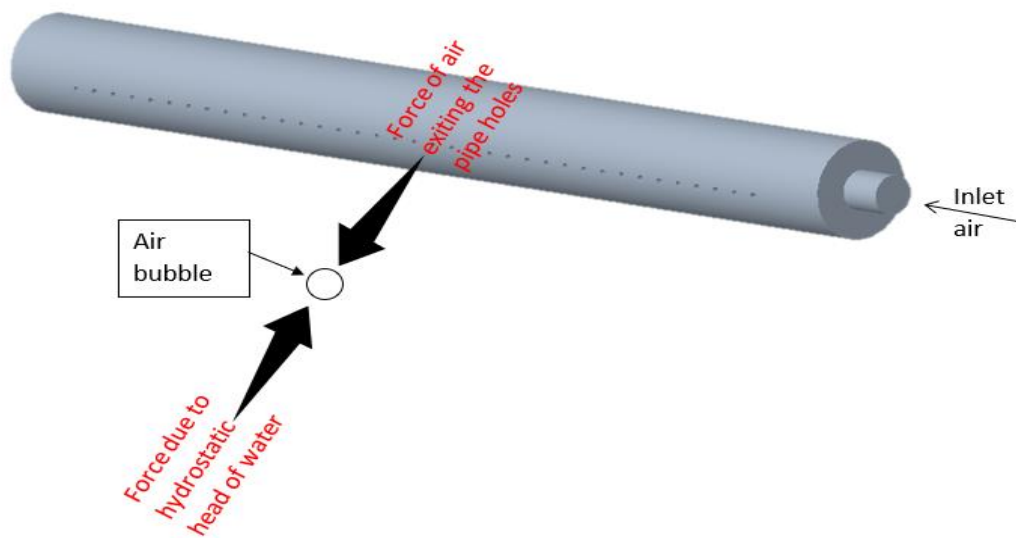
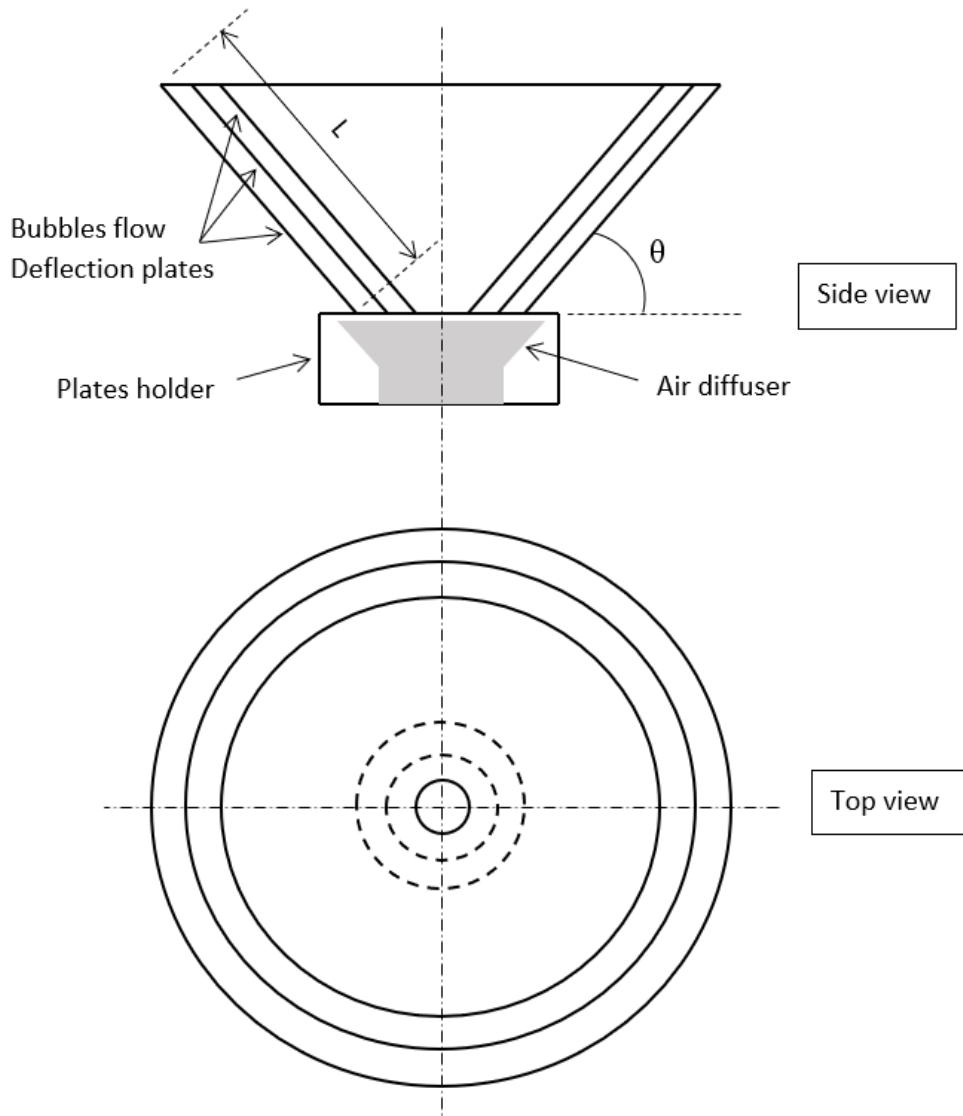


Figure 4.37: Forces acting on the bubbles soon after emerging from the pipe

Based on the findings from bubbles observation. These findings are based on 0.3 m water column. If applied to real case, where the water column is ranging between 2 to 4 m, the required momentum will be 10 times higher than that of the current conditions. Therefore, this study is not feasible, and it will be better to think of another method to force the bubbles to deviate from vertical path without relying on momentum.

We know that forcing the bubbles to take an inclined path when they rise in water will increase the rate of oxygen transfer by increasing the resident time and the transfer area between the air and water, since inclined path is always longer than straight path, and for this case further water regions will be exposed to the bubbles.

A good suggestion to implement that is by installing layers of inclined plates on top of the diffuser as shown in figure 4.38. This design can create bubbles deviation and force the bubbles to take other than vertical path. Also, this can be adjusted for different angle (θ) and different lengths (L) to consider the effect of the inclination on the results. After that, a comparison between this method and the normal diffusion method when the bubbles rising in vertical direction can be conducted based on the standard oxygen transfer efficiency (SOTE). This suggested idea can be added within the recommended future research by following the set up illustrated in figure 4.38.



4.38: Suggested set up for deflecting air bubbles

5. CFD studies on aeration

In wastewater treatment plants, the typical height of aeration tanks ranges between 3 and 4 meters. Since experiments undergone in labs and most labs have limitations regarding the access and containment of such high tanks. Therefore, these limitations pose difficulties when conducting experimental work to test full scale aeration systems. On the other hand, there is an importance to consider high aeration tanks to see how this can affect the oxygen transfer rate. For this reason and more, CFD can be considered a very useful and flexible tool that can be used when such limitation problems arise.

5.1 Effect of water column-CFD modeling

The effect of water column has been investigated experimentally for lab scale aeration systems in section 4.2. Although the findings of this experimental study were interesting, but it would be more interesting to expand these findings to include real scale aeration systems, which is the objective in this section. Three real scale water columns are considered here, which are 2, 2.5, and 3 m.

For such high-water columns, the CFD solution computation time will be significant; to decrease that time, the CFD model will be limited to a single diffuser aeration tank as shown figure 5.1. The air diffuser is a standard aeration diffuser similar to that used for the previous experimental studies. It is submerged at the bottom of a rectangular section water tank. The height of the water tank is the only variable here.

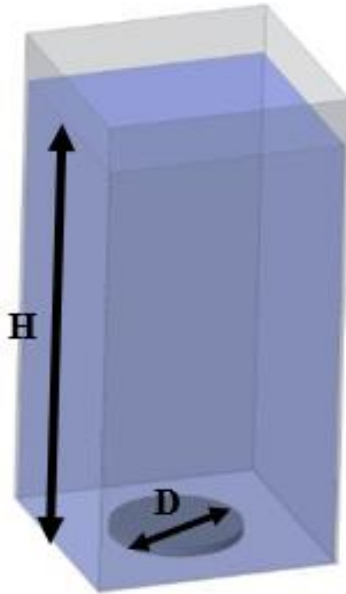


Figure 5.1: CFD model for the aeration system

When using the CFD method, it is important to validate the results obtained from this method by compare it with experimental results with the same conditions. Therefore, an experimental model similar to that used for the CFD was created as shown in figure 5.2. This experimental system consists of the same components as in figure 5.1 but there is and additional component which is the dissolved oxygen probe. This is necessary in any experiment work and it is used for the experimental measurements to obtain the dissolve oxygen evolution with time, which in turn necessary to determine the overall mass transfer coefficient.



Figure 5.2: Experimental model to validate the CFD results

The computational method for the aeration system is based on a two-fluid model, primary and secondary fluids, to set the equations of motion and the forces acting on the bubbles rise in the water. Usually, the primary fluid is the one with the highest density since it will be the fluid that applies the greatest force on the other fluid (less density fluid). Therefore, the water is considered primary and air is secondary fluid.

On the other hand, diffusion occurs in fluids (for gases and liquids) when the concentration is not the same in two or more fluids that are in contact with each other, where there will be a diffusing flux transferring from the high to the low concentration. This diffusing flux is function of time and position, since the concentration is also changing with time and position.

Considering air-water system, the interface between these two phases will be the bubble.

Then, Fick's law at the bubble boundaries is expressed as:

$$N_B = -D_{AB} \frac{\partial c_A}{\partial x} \quad (5.1)$$

Considering the oxygen is transferring from the air to the water, equation 5.1 can be rewritten to account for oxygen addition in water by just changing the sign of the diffusion flux, where A is water and B is oxygen. Therefore equation 5.1 becomes:

$$N_A = D_{BA} \frac{\partial c_A}{\partial x} \quad (5.2)$$

The binary diffusion coefficient is constant and $D_{AB}=D_{BA}$, since $J_A=-J_B$ and $dc_A=dc_B$. Therefore, this coefficient can be considered as a property of the fluids where the diffusion occurs. It is necessary to consider binary diffusion coefficient rather than diffusion coefficient when diffusion occurs in multi fluids or components.

The rising of bubbles will change the static condition of water causing some mixing depending on different factors. One of the most affecting factors that can implicitly agitate the water is the turbulence effect of air flow in the water. Previous studies (chapter 4) showed the effect of mixing due to the air flow in the water can significantly affect the rate of oxygen transfer. Therefore, it becomes necessary to include the velocity or convection diffusion in addition to the molecular diffusion. The unsteady diffusion equation can be expressed as:

$$\frac{\partial c_A}{\partial t} + U \cdot \nabla C_A = D_{BA} \nabla^2 c_A \quad (5.3)$$

Based on the two-film theory (Lewis W., 1924) for gas absorption, there exist a boundary between the two phases where the transport of species can experience some resistance. Therefore, it is

convenient to employ a mass transfer coefficient based on the difference in concentrations between the gas and liquid phases as follows:

$$N_A = k(c_A - c_\infty) \quad (5.4)$$

when combining equations 5.2 and 5.4 and integrating along the bubble interface, the final equation will be given as:

$$\frac{k d_b}{D_{AB}} = \ln \frac{c_{A2} - c_\infty}{c_{A1} - c_\infty} \quad (5.5)$$

The mass transfer data was correlated by using dimensionless groups based on the two-film theory. Equation 5.5 can be expressed in terms of some of the important dimensionless groups which is the Sherwood number as:

$$Sh = \ln \frac{c_{A2} - c_\infty}{c_{A1} - c_\infty} = f(Re, Sc) \quad (5.6)$$

Sherwood number is function of the Reynolds number and the Schmidt number. Both are very important factors in mass transfer of species. The higher the Reynolds number the higher mixing and the higher rate of mass transfer. The Schmidt number depends on the fluid properties. For diffusion in gases, the Schmidt number is of the order of one, while for liquids it can be as high as 40000 (Bird R., 2007). For air – water system, the Schmidt number is 340 (Poling B., 2001).

Equation 5.6 can be applied to the current case by using Higbie – Poissonesq correlation (equation 3.20) (Higbie, 1935) which is obtained from experimental measurements of mass transfer coefficient.

5.1.1 CFD results validation

Figure 5.3 shows the experimental set up used to validate the CFD results. This set up is necessary to conduct the dissolved oxygen (DO) measurements and determine the DO profile and calculate the overall mass transfer coefficient based on that. In addition, same set up was used to measure the bubble diameter and bubble rising velocity by using high speed camera of 2000 frame per second. From that, the average rising velocity and the bubble diameter are

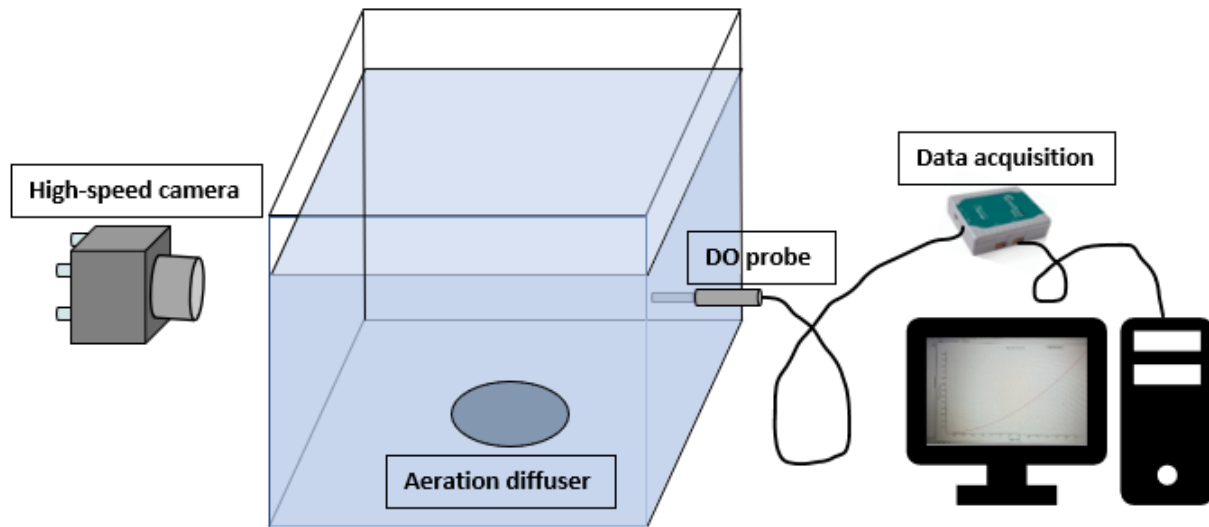
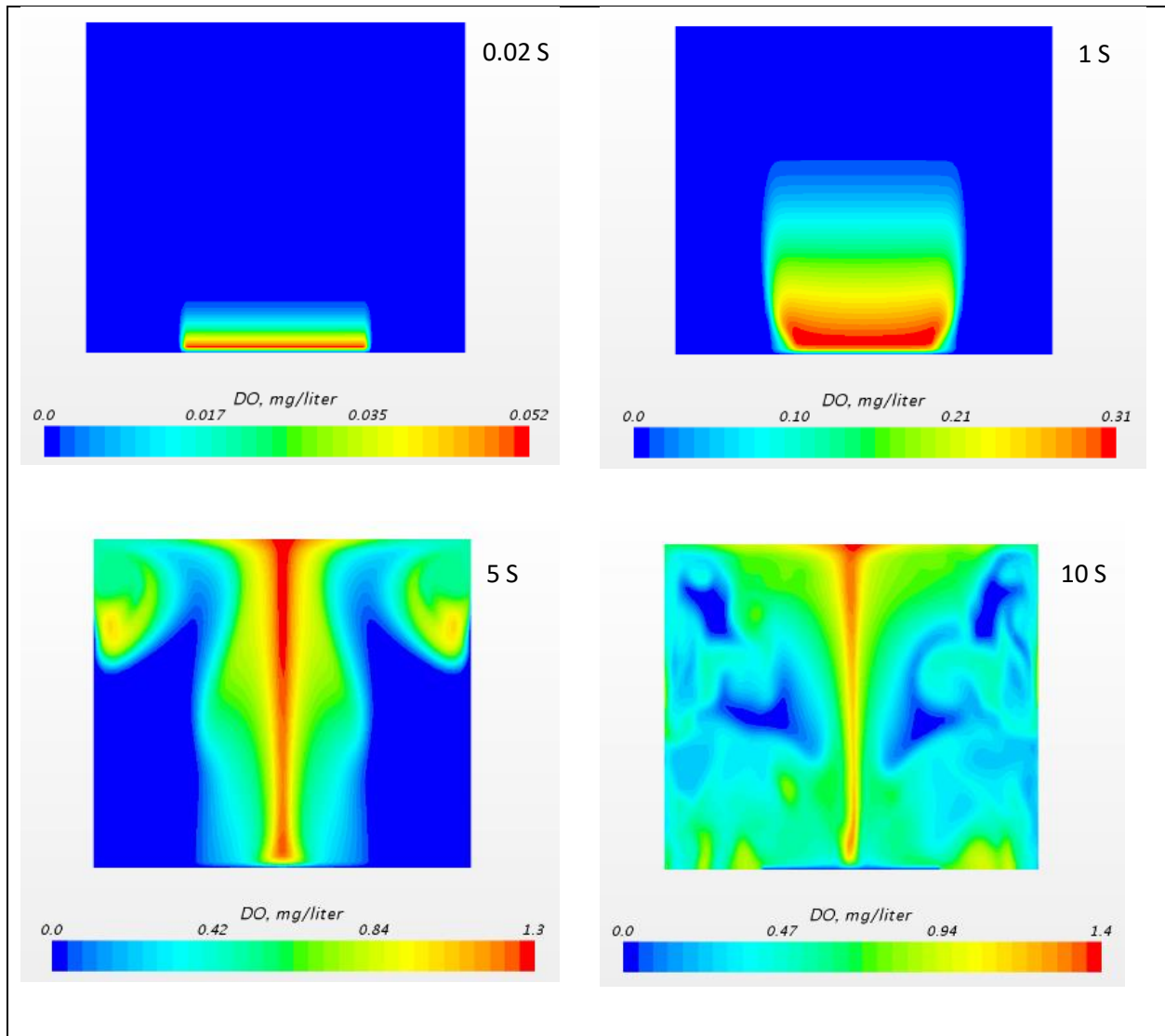


Figure 5.3: Experimental set up for CFD validation

measured and inputted as initial conditions to the CFD simulation to determine the length scale of the dispersed phase and the mass transfer coefficient in terms of the Sherwood number from equation 5.6.

Figure 5.4 shows the dissolved oxygen (DO) contours at different physical times. It shows the onset of DO transfer from the dispersed air phase to the water phase at early physical times. Then, it diffuses to the rest of the water as time goes on until it reaches to a state close to saturation.

It can be noted that the DO diffuses at a faster rate at earlier times than higher times. This is reasonable since the difference in DO contents in air and water decreases as the physical time increases which causes the rate of oxygen transfer to decrease.



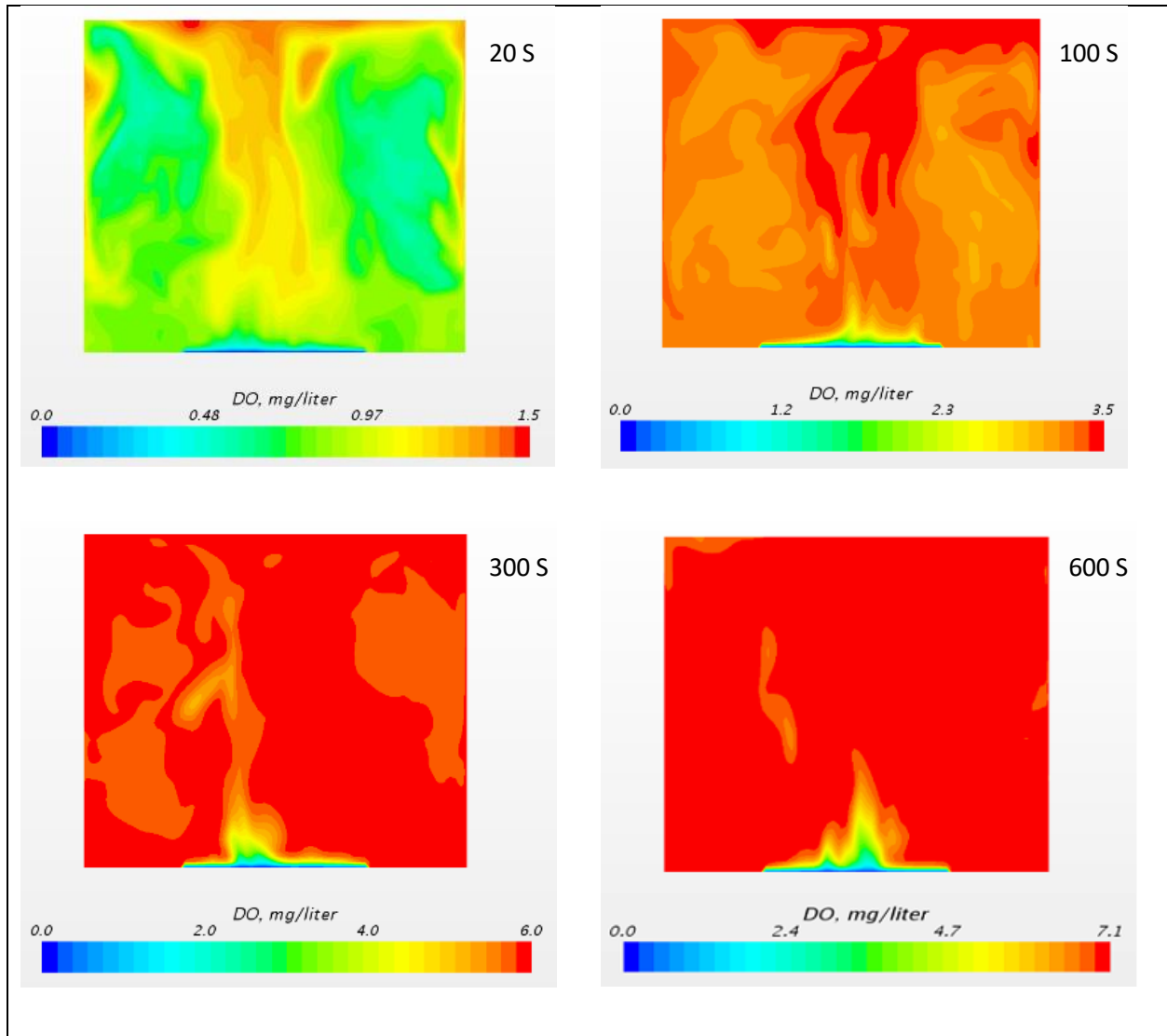


Figure 5.4: Dissolved oxygen evolution with time

The DO evolution with time was obtained after conducting the experimental measurements and completing the CFD simulation for this small-scale aeration system. These CFD and experiment profiles were compared and figure 5.5 shows this comparison. Standard conditions with 27 °C temperature were used for both cases. The two curves take a similar trend at earlier time, but the CFD curve start to diverge from the experimental curve. This divergence can be attributed to the

mesh resolution and this could be improved by applying finer mesh. The number of mesh cells created for the CFD case is 1 million cells. This number is corresponding to 10 million cells when considering the highest water column (3 m). The final parameter that is important to look at for both cases is the overall mass transfer coefficient which can be obtained from equation 3.9, where this equation is used only when the

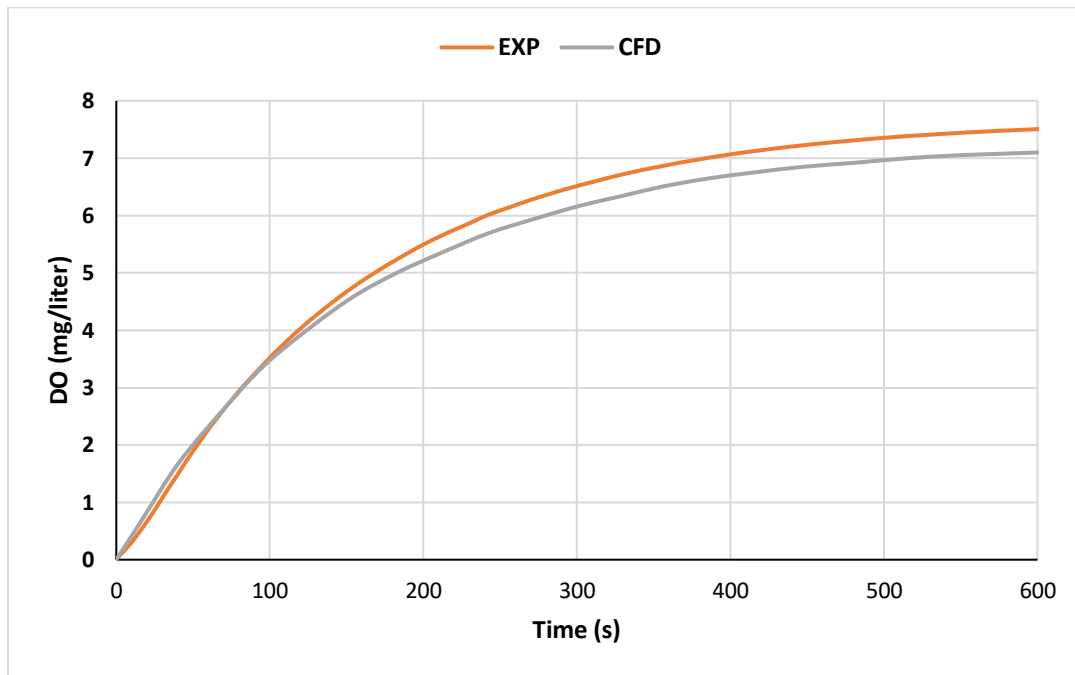


Figure 5.5: DO profile of experiment vs CFD

temperature is 20 °C. To consider different temperatures, equation 3.12 can be used to correlate the overall mass transfer coefficients, which is used for both the CFD and the experiment because the temperature of the water is 27 °C in both cases. When applying this approach, the CFD and the experimental results are close to each other based on the SOTE that is determined from equation 3.11. These were 4.97 % for the experiment and 4.7% for the CFD, which is showing a 5% error, and this can be an acceptable error. Therefore, we can consider the CFD results as acceptable and

we can move on to the next step, which is obtaining the DO profiles for the full-scale aeration systems; 2, 2.5, and 3 m water columns.

5.1.2 CFD results of full-scale aeration systems

Results of the full-scale aeration systems can be obtained by first applying the CFD method and modeling to obtain the DO profile for each case and then using equations 3.9, 3.11, and 3.12 to obtain the SOTE.

Figure 5.6 shows the DO increase with time for each of 2, 2.5, and 3 m water column. These results were obtained based on 27 °C and 1 atm, which entails using equation 3.12 to correlate the mass transfer coefficient at this temperature for all the three water column cases, similar to the results obtained in section 5.1.1. However, the results are showing similar trend as the DO increases from 0 at 0 time to a maximum value that differs based on the water column height. These maximum values are not the steady state values since the DO is not reaching to a constant value yet, but the trend will reach steady state at a certain time greater than the current physical time. Based on that, the standard oxygen transfer efficiency for each of the 2, 2.5, and 3 m is 18.22%, 20.49%, and 21.74% respectively, as shown in figure 5.7.

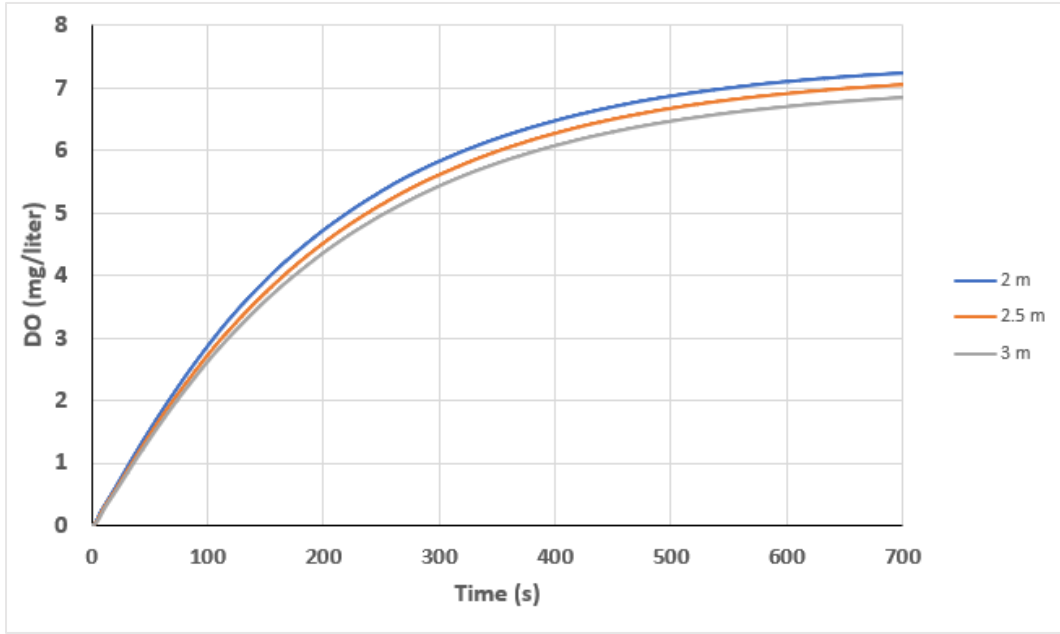


Figure 5.6: DO evolution with time for 2, 2.5, and 3 m water columns

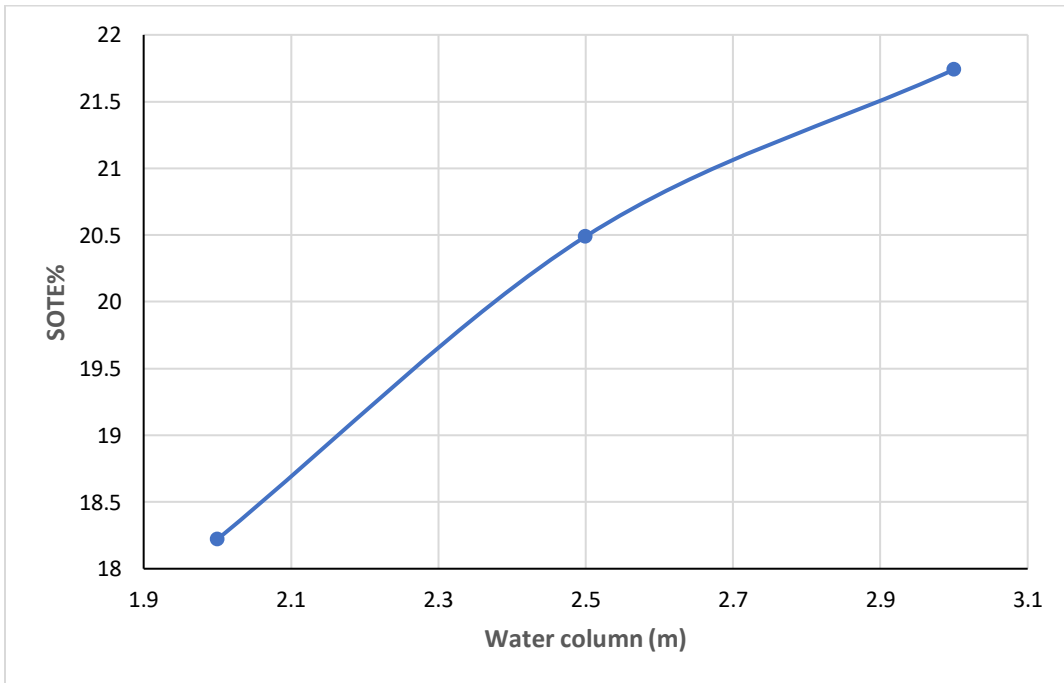


Figure 5.7: SOTE% vs water column-CFD

5.1.3 Conclusions

The conclusions from this study can be considered similar to the effect of water column experimental study of section 4.4.1, where the highest water column is showing better results than the other two lower water columns. Also, the lowest SOTE can be obtained from the lowest water column, while the 2 m water column is in between the highest and lowest water column. Although the high computation time required to complete each simulation, the CFD method was very flexible where it can be used without limitations for zone or equipment requirements. The final physical time obtained for this study is less than the steady state value due to the high cost of computation time if considering a physical time to reach to the steady state value. All the simulations are conducted by using the high-performance computation (HPC) at UWM, otherwise it will take very long computation time that makes completing all the results very difficult. Therefore, it is recommended to use a high-speed computation whenever available.

5.2 Effect of diffusers diffusion order

This work is based on the possibility of further increasing the mixing in the aeration tank by using different diffusion orders, which means that the order of the supplied air to the diffusers will be set in different orientation. Experimental and CFD studies using pulsating air flow method are both considered for this case.

5.2.1 Computational method

The bubbly flow into the water can be considered as dispersion of bubbles in static fluid. Employing computational fluid dynamics (CFD), this can be modelled as a two-phase flow, where the carrier or continuous phase is water and the dispersed phase is air.

The presence of a dispersed phase can modify the turbulence of a continuous phase in different ways. The combination of the drag and buoyancy can directly affect the momentum of

fluids. The rising of the dispersed bubbles and the wake generated can generate turbulence in the continuous phase. The lift force generated due to the irregular rising of bubbles and the interaction between the bubbles can further increase the turbulence. All that lead to increase the mixing in the aeration tank, which is favorable in terms of mass transport of species. This complicated behavior is also leading to the consideration that the dispersion of bubbles in water is in fact turbulent flow, which is the case considered for the current study.

The volume fraction is shared between the two phases. It introduced to the continuity, and momentum equations on condition that the total volume fraction is equal to one. Therefore, the species equation for phase i is given by:

$$\frac{\partial \rho_i Y_i}{\partial t} + \nabla \cdot (\rho_i U_i Y_i) = N_{ji} - N_{ij} + S_i \quad (5.7)$$

The momentum equation is given by:

$$\begin{aligned} \frac{\partial \rho_i U_i Y_i}{\partial t} + \nabla \cdot (\rho_i U_i U_i Y_i) \\ = -Y_i \nabla p + Y_i \rho_i \mathbf{g} + \nabla \cdot \tau_i + U_s (N_{ji} - N_{ij}) + F_D + F_L + F_{vm} \end{aligned} \quad (5.8)$$

The mass transport terms in the species and momentum equations (equations 5.7 and 5.8) are accounted when considering a mass transfer model. Despite the two-phase flow treatment in this work, but there will be no significance from activating a mass transfer model when solving the CFD problem, since no oxygen transfer data is required. Therefore, these terms can be taken out of the computation.

Since the density of the air is very low compared to the water, the turbulence in the water has a dominant effect. In addition to that, the definition of the drag and lift forces should follow the water influence on the air not the opposite. Then, the drag coefficient can be obtained from the Schiller correlation (Schiller & Naumann, A., 1933):

$$C_D = \frac{24(1 + 0.15Re^{0.687})}{Re}, Re \leq 1000 \quad (5.9)$$

Where Re is the dispersed phase Reynolds number and it can be obtained from:

$$Re = \frac{\rho_i(U_i - U_j)d_b}{\mu_i} \quad (5.10)$$

In equation (5.10), the subscripts i and j are referred to the interacting fluids. Where i for primary or carrier fluid (water) and j for secondary or dispersed fluid (air).

The lift coefficient is constant, but the lift force is corrected based on the drag force to account for multi-particle effects and increase the stability of the solution.

The drag and lift forces are calculated based on the interaction length scale. For the current cases, this scale is defined as the water-air interface, which is the air bubble diameter. The bubble diameter is calculated from measuring the bubble horizontal and vertical dimensions obtained from experimental measurements. For these measurements, high-speed camera with 2000 frame/sec is used. Since the rising of bubbles in water are different in size, twenty bubbles at different locations within the target picture frame are captured by the high-speed camera. Then, the average diameter

is considered as the interaction length scale. The bubble size is considered constant since the contact time between the air and water is short for the aeration system considered for this study.

The CFD physical problem and operating conditions are the same as that of the experiment, this is necessary since comparison with the experimental approach is intended from the results of this study.

5.2.2 Experimental method

Although, the rising of bubbles will change the static condition of water causing some mixing, but the mixing extent can be significantly altered by using pulsating airflow method as it was proven in the previous studies. This method is also used to create pulsating effect for both inline and staggered orders. The experimental system can be illustrated in figure 5.8 which consists of a water tank of 1.2 m height and 0.9 m diameter, and four membrane diffusers of 0.23 m diameter. Each diffuser has around 5000 fine pores of around 0.3 mm diameter. These are standard aeration diffusers made of rubber membrane, each has a dynamic wet pressure ranges between 280 to 400 mm depending on the air flow rate. The intermediate distance between the four diffusers is kept constant. Air with different flow rates is supplied to the four diffusers by using pulsating method, where there will always be two diffusers on and two diffusers off. This pulsating effect is created by using an Arduino circuit, where the pulsating time can be changed by the Arduino control circuit. The dissolved oxygen (DO) in the water is measured at three different elevations along the tank height using three optical DO probes of 1 Hz frequency. They can measure oxygen concentration up to 20 mg/liter within $\pm 2\%$ accuracy. The final DO reading is calculated by taking the average of the measurements from all three DO probes.

All experimental DO measurements are conducted under standard conditions. For these measurements, it is necessary to add deoxygenated chemical to strip the water from dissolved

oxygen similar to previous experimental cases. Then, water is reaerated to obtain the DO-time curve. The overall mass transfer coefficient is considered in this case, which can be determined from the measured DO profile based on the two-film theory [12], by using equations 3.9 and 3.12. Then, standard oxygen transfer efficiency (SOTE) is calculated after calculating the rate of oxygen transfer (SOTR) and based on the mass flow rate of the oxygen which is determined from the mass flow rate of the air measured on a flow meter. Therefore, the SOTE can be obtained from equation 5.13, which is similar to the method described in section 3.1:

$$N = K_L A_b (C_\infty - C_O) \quad (5.11)$$

$$dC / dt = K_L a (C_\infty - C_O) \quad (5.12)$$

$$SOTE = \frac{SOTR}{\dot{m}_{O_2}} \quad (5.13)$$

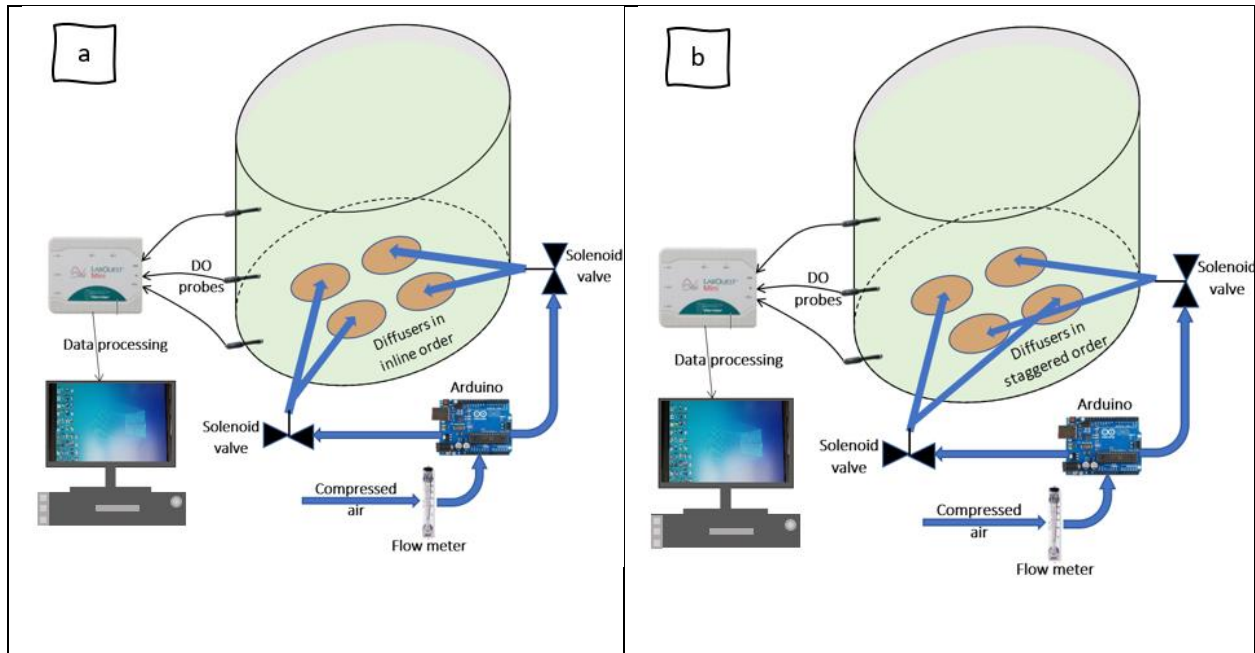


Figure 5.8: Experimental set up; a-Inline order, b-Staggered order

5.2.3 Experimental results

The work included here is based on the effect of diffusion order on the aeration efficiency by diffusing the air from each two diffusers at a certain order and time. This time which is the pulsating time also contributes to the mixing in the water tank. Therefore, for the experimental results, different pulsating time cases are considered. The pulsating times considered are 0.5, 1.5 and 2.5 seconds.

Experimental measurements were conducted to obtain the dissolved oxygen (DO) profile with time in a similar way to that followed in previous work.

Figures 5.9 to 5.11 show the calculated SOTE obtained from experimental measurements for different flow rates and at different pulsating times. All results show decreased trend when the flow rate increased from around 15-25 L/min. Then, the SOTE is increasing beyond 25 L/min. The decreased behavior is attributed to the inverse proportional relation with the air or oxygen flow

rate, this can be indicated from equation 5.13. Then, when the flow rate is increasing, the mixing in the aeration tank becomes higher to a degree that will overcome the inverse proportional relation of the SOTE on the oxygen flow rate. Therefore, the SOTE will keep increasing at higher flow rates, in contrast to the low flow rate region.

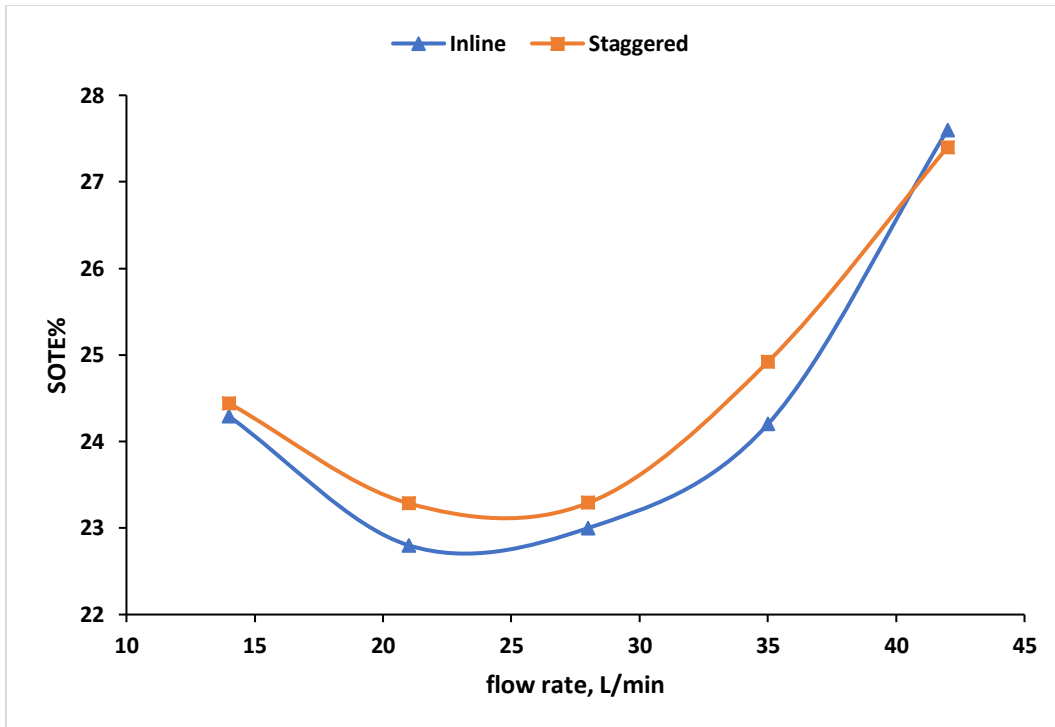


Figure 5.9: SOTE% variation with flow rate at 0.5 Sec pulsating time

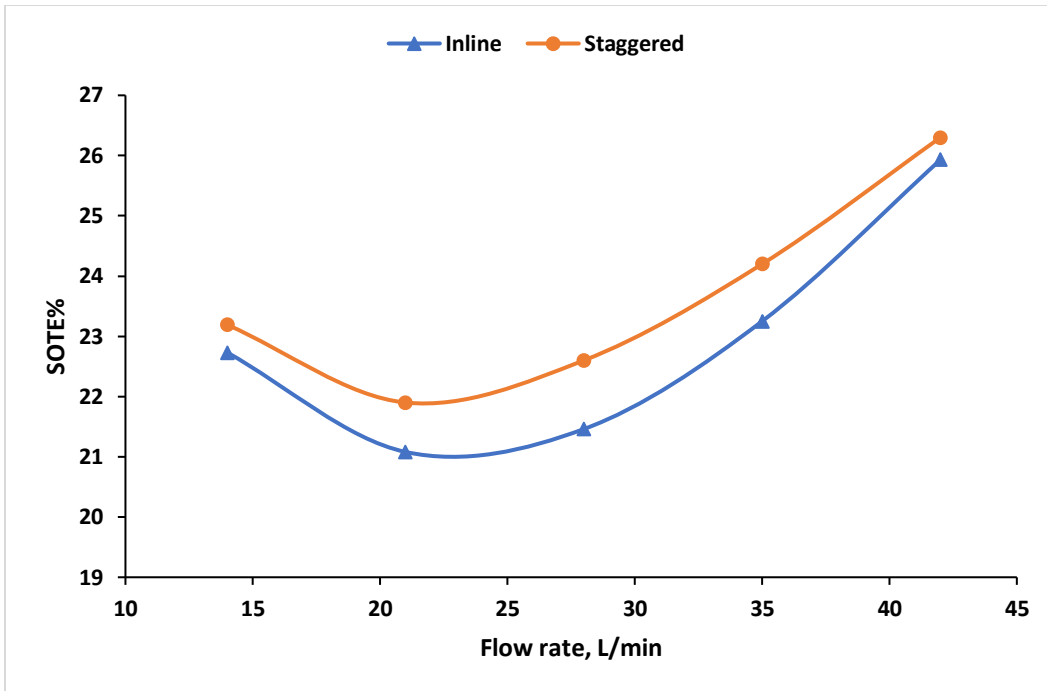


Figure 5.10: SOTE% variation with flow rate at 1.5 Sec pulsating time

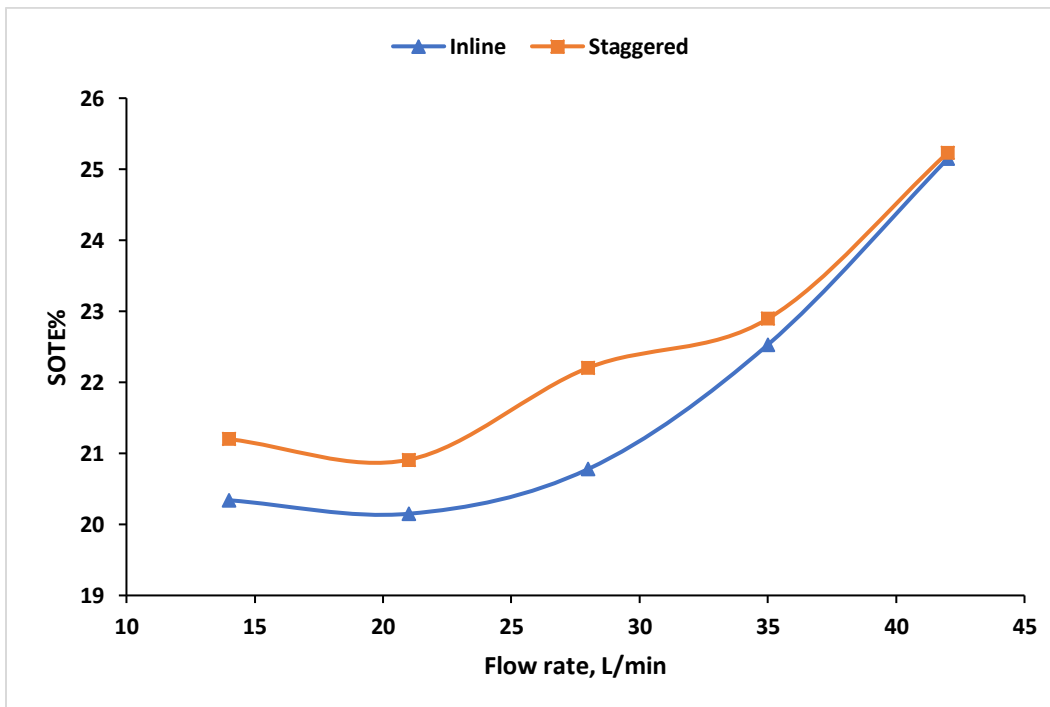


Figure 5.11: SOTE% variation with flow rate at 2.5 Sec pulsating time

Also, the higher SOTE results can be seen when the pulsating time is 0.5 second, then 1.5 second, and the lowest can be seen at 2.5 second as shown in figures 5.12 and 5.13. This is in agreement with the results obtained in section 4.2.

For comparison of the SOTE results, it can be clearly considered that the staggered diffusion order is showing better behavior than the inline diffusion order. But at higher flow rates, the staggered and inline diffusion effects tend to be similar. This is attributed to the wall effect, when the bubbles swarms emerge to the water surface, there will be high intensity waves moving from the center of the water tank to its wall. After impinging on the wall, the surface waves retract back and create more mixing that can alter the effect of diffusion order, whether it is inline or staggered.

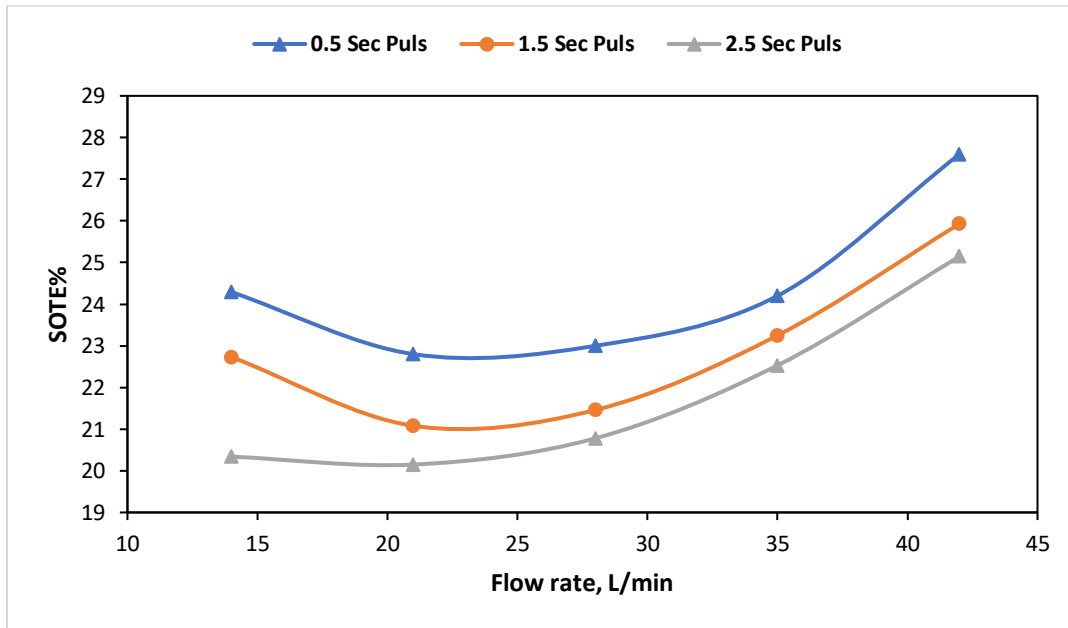


Figure 5.12: SOTE of the 0.5, 1.5, and 2.5 S pulsating time for inline case

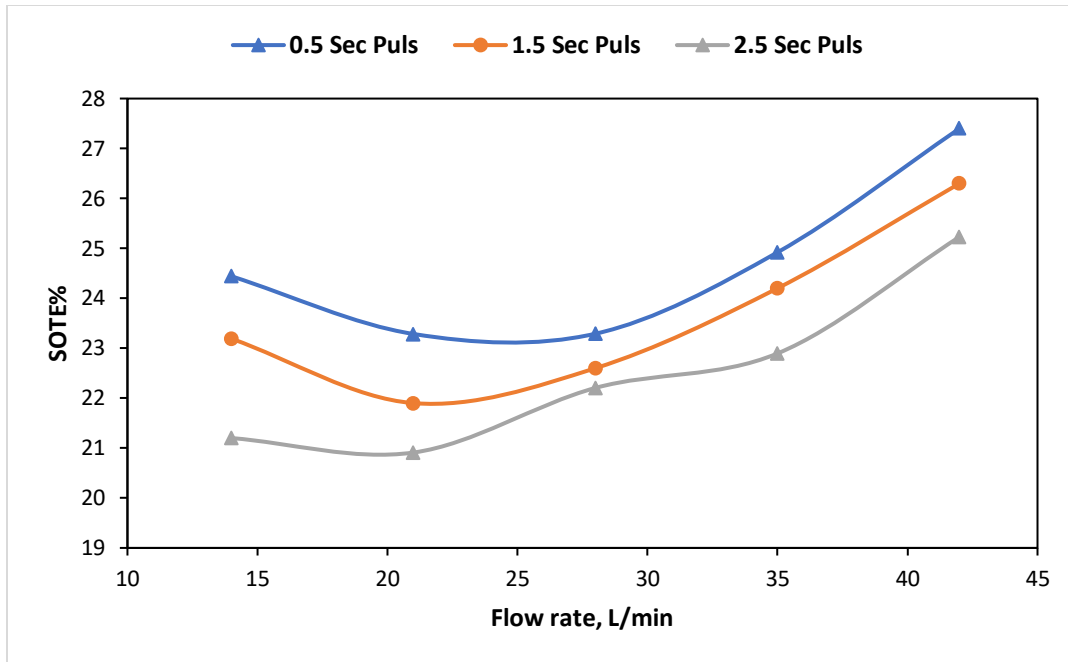


Figure 5.13: SOTE of the 0.5, 1.5, and 2.5 S pulsating time for staggered case

5.2.4 CFD results

For the experimental results, the SOTE was considered to be a measure of the aeration system efficiency. Similarly, it can be assumed that flow vorticity and circulation can render the effect of mixing on the aeration efficiency for the CFD results. This assumption is coming from the fact that, when vorticity or circulation increases, the mixing will increase as well. Since mixing is directly affecting the oxygen transfer rate, then higher vorticity or circulation can enhance the efficiency of the aeration system. For better rendering of this effect, results of the vorticity and circulation are obtained at different locations and at a certain physical time. On the other hand, the CFD results are limited to the lowest pulsating time (0.5 second) only because of the higher computation time required when considering higher pulsating time.

As a first step towards comparing the results with experimental data, figure 5.14 shows the surface jump obtained when the diffused air reaches the surface after 1 second of physical time.

The jump is measured about 7 cm, which agrees with the jump height obtained in section 4.3 for the same flow conditions.

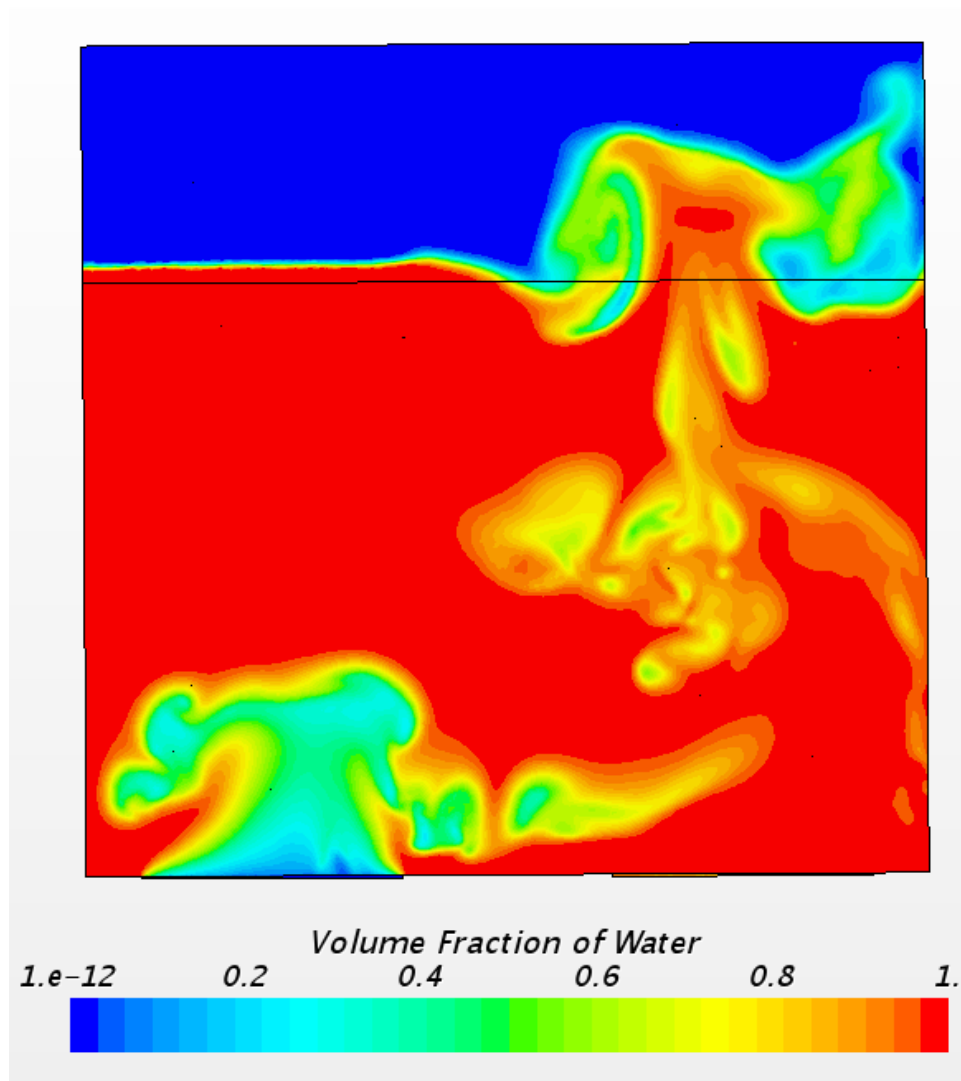


Figure 5.14: Water jump at the air-water interface

Figures 5.15 and 5.16 show the vorticity and circulation variation with time for each of the inline and staggered order. The vorticity results in figure 5.15 were calculated at a plane on the water surface. Similarly, the circulation in figure 5.16 was also obtained at the same plane. The vorticity is first stay constant at low value close to zero then, it starts increasing to a maximum value. Then,

two peaks can be seen, the first peak is generated at about 1 s due to the onset of one flow streams of bubbles at the surface. Then, the second bubbles swarm from the second set of diffusers will rise to the surface, this is where the second peak will start to generate, around 1.5 to 2 s. Figure 5.16 show the circulation of the flow for each of the inline and staggered cases. The circulation of flow was calculated by integrating the vorticity over the region of interest, for this case the region is the surface of the water. Similar to the vorticity, the circulation results were obtained at a plane on the water surface. The circulation results from figure 5.16 show similar trend to that of the vorticity results except lower fluctuation can be seen in this case, which is reasonable considering the integral of vorticity to obtain the circulation.

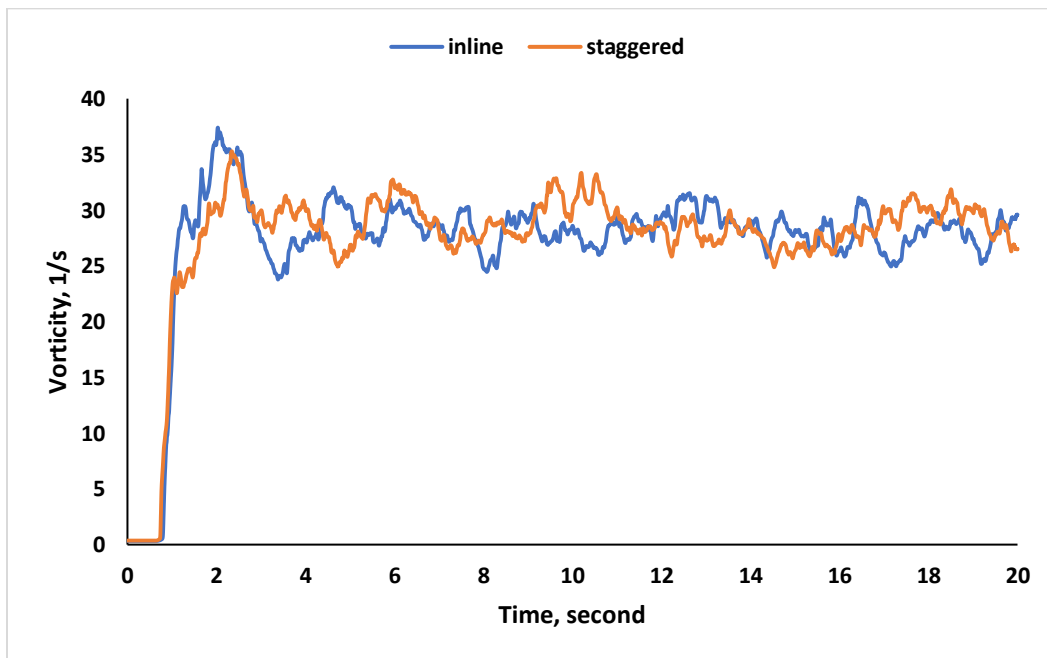


Figure 5.15: Vorticity variation with time at a plane on the water surface

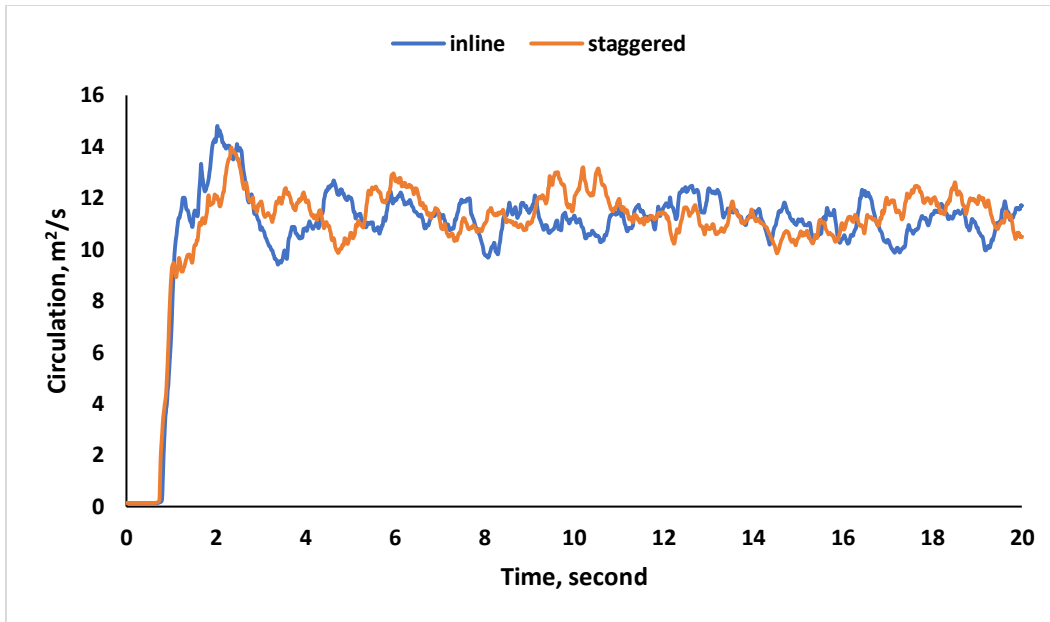


Figure 5.16: Circulation variation with time at a plane on the water surface

Figure 5.17 and 5.18 show the vorticity and circulation at a plane parallel to the water surface and lies 0.2 m below the surface. Due to the high computation time required, these results were limited to a period of 0 to 4 seconds. It is intended from these results to see the flow behavior at a plane other than the surface. Similar behavior to that of figure 5.15 and 5.16 can be seen. Where the trend of vorticity or circulation increases and then fluctuates around an average value same as that obtained at the water surface.

All the foregoing results show a maximum vorticity occurs around 1.5 to 2 seconds, which is the case when the two bubble swarms first emerge to the planes where these results are calculated. Then, results take a steady fluctuation about an average value.

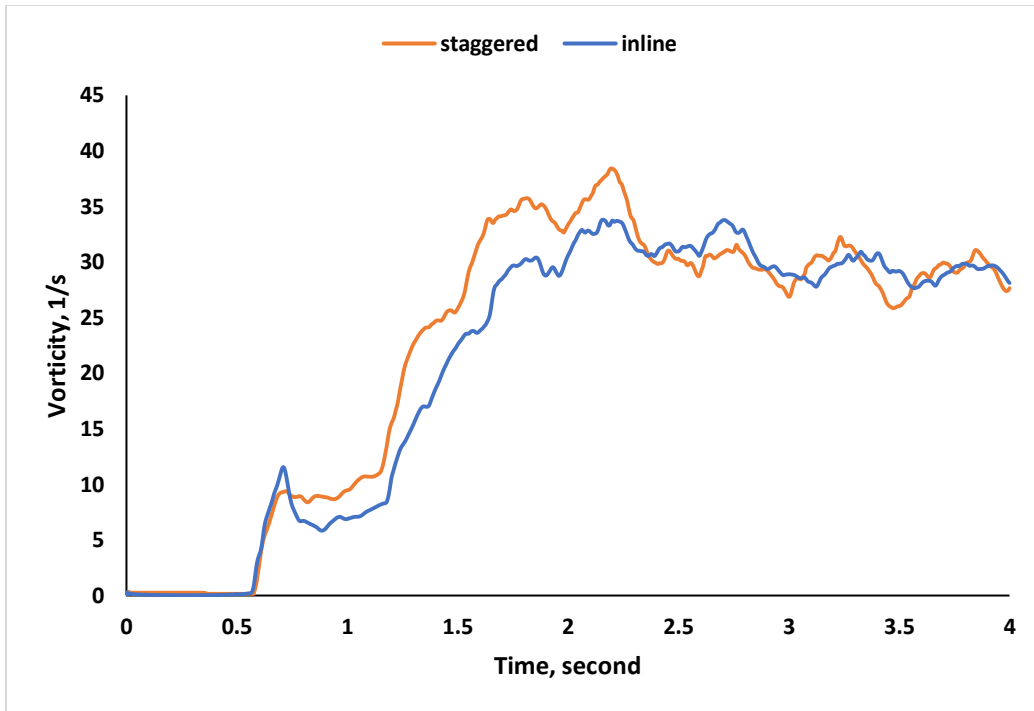


Figure 5.17: Vorticity variation with time at a plane 0.2 m below the water surface

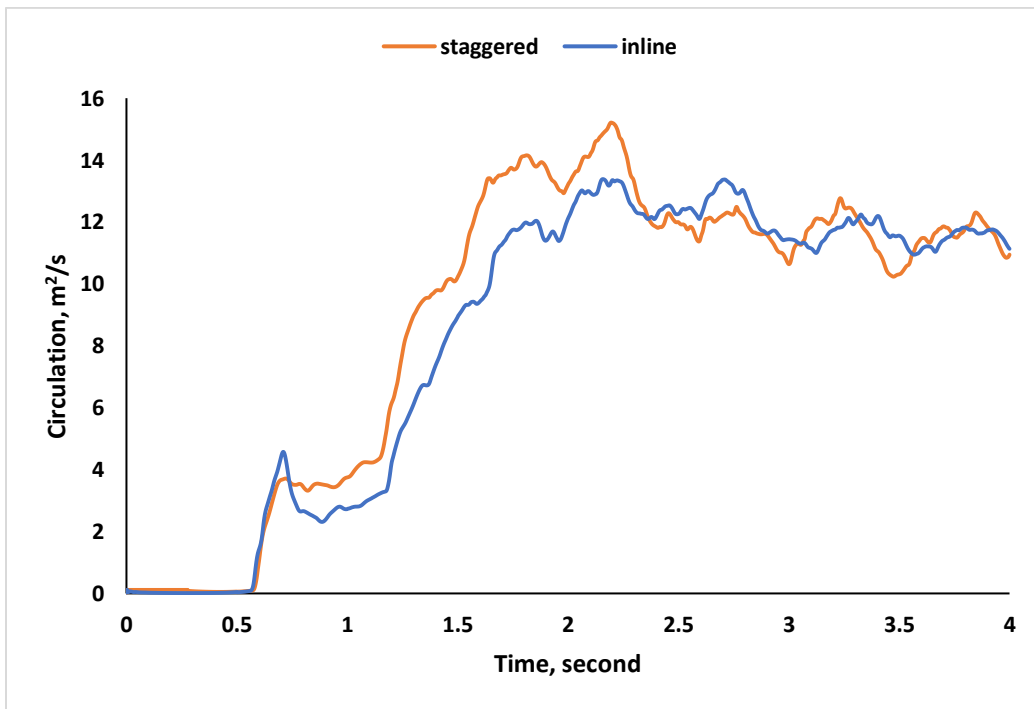


Figure 5.18: Circulation variation with time at a plane 0.2 m below the water surface

For all of the CFD results, it would be more realistic to consider a later physical time because the flow tends to be more stable as physical time increases as shown in figures 5.19 and 5.20. In this case, 2.5 s can be considered as that time where flow starts to stabilize, and results can be more accurate beyond that point. Also, it would be more reasonable to assume an average value in which the steady state results can be settled on as time approaches infinite (time-averaged value). These steady state values can be found in table 5.1.

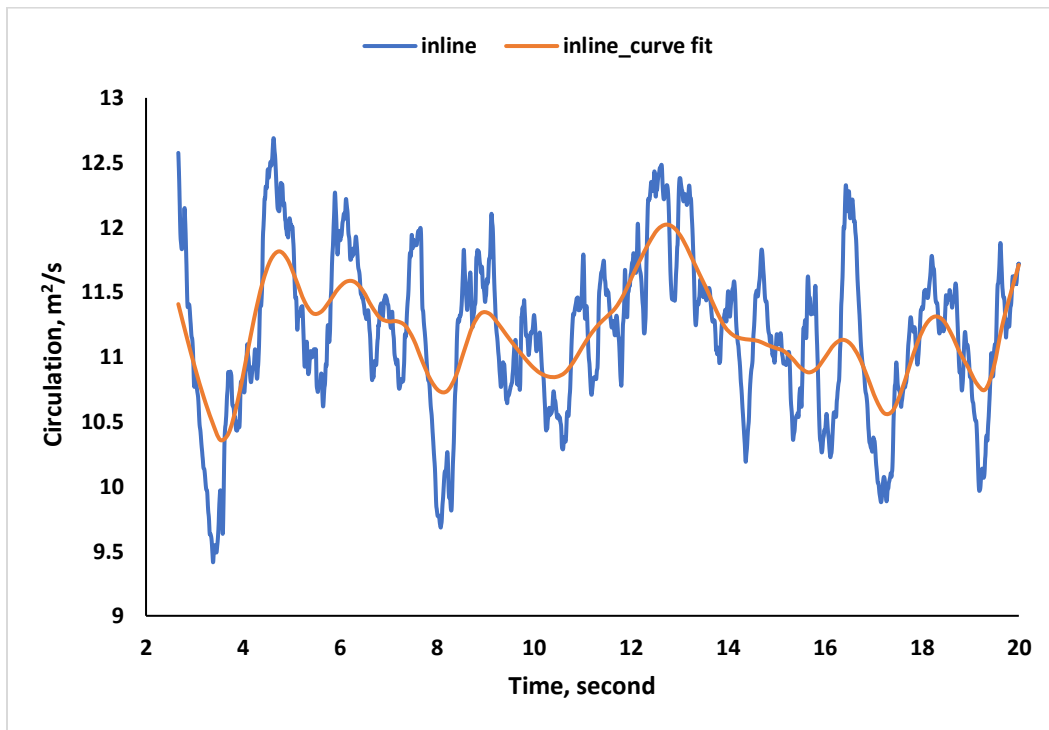


Figure 5.19: Curve fitting of the circulation variation for the inline order from figure 9 starting at 2.5 s time

Table 5. 1: Time-averaged vorticity and circulation

	Inline order	Staggered order
Vorticity, 1/s	28.3	28.7
Circulation, m ² /s	11.2	11.4

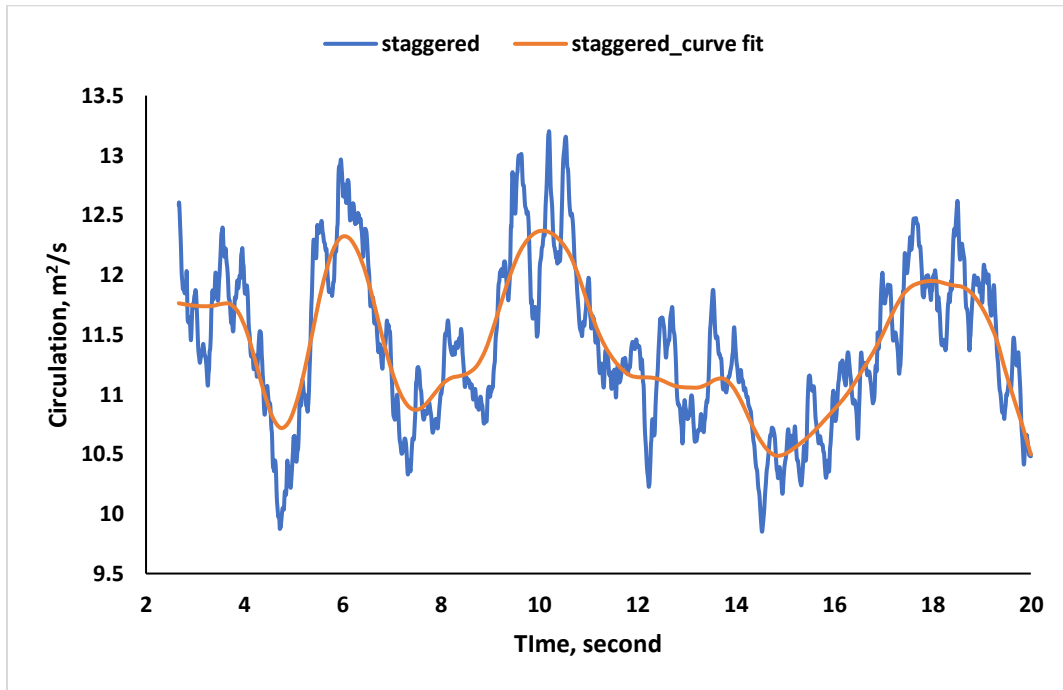
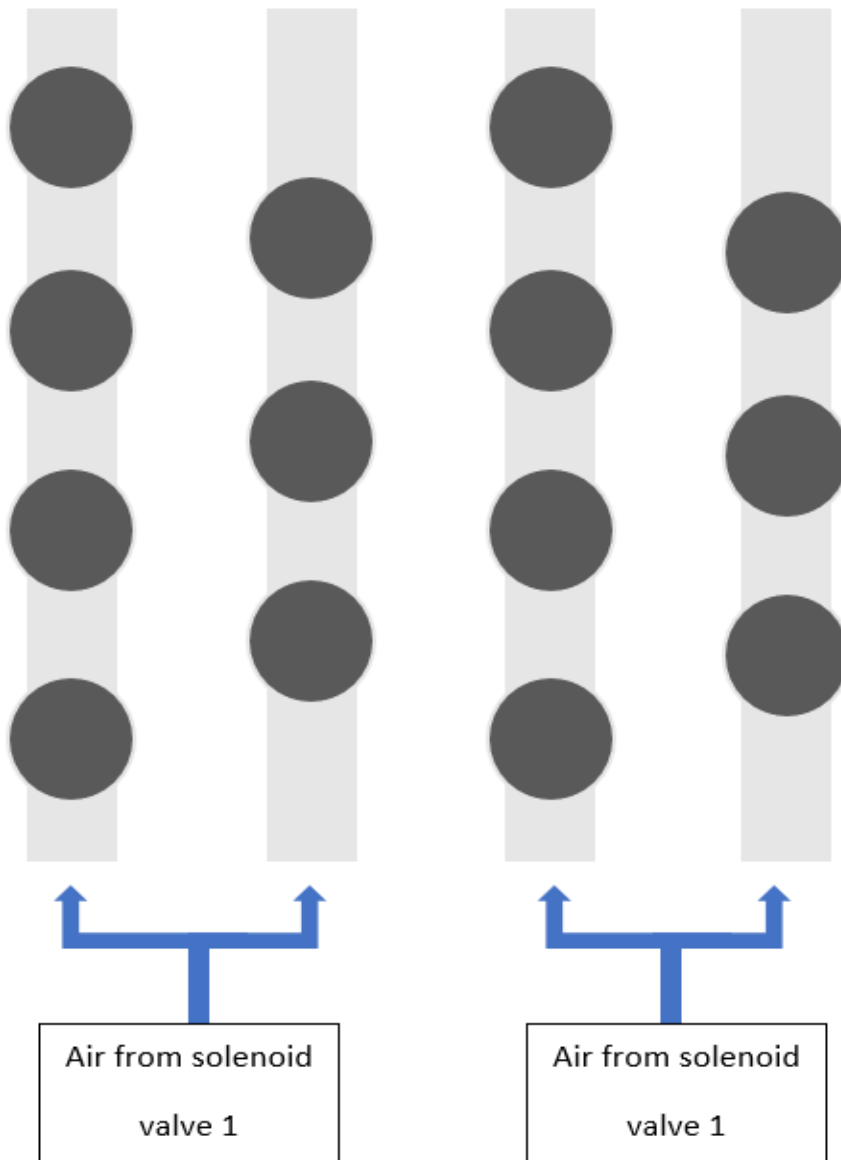


Figure 5.20: Curve fitting of the circulation variation for the staggered order from figure 9 starting at 2.5 s time

When considering the vorticity or circulation as a measure for the rate of oxygen transfer due to mixing, then higher vorticity or circulation mean higher oxygen transfer rate. This is analogous to the SOTE from the experimental results. Based on that, compared with the experimental results (figure 5.9) the CFD results are also showing that the staggered order diffusion better than the inline order in terms of oxygen transfer efficiency.

5.2.5 Application to real case

The air diffusers are distributed in inline order in wastewater treatment plants; therefore, it will be necessary to reflect the design of the staggered and inline order of the study on the real case. Due to the large number of diffusers in any wastewater treatment plants, the best way is to lay the pipes in parallel. Figure 5.21 shows the suggested order layout of the diffusers. The design of the air diffusion to the diffusers based on this layout can be done by supplying the air to each two consecutive pipes. For staggered order as shown from figure 5.21, the pipes or diffusers can be installed so that staggered order can be created. This layout is sufficient to create the staggered layout while keeping the pipes parallel to each other. An Arduino circuit should be provided to give the pulsating effect, where for this case, each two pipes can be connected to a single solenoid valve as shown in figure 5.21. Multiplying this layout can cover all the piping and diffusers for any wastewater treatment plant.



5.21: Suggested staggered order layout for implementing the diffusion order on real case

5.2.6 Conclusions

The CFD approach of such a complicated application can promise a significant influence when computation time is of critical importance. By considering this approach, the results obtained will compensate for the necessity to run CFD simulations of very high physical time to determine the DO profile. This physical time is equal to the physical time required to complete the DO experimental measurements according to the experimental approach.

The experimental approach shows the staggered diffusion order is better than the inline order for all the pulsating time considered for this study. Except the cases when flow rate is high, due to the water tank wall effect, this can alter the behavior of the SOTE results. On the other hand, when comparing the effect of pulsating time in the experimental case, the 0.5 second shows the best case, this behavior is agreed with the results from the experimental work discussed in the previous sections.

It can also be concluded from this study that the CFD results show similar behavior as the experimental results. But this approach needs to include more operating conditions such as airflow rate and water column to expand the CFD results and apply more conditions based on the experimental approach.

Chapter 6 Recommendations for future research

- 1- The literature shows promising results when using ultrasonic to increase the dissolve oxygen concentration level in water, therefore, this method can be conducted by inserting ultrasonic vibrator above the air diffusers while dispersing bubbles from the air diffusers. Then compare the SOTE results with and without ultrasonic
- 2- Since the bubbles rising velocity is increasing with bubble size, applying pulsating air flow method to coarse bubble membrane diffusers can increase the rising velocity which will increase the intensity of the surface waves and increase mixing in the aeration tank. This study can be compared with fine bubble diffusers which are already investigated to determine its significance.
- 3- Conduct a comparison study between ceramic and membrane diffusers for high water columns, in the range of 2 to 3 m.
- 4- Conduct aeration study for comparison between ceramic and membrane diffusers using continuous air flow
- 5- Considering the same set up shown in figure 4.34 to convert the bubbles rising path from vertical to inclined to increase the resident time and transfer area between the air and water
- 6- At stagnant condition, the water level will be less than that when air bubbles existed. Therefore, there will be a water column difference between stagnant

and bubbly flow. This difference in water column can be used as potential energy.

- 7- The CFD study of the effect of diffusion order on the oxygen transfer efficiency was limited to one case. This study can be expanded to include more flow rates and water columns to see the effect of more parameters and also increase its applicability.
- 8- Using CFD, consider more diffusers (for example 9 instead 4) to investigate more diffusion orders and more mixing.
- 9- Investigate the effect of creating wave motion within the diffuser membrane to avoid the bubbles attachment to the membrane surface
- 10- The vacuum degasification method was proven to extract the dissolved oxygen in the water more efficiently than adding Sodium Sulfite, but this method is applied to small scale system. This method can be expanded to include full-scale aeration system by using higher capacity vacuum system.
- 11- Using Ultrasonic method for degassing of Oxygen in water

References

- Ajay Kumar, P. G. (2004). Gas - Liquid mass transfer studies in sonochemical reactors. *j. Ind. Chem. Res.*, 1812-1819.
- Alkhafaji, A., Alkhalidi, A., & Amano, R. (2018). Effect of water column height on the aeration efficiency using pulsating air flow. *JJMIE*, 45-50.
- Alkhafaji, A., Alkhalidi, A., & Amano, R. S. (2017). Study of aeration by using pulsating air flow. *55th AIAA Aerospace Sciences Meeting*. Texas.
- Alkhalidi, A. A., & Amano, R. S. (2015). Factors affecting fine bubble creation and bubble size for activated sludge. *Water and Environmental Journal*, 105-113.
- Alkhalidi, A. A., Alba'ba'a, H. B., & Amano, R. S. (2016). Wave generation in subsurface aeration system: a new approach to enhance mixing in aeration tank in wastewater treatment. *Desalination and Water Treatment*, 1-8.
- ASCE. (1993). *Measurement of oxygen transfer in clean water*. Retrieved from Front Matter and Software: doi: 10.1061/9780872628854.fm
- Ashley, K., Hall, K., & Mavinic, D. (1991). Factors influencing oxygen transfer in fine pore diffused aeration. *Water Research*, 1479-1486.
- Behzadi, A., Issa, R., & Rusche, H. (2004). Modelling of dispersed bubble and droplet flow at high phase fraction. *Chemical Engineering Science*, 759-770.
- Bewtra, J. K., & Nicholas, W. R. (1965). Oxygenation from diffused air in. *Water Pollution Control Federation*, 1195-1224.
- Bird R., S. W. (2007). *Transport Phenomena*. New York, NY: John Wiley & Sons Inc.
- Chow, V. T. (1959). *Open channel hydraulics*. Tokyo: McGraw Hill Book Company, INC.
- Cockx, A., Do-Quang, Z., Line, A., & Roustan, M. (1999). Use of computational fluid dynamics for simulating hydrodynamics and mass transfer in industrial ozonation towers. *Chemical Engineering Science*, 5085-5090.
- Colombet, D., Legendre, D., Cockx, A., Guiraud, P., Risso, F., Daniel, C., & Galinat, S. (2011). Experimental study of mass transfer in a dense bubble swarm. *Chemical Engineering Science*, 3432-3440.
- Colombet, D., Legendre, D., Risso, F., Cockx, A., & Guiraud, P. (2014). Dynamics and mass transfer of rising bubbles in a homogeneous swarm at large gas volume fraction. *Journal of Fluid Mechanics*, 254-285.
- Dani, A., Guiraud, P., & Cockx, A. (2007). local measurement of oxygen transfer around a single bubble by planar laser-induced fluorescence. *Chemical Engineering Science*, 7245-7252.

- Das, A., Das, P., & Saha, P. (2011). Formation of bubbles at submerged orifices - Experimental investigation and theoretical prediction. *Experiemntal Thermal and Fluid Science*, 618-627.
- Davis, M. (2010). *Water and wastewater engineering*. New York, NY: McGraw-Hill Science.
- EPA. (1998). *How wastewater treatment works...The basics*. Washington D.C: Environmental protection agency.
- EPA. (1999). *Wastewater technology fact sheet fine bubble aeration*. Washington, D.C: Environmental protection agency.
- Eskin D., A.-H. K. (2015). Application of a plate sonotrode to ultrasonic degassing of aluminum melt: Acountic measurements and feasibility study. *Journal of Materials Processing Technology*, 148-154.
- Eskin, D. (2017). *Overview of ultrasonic degassing development*. London: Brunel University.
- Fayolle, Y., Cockx, A., Gillot, S., Roustan, M., & Heduit, A. (2007). Oxygen transfer prediction in aeration tanks using CFD. *Chenical Engineering Science*, 7163-7171.
- Guyurgina, I. (2016, March 19). *sonomechanics*. Retrieved from Removing Air From Oils, Epoxies, Hydraulic Fluids, Adhesives, Waxes and Other Liquids: <https://www.sonomechanics.com/liquid-degassing-deaeration/>
- Henry, W. (1803). Experiments on the quantity of gases absorbed by water, at different temperatures, and under different pressures. *Philosophical Transactions*, 29-274.
- Higbie, R. (1935). The rate of absorption of a pure gas into a still liquid during short time of exposure. *Transactions of the American Institute of Chemical Engineers*, 365-389.
- Hikaru Miura, M. N. (2015). Increasing unsaturated dissolved oxygen concentration in water by fine bubbles induced by ultrasonic vibrations. *J. Acoust. Sci. & Tech*, 240-247.
- Ishii, M. (1975). *Thermo-fluid dynamics, theory of two-phase*. Eyrolles.
- Khan, M. P. (2013). Inter-phase slip velocity and turbulence characteristics of micro particles in an obstructed two-phase flow. *J. Environ. Fluid Mech.*, 371-388.
- Khan, M. P. (2013). Inter-phase slip velocity and turbulence characteristics of micro particles in an obstructed two-phase flow. *J. Environ. Fluid Mech.*, 371-388.
- Khudenko, B., & Shpirt, E. (1986). Hydrodynamic parameters of diffused air systems. *Water Research*, 905-915.
- Lance, M., & Bataille, J. (1991). Turbulence in the liquid phase of a uniform bubbly air-water flow. *Journal of Fluid Mechanics*, 95-118.
- Lawrence, K., Yung, H., & Nazih, K. (2006). *Advanced physicochemical treatment processes*. Totowa, New Jersey: Humana press.

- Lewis W., W. W. (1924). Principles of gas absorption. *68th Meeting of the American Chemical Society*. Ithaca, N.Y.
- Matthew McCartney, C. S. (2008). Salinity implications of wastewater after irrigation in Musi river catchment in India. *J. Sci. (Bio. Sci.)*, 49-59.
- McGinnis, D., & Little, J. (2002). Predicting diffused-bubble oxygen transfer using the discrete-bubble model. *Water Research*, 4627-4635.
- Miyagi, O. (1925). The motion of an air bubble rising in water. *Philosophical Magazine*, 112-140.
- Mooers Products Inc.* (2013). Retrieved from <http://www.mooersproductsinc.com/bubble-diffuser-aeration-differences/>
- Pabi, S., Amarnath, A., Goldstein, R., & Reekie, L. (2013). *Electricity use and management in the municipal water supply and wastewater industries*. Palo Alto, California: Electric research institute.
- Poling B., P. J. (2001). *The properties of gases and liquids*. McGraw-Hill Companies Inc.
- Schiller, L., & Naumann, A. (1933). Uber die grundlegenden Berechnungen bei der Schwerkraftaufbereitung. *VDI Zeits*, 318-320.
- Star-ccm+ 2013, Siemens Inc., University of Wisconsin-Milwaukee Research License 2019. (n.d.).
- Tomiyaama, A., Kataoka, I., Zun, I., & Sakaguchi, T. (1998). Drag coefficients of single bubbles under normal and micro gravity conditions. *JSME International Journal*, 472-479.
- Tomiyaama, A., Tamai, H., Zun, I., & Hosokawa, S. (2002). Transverse migration of single bubbles in simple shear flows. *Chemical Engineering Science*, 1849-1858.
- Walther, E. (2009). *Energy efficiency and GHG reduction in wastewater facilities*. Northern California Chapter Meeting.
- Welty J., R. G. (2014). *Fundamentals of momentum, heat, and mass transfer*. New Jersey: Wiley.
- Wilkinson, P. M., & Haringa, H. (1994). Mass transfer and bubble size in a bubble column under pressure. *Chemical Engineering Science*, 1417-1427.

Appendix A: Image Processing Code

```
% CFD and Experimental evaluation and comparison for Air fraction
% The purpose of this script, for both CFD and Experimental images, is to calculate the
% total percent of air fraction with respect to the area of the experimental set up.
% After which, the values are compared
% The steps are:
% 1: Processing and analyzing the air infraction in the CFD images.
% 2: Processing and analyzing the air infraction in the Experimental images.
% 3: Evaluating the difference and percent error in the Calculated CFD and Experimental Air
Infraction.
% 4: Exporting all data to an excel spreadsheet
%% Script start
clear variables; close all; clc % Give fresh window
dbstop if error % Stop script if error occurs
format long g % Format numerical outputs
directory = ( 'C:\Users\..... '); % Define path
images = dir( strcat( directory , '*.png' ) ); % Define file type
% pre-difined variables
test_area_h = 0.6; % Test area height in m
test_area_w = 0.9; % Test area width in m
test_area = test_area_h * test_area_w; % Total area of test section in m^2
%% For CFD image
```

```

cfd_xy1 = [ 364 , 63 ]; % Coordinates of top left corner of CFD section
cfd_xy2 = [ 1126 , 571 ]; % Coordinates of bottom right corner of CFD section
cfd_area_pxl = ( cfd_xy2( 1 , 1 ) - cfd_xy1( 1 , 1 ) ) * ( cfd_xy2( 1 , 2 ) - cfd_xy1( 1 , 2 ) ); %
Area of CFD in pixels^2
cfd_pxl_scl = test_area / cfd_area_pxl; % CFD ( meters^2 / Pixel^2 ) conversion factor
cfd_img = imread( 'Scalar_Scene_1_image_1.000000e+00.PNG' ); % Defines CFD image being
analysed
crop_cfd = imcrop( cfd_img , [ 364 , 63 , 366 , 508 ] ); % Isolates Air Infraction within a Region
of Interest
% Creating background image, removes all blue from image
red = zeros( 509 , 367 ); % Defines red plane with no red color
green = zeros( 509 , 367 ); % Defines green plane with no green color
blue = ones( 509 , 367 ) * 255; % Defines Blue plane with highest blue contrast
background = uint8( cat( 3 , red , green , blue ) ); % Creates 3D matrix representing a blue image
subtracted_cfd = crop_cfd - background; % Removes blue background from image
gray_cfd = rgb2gray( subtracted_cfd ); % Creates a 2D matrix representing a 3D matrix, results
in grayscale image
adjust_cfd = imadjust( gray_cfd ); % Saturates top 1% and bottom 1% of all pixels, highlighting
contrast
bin_cfd = imbinarize( adjust_cfd ); % Represents image as a logical array.
air_infraction_cfd = sum( sum( bin_cfd ) ); % Calculates area of Air Infraction in Pixels^2,
Counts all 1's in binary image

```

```

air_infraction_area_cfd = air_infraction_cfd * cfd_pxl_scl; % Converts from Pixels^2 to
meters^2

air_infraction_percent_cfd = ( air_infraction_area_cfd / test_area ) * 100; % Calculates percent
of Air Infraction of CFD image in test area

%% For Experimental Image

data = imread( '1_S.PNG' ); % Experimental Image

exp_sz = size( data ); % Size of Matrix

exp_pxl_h = exp_sz( 1 , 1 , : ); % Experimental height in Pixels

exp_pxl_w = exp_sz( 1 , 2 , : ); % Experimental width in Pixels

exp_area_pxl = exp_pxl_h * exp_pxl_w; % Experimental Area in Pixels^2

exp_pxl_scl = test_area / exp_area_pxl; % Experimental (meters^2 / Pixel^2 ) conversion factor

d2 = rgb2gray( data ); % Creates a 2D matrix representing a 3D matrix, results in grayscale
image

tophat_image = imtophat( d2 , strel( 'disk' , 20 ) ); % Filtering out background with a tophat filter

adjust_image = imadjust( tophat_image ); % Saturates top 1% and bottom 1% of all pixels,
highlighting contrast

adapt_image = adapthisteq( adjust_image ); % Histogram adaption further enhancing contrast

back_sub1 = adapt_image - d2; % Method to subtract filtered background (line

back_sub2 = adapt_image - back_sub1; % Mathematically using just variables, this does not
work

bin_exp1 = imbinarize( back_sub2 ); % Represents subtracted filtered image as a logical array.

bw1 = bwareafilt( bin_exp1 , 1 ); % Captures largest detected area

cloud1 = imfill( bw1 , 'holes' ); % Fills largest detected area

```

```

bin_exp2 = imbinarize(adapt_image); % Represents filtered image as logical array
bw2 = bwareafilt( bin_exp2 , 1 ); % Captures largest detected area
cloud2 = imfill( bw2 , 'holes' ); % Fills largest detected area
comp1 = imcomplement(cloud1); % Changes 1's to 0's and vice verses in logical array
comp2 = imcomplement(cloud2); % Changes 1's to 0's and vice verses in logical array
comp = comp1 + comp2; % Captures Area without noise
cloud = imcomplement( comp ); % Change back to needed logical array
correction_factor = 0.6; % Given correction value
air_infraction_exp = abs(sum( sum( cloud ) ) ); % Calculates area of Air Infraction in Pixels^2,
Counts all 1's in binary image
corrected_air_fraction_exp = air_fraction_exp * correction_factor; % Accounts for correction
factor
air_fraction_area_exp = corrected_air_fraction_exp * exp_pxl_scl; % Converts from Pixels^2 to
meters^2
air_fraction_percent_exp = ( air_fraction_area_exp / test_area ) * 100; % Calculates percent of
Air fraction of CFD image in test area
%% Data comparison
Error = ( ( air_fraction_area_exp - air_fraction_area_cfd ) / air_fraction_area_cfd ) * 100;
Diff = air_fraction_percent_exp - air_fraction_percent_cfd;
% % xlswrite
% cd C:\Users\
%
% col_header = { 'Time(s)' , 'CFD' , 'Experiment' , 'Difference' };

```

```
% Time = { '0.5' , '1' , '1.5' , '2' };  
% xlswrite( 'air fraction' , col_header , 1 , 'A1' )  
% xlswrite( 'air fraction' , Time , 1 , 'A2:A5' )
```

Curriculum Vitae

Ahmed A. Alkhafaji

Place of birth: Baghdad, Iraq

Education

B.S., Baghdad University, June 1997

M.S., Baghdad University, January 2001

Dissertation title: Numerical and Experimental Investigation of Aeration Self Mixing by Using Pulsating and Continuous Air Flow

Teaching Assistant, August 2016 to December 2018

Research Assistant, January 2018 to December 2020

Publications:

1. Alkhafaji, A., Alkhalidi, A., & Amano, R. S. (2017)., Study of aeration by using pulsating air flow, 55th AIAA Aerospace Sciences Meeting, Texas
2. Alkhafaji, A., Alkhalidi, A., and Amano, R. 2018, Effect of Water Column Height on the Aeration Efficiency Using Pulsating Air Flow, JJMIE.
3. Alkhafaji, A., Strickler, J. Rudi, Amano, R. Jiang, H., Sikkel P. Kohls, N., marine zooplankton olfaction simulation using computational fluid dynamics, FEDSM 2020 ASME Meeting
4. Alkhafaji, A., A., Amano, R., S., 2020, Evaluation of ceramic and membrane diffusers under different water columns with pulsating air flow method, IJECE
5. Alkhafaji, A., A., Amano, R., S., 2020, Experimental and computational study on the effect of diffusion order in aeration systems, IJECE